NOTICE

The quality of this microform is heavily dependent upon the quality of the original thesis submitted for microfilming. Every effort has been made to ensure the highest quality of reproduction possible.

If pages are missing, contact the university which granted the degree.

Some pages may have indistinct print especially if the original pages were typed with a poor typewriter ribbon or if the university sent us an inferior photocopy.

Reproduction in full or in part of this microform is governed by the Canadian Copyright Act, R.S.C. 1970, c. C-30, and subsequent amendments.

AVIS

La qualité de cette microforme dépend grandement de la qualité de la thèse soumise au microfilmage. Nous avons tout fait pour assurer une qualité supérieure de reproduction.

S'il manque des pages, veuillez communiquer avec l'université qui a conféré le grade.

La qualité d'impression de certaines pages peut laisser à désirer, surtout si les pages originales ont été dactylographiées à l'aide d'un ruban usé ou si l'université nous a fait parvenir une photocopie de qualité inférieure.

La reproduction, même partielle, de cette microforme est soumise à la Loi canadienne sur le droit d'auteur, SRC 1970, c. C-30, et ses amendements subséquents.

Canada

Combinational PPAM Signaling and PWM Equalization over a Fiber Optic Channel

Tino Zottola

A Thesis

In

The Department

of

Electrical and Computer Engineering

Presented in Partial Fulfillment of the Requirements
for the degree of Master of Engineering
Concordia University
Montréal, Québec, Canada

October 1988

ISBN 0-315-49061-6

ABSTRACT

COMBINATIONAL PPAM SIGNALING AND PWM EQUALIZATION OVER A FIBER OPTIC CHANNEL

Tino Zottola

The performance of a combinational PPAM modulation scheme over an optical channel is evaluated and compared to conventional PAM and PPM schemes. Then the combinational PPAM scheme is examined in two different scenerios: with the conventional integrate-and-dump receiver and with the proposed ratio receiver tailored to the new combinational PPAM wave shape.

An equalizer for a PWM optical channel with Poisson statistics and additive white noise is presented. A linear equalizer is found using the zero forcing (LE-ZF) and mean square error (LE-MSE) criterion.

ACKNOWLEDGEMENT

I would like to express my gratitude to my thesis supervisor Dr. A.K. Elhakeem for his constant guidance throughout this research, and for his suggestions and constructive critism during the course of this thesis.

Furthermore, I would like to extend much thanks to Dr. J.F. Hayes for allowing me to participate in the implementation of his fiber optic based star LAN at Concordia. This has provided me with a wealth of practical knowledge in fiber optic systems.

Table of Contents

LIST OF FIGURES

LIST OF SYMBOLS

e	: electronic charge
$\overline{e^2}$	: mean square error of equalizer
f	: frequency
h	: Planck's constant
h_f	: Impulse response of optical fiber
h_l	: Impulse response of laser
h_R	: receiver filter
i_e	: APD electron current
i_h	: APD hole current
m_I	: mean of ISI
m_S	: mean of desired symbol
m_{th}	: mean of thermal noise
m_V	: mean of data symbol V_k
m_x	: mean of α_i
m_y	: mean of β_i
n_1	: refraction index
n_2	: refraction index
n_t	: noise voltage
p(t)	: optical pulse output of fiber
p_G	: Gaussian probability density function
p_P	: Poisson probability density function
p_R	: ratio receiver probability density functiom
p_T	: joint Poisson-Gaussian probability density function
r(t)	: composite pulse formed from α_i and β_i
t_r	: pulse rise time

$(t_{tr})_e$	: electron transit time
$(t_{tr})_h$	: hole transit time
t_A	: time required for avalanche to develop
v_{se}	: electron drift velocity
v_{sh}	: hole drift velocity
w_A	: avalanche distance
w_2	: distance of depletion layer
A	: amplifier gain
A_i	: threshold amplitude
APD	: avalanche photo-diode
B	: bandwidth
C	: capacitive element
C_n	: equalizer tap weight coefficients
DFE	: decision feedback equalizer
E	: energy component
E(x)	: expectation of x
ECC	: error control coding
F	: noise factor
F_e	: noise factor due to electron initiated avalanche
F_h	: noise factor due to hole initiated avalanche
G	: avalanche multiplication factor
$<G>$	: first moment of APD gain
$<G^2>$	: second moment of APD gain
G_e	: avalanche multiplication factor for injected electrons
G_c	: carrier generation
G_h	: avalanche multiplication factor for injected holes
$\bar{I}$	: mean of a randomly generated current

$(I_A^*)^2$: mean square of amplifier noise current

$(I_m^*)^2$: mean square of current in avalanche region

$(I_{sh}^*)^2$: mean square of shot noise current

$(I_{th}^*)^2$: mean square of thermal noise current

$(I_T^*)^2$: mean square of the sum of all noise currents

ISI : inter-symbol interference

K_B : Boltzmann's constant

L : number of PAM levels

LE : linear equalizer

LED : light emitting diode

M : number of PPM slots

N : number of carrier pairs

N_o : thermal noise spectral density

NRZ : non-return to zero

OOK : on-off keying

P_e : probability of error

P_{op} : optical power incident to APD

P_{sh} : shot noise power

P_{th} : thermal noise power

P_S : APD signal output power

PAM : pulse amplitude modulation

PDF : probability density function

PIN : Positive - Intrinsic - Negative

PN : Positive - Negative

PPAM : combinational pulse amplitude-position modulation

PPM : pulse position modulation

PWM : pulse width modulation

R_n : autocorrelation of thermal noise component

R : resistive element

R_{APD} : APD load resistor

RZ : return to zero

S : transfer function

S_o : frequency independent transfer function

S/N : signal-to-noise ratio

T : data frame period

T^o : receiver temperature

$(V_A^*)^2$: mean square of amplifier noise voltage

V_B : APD breakdown voltage

V_k : data symbol

V_N : amplifier output noise voltage

V_S : amplifier output signal voltage

$(V_{th}^*)^2$: mean square of amplifier noise voltage

$X(t)$: message source input to the transmitter

$X_C(t)$: laser current

$X_L(t)$: optical output of laser

$X_S(t)$: APD output

$Y(t)$: equalizer signal input

$Z(t)$: equalizer signal output

α_i : first component of composite pulse

α_e : electron ionization probability

α_h : hole ionization probability

β_i : second component of composite pulse

γ : ISI decay factor

$\delta(t)$: impulse function

ξ_{ph} : photon energy

ξ_R : received optical energy

$\lambda(t)$: mean instantaneous rate of primary electrons

λ_o : dark current

η : detector efficiency

π : constant = 3.1415926

σ_{sh}^2 : variance of shot noise

σ_{th}^2 : variance of thermal noise

σ_I^2 : variance of ISI

σ_N^2 : variance of number of carrier pairs

σ_S^2 : variance of desired symbol

σ_x^2 : variance of α_i component

σ_y^2 : variance of β_i component

τ : data slot period

τ_{APD} : avalanche response time

θ_i : angle of transmitted light w.r.t. normal

θ_r : angle of reflected light w.r.t. normal

θ_t : angle of refracted light w.r.t. normal

υ : frequency of light

Δf : system bandwidth

$\Delta\tau$: timing error

Ω_S : outcome of decision logic when desired signal is present

Ω_I : outcome of decision logic when ISI is present

Ωth : outcome of decision logic when thermal noise is present

$\Phi_R(f)$: Fourier transfom of received optical signal

Θ_{mn} : autocorrelation of symbols V_m and V_n

CHAPTER ONE

INTRODUCTION

It can be said the era of optical fiber communicaton began in 1880 when Alexander Graham Bell used his photophone to communicate using light over a distance of a mile. In the last 20 years fiber optic technology has been developing at an incredible rate. In this short time it has evolved from a laboratory curiosity to an integral part of many modern communications. In 1967 rudimentary fiber optic cable had a prohibitive loss of 1000 dB/km. This high attenuation can be attributed to the crude refining techniques, of the yet undeveloped technology, used to make fiber optic cable which left a high concentration of impurities in the glass fiber. This factor limited the cable's usefulness to very small distances indeed. Modern fiber optic cable can be manufactured with an attenuation as low as 0.2 dB/km, which makes it an excellent contender for long haul applications. Furthermore, new solid state devices such as laser LEDs (Light Emitting Diodes) and APDs (Avalanche Photo-Diode) detectors give modern fiber optic systems bandwidths in the gigahertz range. Hence, many North American telecommunication companies are currently replacing many of their transcontinental microwave links with optical fiber networks.

Communications via optic fiber is quickly replacing conventional microwave links and copper wire trunk lines in many applications. Optic fiber offers many advantages over its competitors. These advantages include the following:

(1) The attenuation of optic fiber is considerably less than that of similar lengths of coaxial cable or twisted pair. Modern optic fiber has a loss of less than 1 dB/km. Therefore optic fiber can span greater distances than copper wire before a repeater station is required. This translates into lower installa-

tion and maintanence costs.

(2) Optical fiber provides a high level of security since tapping into optical fiber requires physical contact with the fiber. Hence this loss of optical power can easily be detected at the receiving end. Whereas copper wire based trunk lines can easily be eavesdropped upon by either capacitive or inductive pickup devices and hence escape any detection since no physical contact is ever made.

(3) Similarly the electromagnetic leakage previously described also introduces another problem in copper wire based system, namely crosstalk. This is the undesired transfer of signal from one wire to its neighbouring wires. Due to the closed construction of fiber optic cable, which is attributed to the cladding around the cable, emissions from optical fiber sytems are virtually non-existent. Similarly the same construction of optical fiber also makes it immune to the effects of external electromagnetic interference.

(4) The inert nature of glass makes optic fiber immune to environmental abuses. This makes optic fiber much more rugged than more volatile copper wire systems.

(5) One of the most important features of optic fiber is its ability to handle very large bandwidths with ease. Just one percent, of the frequency of light used over optic fiber, is capable of accommodating over 5 million simultaneous television channels.

(6) The small size of optic fiber allows a greater number of communication circuits to occupy the same space of a copper wire trunk. Typical fiber optic cable is slightly thicker than a human hair and can carry thousands of telephone calls.

Fiber optic cable is not without some problems. One main problem is that fiber optic systems are not as easy to install and modify as copper wire ones. Special connectors, special tools, and procedures are required to install to route, splice, and align the optic fiber cables. Furthermore, fiber optic connectors and splices introduce a small loss in optical signal flow. But the advantages far outweigh the disadvantages and hence optic fiber remains quite a formidable opponent for copper wire systems.

The focus of this thesis will be on some unexplored areas of fiber optic technology. The performance of conventional digital modulation techniques such as PAM (Pulse Amplitude Modulation), and, PPM (Pulse Position Modulation) will compared with that of the proposed combinational PPAM (Pulse Position-Amplitude Modululation) scheme. The performance of the combinational PPAM scheme will be evaluated and compared using a conventional receiver and the proposed ratio receiver. The combinational PPAM system will be compared with the performance of purely PAM and purely PPM systems under similar conditions and with equal data rates and equal power budgets.

The detection and equalization of a PWM (Pulse Width Modulation) optical system will be examined. Methods for equalization of PAM signals by Messerschmitt [1] and for PPM signals by Gagliardi [2] have been described. Only PWM equalization apparently is not found in current literature. In chapter 4 these formulations are used as basis for solving equalizer coefficients for a PWM optical fiber system.

CHAPTER TWO

FIBER OPTIC COMMUNICATIONS

2.1 Introduction

An optical fiber communication system consists of three major sections: The transmitter, the optical fiber medium, and the receiver. The transmitter and receiver sections are shown in figures 1 (A) and 1 (B), respectively.

The transmitter section consists of a data source, an optional data encoder, and an optical source. The data can be passed through a data encoder if improvements of the system performance are desired, at the expense of system complexity. The optical source is in turn modulated by one of many different techniques such as OOK, PAM, PWM, or PPM. The optical source is usually an LED for low to medium capacity systems and a laser for high capacity systems. The use of lasers is becoming widespread in all systems, due to cheaper laser diodes as a result of CD (Compact Disk) player mass production.

The receiver consists of an optical detector such a PIN diode for bandwidths not more than a few hundred megahertz and the APD diode for bandwidths in the gigahertz range. The detector is followed by a low pass filter, an amplifier, an equalizing filter, and then the decision logic. The optical detector is a photosensor used to convert the weak optical signal from the fiber into an electrical signal. The photosensor must have the following characteristics: high sensitivity, high noise immunity, and practical design for manufacturing. The amplifier must be capable of boosting the nanowatt output of the photosensor to a level suitable for the decision logic. The equalizing filter is used to compensate incoming pulses distorted by ISI. The decision logic is configured to match the modulation scheme used at the transmitting end.

2.2 Data Encoding

Although an encoder is not absolutely necessary, it is sometimes used to enhance the performance of a fiber optic system.

An encoder can take the form of a Manchester encoder. The Manchester encoder requires twice the bandwidth, that the same unencoded signal occupies. At the expense of bandwidth, the bi-bit structure of the Manchester waveform allows for easy clock extraction by the receiver's Manchester decoder. This is possible because transitions are always present in middle of the Manchester symbol. Therefore the clock can always be derived, even when a long series of zeros or ones are sent. This is not the case with conventional RZ and NRZ systems. At the expense of system bandwidth, a simple clock extraction scheme is obtained.

The scenerio where a long string of zeros or ones exists makes the task of synchronization difficult. One alternative method to eliminate this scenerio and to make clock recovery easier is to scramble the transmitted signal by multipling it with a pseudo-random code string. The long string of zeros and ones is gone and the received scrambled signal is fed into a PLL (Phase Lock Loop) to obtain a clock signal. Then the scrambled signal is multiplied once again with the same pseudo-random string used at the transmitter to recover the original data. At the expense of more complex circuitry, system bandwidth is used much more efficiently then was the case with the Manchester scheme.

Encoders can be used for reasons other than easy clock extraction. For example a delay or Miller encoded signal is used to improve the spectral characteristics of the transmitted signal. A Miller encoded signal occupies less bandwidth than an unencoded signal. This is accomplished by a reduction of the number of transitions in the encoded signal. A "1" is represented by a signal transition at the midpoint of the bit interval. A "0" is represented by no

transition unless it is followed by another "0", in which the signal transition takes place at the end of the bit interval.

Data can also be encoded for improved reliability. At the expense of redundant information, an ECC (Error Control Coded) signal allows for the detection and correction of a limited number of corrupted bits at the receiver. The simpliest ECC scheme is an ASCII byte where a one parity bit is tagged onto a seven bit symbol. If odd parity is used, then an eighth bit is added to make the sum of the seven bits and that of the parity bit odd. If even parity is used then the sum is made even. Of course with such a simple scheme, if more than one error occurs the coding is rendered ineffective. With all ECC schemes when an error is detected, retransmission of the corrupted data is required, which reduces system throughput.

Sometimes data is encoded for security reasons. If a fiber optic line is tapped by an unauthorized party, scrambling provides a certain level of security. Such a scheme is designed such that an extremely large number of incorrect keys are possible to deter eavesdroppering. The received data will be meaningless to anyone, except the user who has the corresponding decryption key.

Therefore at the expense of bandwidth, which is plentiful in fiber optic systems, the overall performance of the fiber optic system can be improved by one or more of the previously described methods. In the cases of the scrambled signal and the Miller encoded signal, at the expense of more complex equipment, a reliable clock extraction or a reduction of system bandwidth are obtained, respectively.

2.3 The LED Optical Source

One of the key components in an optical fiber system is the optical source which converts our electrical signal into a corresponding optical signal. In short haul systems the LED is used extentsively. It offers the following advantages: low cost, simple to fabricate, simple interface circuitry, and temperature insensitivity. However, since LEDs are an incoherent source of light, their coupling efficiency is much less that of coherent devices such as lasers. Furthermore, LEDs have a maximum bandwidth of no more than two to three hundred megahertz.

The LED consists of PN junction between two electrodes. The PN junction radiates light in the form of photons which are generated by the recombination of the injected hole and electrons carriers. Normally there exists an energy barrier which inhibits recombination, but when the diode PN junction is forward biased, the hole and electron carriers have sufficient energy to cross the energy barrier and recombine as shown in Figure 2.

The energy of the radiated photons is proportional to the energy required to free the valence electrons required for recombination with a corresponding hole. The light total energy emitted is directly related to the number of valence electrons that recombine in given interval of time.

The quantum efficiency of an LED is typically less than 5 percent. This low efficiency stems from the internal reflections and absorption of emitted light that take place in the LED device. Light is emitted from the PN junction in random directions which also contributes this low efficiency. Efficiency can be improved several fold by surrounding the emitter junction with a transparent dome. This dome structure discourages internal reflections and facilitates the light emission from the LED junction. This form of construction raises the LED efficiency to at least 15 percent.

2.4 The Laser Optical Source

The laser semiconductors have many redeeming characteristics that make them more desirable than LED optical source in long distance and high capacity fiber optic systems. They include the following:

(1) A laser's emissions spread over only a narrow band of wavelengths, hence the problem of pulse dispersion is greatly reduced and therefore ISI is minimized to a greater extent than typical LED devices.

(2) Lasers are highly directional, thus transfer efficiency to the optic fiber is great improved and very little optical power is wasted.

(3) Most importantly the modulation bandwidth of lasers is very high, extending into the gigahertz region, whereas the bandwidth of LED devices is less than a few hundred megahertz. Hence, lasers complement the high bandwidth of optic fiber and APD devices quite nicely.

However lasers do have the problem of being difficult to construct and hence are rather expensive. Furthermore the proper operation of a laser is quite dependent on environmental temperature. But their superior performance overshadows these short comings.

Laser action takes place in three steps: absorption, spontaneous emission, and stimulated emission as shown in figure 3. Laser emission is possible when a semiconductor has a carrier population inversion. This semiconductor has two energy levels, an upper energy level E_2 and lower energy level E_1 . The higher level has a probability of being occupied by electrons greater than that of the lower level. The probability of a photon of energy $E = h\upsilon$ inducing an electron downward exceeds the probability of an upward transition (i.e. photon absorption). When electrons fall to a lower level a photon is released (i.e. spontaneous

emission). When a photon causes the electron to fall, this is known stimulated emission. Hence, this original photon produces an addditional photon. Then these two electrons in turn produce four. This multipication process continues until all possible photons have been emitted. Then the fallen electrons return to their original levels and the process repeat itself as long as the laser semiconductor material is forward biased. Hence, the name LASER comes from the ancronym for Light Amplification by Stimulated Emission of Radiation. In summary initial photons causes low energy electrons to rise to higher level, then a second group of photons causes the elevated electrons to drop and emit photons. Hence by the time the photons exit the laser semiconductor a vast quantity of photons is present. Since all photons are stimulated by previous electrons, the new and old photons are all in phase (i.e. coherent). The advantage of having a coherent light source is that an intense and highly directional beam is delivered with minimumal pulse dispersion.

2.5 The Theory of Light Transmission via Fiber Optic Cable

Light always travels in straight parallel rays unless a change in the medium is encountered. At the medium boundary two things can occur. First a portion of the light rays are reflected into the original medium. The angle of the reflected light rays is equal to the angle of incidence with respect to the normal of the medium boundaries. Secondly, light rays can cross the into the second medium. These rays are said to have been refracted since the rays have changed their angular position in the new medium. An illustration of these two phenomena is shown in figure 4. The angle of refraction with respect to the normal of the medium boundaries can be given by the ratio of their refractive indexes by Snell's law in equation (2.4.1).

$$\frac{Sin\,\theta_t}{Sin\,\theta_i} = \frac{n_1}{n_2} \tag{2.4.1}$$

When the first medium has a much greater refractive index than that of the second medium and when θ_i is sufficiently large, a situation occurs where the refracted rays are propagated along the medium boundaries (i.e. $\theta_t = 90^o$). The point where θ_i causes this to occur is called the critical angle. This phenemona is better known as total internal reflection. Total internal reflection happens when θ_i is equal to or greater than the critical angle.

Typical fiber optic consists of three main components. The inner core is fabricated from silica glass and is where the optical signal propagates. Then this silica core is covered with another layer called cladding. The purpose of the cladding is to contain the optic signal within the inner glass silica core. This cladding is in turn covered by an outer protective jacket. It's primary purpose is to insulate the silica glass fiber fom the external environment.

The refractive index of the core material is much greater than that of the cladding around the core. Hence all light rays are contained within the fiber. Propagation takes place via multiple internal reflections. All light rays having angles between 90^{o} and the critical angle are permitted to propagate, while all other rays greater than the critical angle are severly attenuated. These allowed directions of propagation correspond to the modes of the optical waveguide. Two classes of optical fiber exist: single mode and multi-mode fiber.

(1) Single mode fiber causes the optical signal to travel by only one path. It has the advantage of having a high bandwidth and having minimal pulse distortion. However it difficult to interface with optical devices and is hard to splice because of the critical alignment between fiber and devices required.

(2) Multi-mode fiber allows the optical signal to travel via manv different paths en route to it's destination. Multi-mode optic fiber has the advantage of being easily interfaced to the optical periphals and can be easily spliced. However it introduces considerable pulse spreading and hence is limited to low frequency applications only. It easy installation makes it quite a popular choice in low cost and inexpensive systems.

As in any communication medium optical fiber attenuates the signal that is propagating through it. There are several phenomena responsible for this loss: absorption, scattering, and radiation.

(1) Absorption losses are due to impurities remaining after the refinement of the glass silica. The impurities include water ions and metals such as iron. The minimization of the impurities is critical. To obtain losses as low as 10 dB/km the impurities present should less than a few parts-per-billion since their effect is accumulative. Absorption losses basically "steal" energy from the optical signal and convert it into any form such as heat.

(2) Scattering losses (also known as Raleigh Scattering) are to due minute inconsistencies in the refractive index along the fiber. The small changes tend to disperse the optical signal. Since 1976 when quality fiber optic cable with extremely small absorptive losses was available, scattering losses account for most of the losses in modern day fiber optic cable. Such losses are susceptible to thermal variations.

(3) Radiation losses are due to minute holes in the cladding which permit signal leakage. This is predominate where the fiber optic cable is subject to strain and pressure. Radiation losses are quite common at locations along the fiber where there are many bends and turns. The protective jacket on the cladding helps minimize these losses somewhat.

2.6 The PIN Diode

In low cost fiber optic systems the PIN diode is a popular choice. The PIN diode used in fiber optic systems is an improved version of the conventional PN photodiode. The typical PN consists of a photosensitive PN junction between two electrodes. During normal operation the PN junction is reversed biased. This reverse voltage produces an electric field which causes the holes to be attracted to P side and the electrons to be attracted to N side of the device. When this junction is exposed to a photons whose energy is greater the band gap energy level that exists at the PN boundary the hole and electron carriers traverse the boundary. And as the photons impart their energy to the carriers, a reverse displacement current is generated. This resulting current is proportional to the optic energy incident on the photodetector surface.

The PIN diode differs from its PN counterpart as shown in figure 5. The depletion (absorption) region in the PN diode is confined to the PN boundary. In the PIN diode the depeletion region runs the full length of the device.

The depeletion region, better known as the I (intrisic) region, is a lightly doped region in contrast with the highly doped P and N regions. The PIN derives its name from this structure consisting of these three main areas. This large I region means more incident light is absorbed by the device and translates into a more efficent and sensistive photodiode. However this increase in length results in a larger distance for the hole and electrons to travel, which slows down the response time of the device. But since the extra time is only a few nanoseconds it can be neglected for most low to medium data rate applications.

The PIN diode suffers the lack of one important feature, which is the lack of a gain mechanism. This limits PIN devices to low noise environments. This is where APD diode comes into play.

2.7 The Avalanche Photo Diode

The emphasis of the thesis will be on APD (Avalanche Photo-Diode) based detectors since their superior performance makes them a logical choice over other alternatives such as the PIN diode. The APD offers a large bandwidth, low noise, and inherent amplification through its avalanche mechanism. These are all highly desirable properties for a photosensor.

The average current produced by the APD detector is directly proportional to the incident optical power on the detector surface. The APD is biased in such a fashion as to produce a high electric field throughout the semiconductor substrate which in turn sets up the conditions necessary for the avalanche effect. The construction of the APD is shown in figure 6 (A) and the electric field distribution is shown in figure 6 (B).

The electrons flow in the high electric field where they experience ionizing collisions which generate a source of secondary electrons for each primary electron. The photo-electric conversion is a two stage conversion process. First, a photon counting takes place where incident photons are converted into a primary detector current. Secondly, each primary electrons then produces a large number of secondary electron-hole pairs via the avalanche mechanism of the APD diode. Both the new electron and hole may go on to produce even further excitations. Accordingly this effect also multiplies the shot noise generated during the photo-electric process. It is this multiplication mechanism which makes the APD detector far more desirable over devices such as the PIN detector. The lack of an amplification mechanism in the PIN diode makes its low output current highly susceptable to noise. The APD is solid state predecessor of the archaic vacuum tube photomultiplier which also has an electron multiplication mechanism.

For each photogenerated primary carrier an average of G carriers are produced for each primary electron at the end of multiplication process. Signal current is multiplied by a factor of G and rms shot noise level is increased by a factor of $GF^{1/2}$. Noise factor F is greater than unity and is an increasing function of G. For any given avalanche diode there exists an optimal value of G for the best overall SNR (Signal to Noise Ratio) that can be obtained.

2.8 Avalanche Multiplication Theory

APD have ionization coefficients for electrons α_e and for holes α_h associated with them. The term α_e and α_h represent the probability that a given carrier will excite an electron-hole pair in unit distance. The ratio $k = \alpha_h / \alpha_e$ is usually in the range of 0.01 to 100 and depends on the material and doping profile of the APD device.

A high voltage, in the neighbourhood of several hundred volts, is applied to the APD device to generate the high electric field necessary to enable the hole-electron carriers to experience ionizing collisions and begin the avalanche effect. The negatively charged electrode of the APD device is referenced by $x = 0$, while the positively charged electrode is referenced by $x = w$. The distance w is the width of the high electric field region. The distance of the hole-electron pair initiating the avalanche is given by $1/\alpha_h$ from the $x = 0$ electrode or by $1/\alpha_e$ from the $x = w$ electrode.

An electron current $i_e(0)$ in the steady state situation crosses the depletion layer of width w at plane $x = 0$. For any point x, where $0 < x < w$, the rate of carrier generation is given by (2.8.1) as described by Gowar [3].

$$\frac{di_e(x)}{dx} = \alpha_e i_e(x) + \alpha_h i_h(x) \tag{2.8.1}$$

The sum of electron and hole current at every point is given by

$$I = i_e(x) + i_h(x) = \text{constant} \tag{2.8.2}$$

where I is the total current flow in the semiconductor. If there is no hole injection at $x = w$ and $i_h(w) = 0$, then $i_e(w) = I$. Equation (2.8.1) can be put in the following standard form.

$$\frac{di_e(x)}{dx} - (\alpha_e - \alpha_h) i_e(x) = \alpha_h I \tag{2.8.3}$$

Solving for this first order differential equation, the electron current is given by

$$i_e(x) = \frac{i_e(0) + \int_0^x \alpha_h I \exp\left[-\int_0^x (\alpha_e - \alpha_h)\, dx' \right] dx}{\exp\left[-\int_0^x (\alpha_e - \alpha_h)\, dx' \right]} \tag{2.8.4}$$

Multiplication factor for injected electrons is defined as the ratio of electrons after the avalanche to electrons before the avalanche.

$$G_e = \frac{I}{i_e(0)} = \frac{i_e(w)}{i_e(0)} \tag{2.8.5}$$

By substituting (2.8.4) into (2.8.5) the result becomes

$$G_e = \frac{1}{\exp\left[-\int_0^w (\alpha_e - \alpha_h)\, dx \right] - \int_0^w \alpha_h \exp\left[-\int_0^x (\alpha_e - \alpha_h)\, dx' \right] dx} \tag{2.8.6}$$

Further simplification results in the following

$$G_e = \frac{1}{1 - \int_0^w \alpha_e \exp\left[-\int_0^x (\alpha_e - \alpha_h)\, dx' \right] dx} \tag{2.8.7}$$

Breakdown of the APD semiconductor material occurs as $G \rightarrow \infty$ and hence

$$\int_0^w \exp\left[-\int_0^x (\alpha_e - \alpha_h)\, dx' \right] dx = 1 \tag{2.8.8}$$

If we include carrier generation $G_c(x)$ and hole injection $i_h(w)$ when

$\alpha_e = \alpha_h$ then total current flow is

$$I = \frac{i_e(0) + i_h(w) + \int_0^w e G_c(x)\,dx}{1 - \int_0^w \alpha_e\,dx} \tag{2.8.9}$$

The current I becomes critically dependent on electric field strength when $k = 1$ and when $G > 10$. When it assumed that avalanche occurs in the region of uniform electric field, then α_e and α_h are independent of x hence from Gowar [3]

$$G_e = \frac{(1-k)}{\exp(-(1-k)\alpha_e w) - k} \tag{2.8.10}$$

As $k \rightarrow 1$ then $G_e \rightarrow \dfrac{1}{1 - \alpha_e w}$

Two factors limit the increase of the multiplication ejection factor G_e from continuing indefinitely. The first factor is the series resistance R_s of the bulk semiconductor between the junction and diode terminals. Secondly, the rise in temperature from the increased dissipation as the total current rises has an effect. This reduces the values of α_e and α_h and raises the junction breakdown voltage thus limiting current I. It also increases the rate of thermal generation of carriers and hence dark current. Multiplication factor G_e expressed in terms of applied terminal voltage is (2.8.11) from Gowar [3].

$$G_e = \frac{1}{[1 - (V_{APD} - IR')/V_B]^n} \tag{2.8.11}$$

where $R' = R_s + R_{th}$ is the sum of the series resistance and effective thermal resistance. V_B is the breakdown voltage of the semiconductor. The index n is a function of design details and diode material.

2.9 APD Bandwidth

The bandwidth of an APD is determined by three parameters overall.

(a) electron transit time across the drift region, $(t_{tr})_e = w_2/v_{se}$,

(b) time required for the avalanche to develop, t_A, where t_A is function of k.

(c) the transit time of the last holes produced in the avalanche back across the drift region, $(t_{tr})_h = w_2/v_{sh}$.

where w_2 is the distance of the drift region and where v_{se} and v_{sh} are the electron and hole carriers drift velocities, respectively.

When $k = 0$ an avalanche develops within the normal electrons transit time across w_A/v_{se}. Assuming $w_A \ll w_2$ and $k > 0$ for a large G and where $0 < k < 1$. The term w_A is the width of the avalanche region.

$$t_A \approx Gkw_A/v_{se} \tag{2.9.1}$$

the overall response time is given τ_{APD}.

$$\tau_{APD} = \frac{(w_2 + Gkw_A)}{v_{se}} + \frac{(w_2 + w_A)}{v_{sh}} \tag{2.9.2}$$

The - 3 dB bandwidth for typical APDs has been approximated by Gower [3] as

$$\Delta f_{(-3dB)} \approx \frac{0.44}{\tau_{APD}} \tag{2.9.3}$$

2.10 APD Detector Noise

The noise factor F and its variation with multiplication factor G is of great importance when optimizing the optical fiber receiver. The relationship between these two parameters is given by (2.10.1.) .

$$F \approx G^x \tag{2.10.1}$$

The index x varies from 0.2 to 1.0 and is dependent on the APD material and the carrier type initiating avalanche. According to Mc Intyre [3] when electrons initiate the avalanche the noise factor is given by (2.10.2) .

$$F_e = G_e \left[1 - (1-k)\frac{(G_e - 1)^2}{G_e^2} \right] \tag{2.10.2}$$

and when the holes initiate the avalanche the noise factor becomes (2.10.3) .

$$F_h = G_h \left[1 + \frac{(1-k)}{k}\frac{(G_h^2 - 1)^2}{G_h^2} \right] \tag{2.10.3}$$

To evaluate noise generation we consider the multiplication factor $G(x)$

$$G(x) = 1 + \int_0^x \alpha_h G(x')dx' + \int_x^w \alpha_e G(x')dx' \tag{2.10.4}$$

The first term represents the initial electron generated in the photo-electric conversion process. The second term describes the multiplication of holes at x as they travel back to $x = 0$. Whereas the third term describes the electrons as they travel from point x to point w. Differentiation of (2.10.4) yields

$$\frac{dG(x)}{dx} = -(\alpha_e - \alpha_h)G(x) \tag{2.10.5}$$

Solving for this first order differential equation

$$G(x) = G(0) \exp\left[-\int_0^x (\alpha_e - \alpha_h) dx' \right] \tag{2.10.6}$$

from equation (2.8.5) $G(0) = G_e$

For $x = w$

$$G(w) = 1 + \frac{k}{1-k} \int_0^w (\alpha_e - \alpha_h) G(x) dx \tag{2.10.7}$$

where $k = \alpha_h / \alpha_e = constant$

$$G(w) = 1 - k(G(0) - 1) \tag{2.10.8}$$

$$2\int_0^w \alpha_h G^2(x) dx = \frac{k}{1-k} \left[G^2(0) - G^2(w) \right] \tag{2.10.9}$$

Therefore avalanche noise is based on two phenomena.

(a) That carrier pairs generated at x will be multiplied by $G(x)$.

(b) That carrier pairs generated at x are created in independent random processes, and thus carry full shot noise.

Mean square shot noise per unit bandwidth associated with a randomly generated is $2e\bar{I}$. Thus mean square noise spectral density is

$$(I_{sh}^2) = 2e\bar{I} \tag{2.10.10}$$

The current of electrons generated in element dx at x is

$$di_e(x) = \alpha_e i_e(x) + \alpha_h i_h(x) dx \tag{2.10.11}$$

Of course an equal current of holes exists, but it was chosen arbitrarily to work

in terms of electron current. Total mean square noise spectral density $(I_m^*)^2$ in the avalanche region is given by

$$(I_m^*)^2 = 2e\int_0^w G^2(x)di_e(x)dx \tag{2.10.12}$$

Recall total current $I = i_e(x) + i_h(x) = G(0)i_e(0) = i_e(w)$ and since $i_h(w) = 0$ then

$$(\alpha_e - \alpha_h)i_e(x) = \frac{di_e(x)}{dx} - \alpha_h I \tag{2.10.13}$$

Thus mean square noise spectral density is

$$(I_m^*)^2 = 2eI\left[G(0) + \frac{k}{(1-k)}G^2(0) - \frac{G^2(w)}{(1-k)}\right] \tag{2.10.14}$$

The mean square noise generated in the multiplication process $(I_m^*)^2$ must be added to the multiplied mean square noise fed in on the initial electron current. Using equation (2.10.10) and the fact $I = i_e(x)+i_h(x) = G(0)i_e(0)$ results in

$$G^2(0)(I_{sh}^*)^2 = G^2(0)2ei_e(0) = 2eIG(0) \tag{2.10.15}$$

The noise factor $F=F_e$ is defined as the ratio of the total noise to this multiplied shot noise such that

$$F_e = 1 + \frac{(I_m^*)^2}{2eIG(0)} \tag{2.10.16}$$

Thus

$$F_e = 1 + 1 + \frac{[kG^2(0) - G^2(w)]}{(1-k)G(0)} \tag{2.10.17}$$

Using equation (2.10.8)

$$kG^2(0) - G^2(w) = k(1-k)G^2(0) - 2k(1-k)G(0) - (1-k)^2 \qquad (2.10.18)$$

By substituting G_e for $G(0)$

$$F_e = G_e\left[1 - (1-k)\frac{(G_e - 1)^2}{G_e^2}\right] \qquad (2.10.19)$$

when G is large the following approximation can be made

$$F_e \approx kG_e \qquad (2.10.20)$$

which stresses the importance of obtaining k as small as possible.

2.11 Receiver Noise

After the APD detector an amplifier is required to boost and convert the low level current, usually in the nanoamperes, to voltage suitable to drive the decision logic. An attenuation loss is incurred in the fiber optic cable due to two phenomena. First, absorptive losses occur due to impurities in the fiber. Secondly, scattering losses occur due to refraction in the fiber. As in all communication receivers where the signal is the weakest (i.e. at the first amplifier stage), is where the most pronounced affect on the total S/N ratio will occur. Hence, it is very important to optimize this stage for maximum S/N ratio. As seen previously the average unmultiplied photodiode current is $2e\bar{I}\Delta f$ where $\Delta f = B/2$ is the bandwidth of the system. As with other noise sources the mean square fluctuation increases in direct proportion with the bandwidth. Hence, the mean square spectral density of the multiplied APD shot noise is

$$(I_{sh}^{*})^2 = 2e\bar{I} \tag{2.11.1}$$

In addition thermal or Johnson noise is present to the random thermal motions of the charge carriers in the resistive elements of the system such as the APD load resistor and resistors present in the first amplifier stage. The mean square spectral densities for thermally induced noise voltage and noise current are

$$(V_{th}^{*})^2 = 4K_B BT^{o} R \tag{2.11.2}$$

$$(I_{th}^{*})^2 = 4K_B BT^{o}/R \tag{2.11.3}$$

respectively. where K_B is Boltzmann's constant, T^{o} is the component temperature in degrees Kelvin and where B is the receiver bandwidth in hertz (i.e. B = 1/T where T is data bit period).

The stages following the first amplifier produce only marginal noise in compared to that of the first stage. Hence, it is at the first stage where the most emphasis is placed. Furthermore, a third source of noise comes the amplifier stage itself. The multiplied detector current is given by Gowar [3] .

$$GI(f) = GR_{APD}\,\Phi_R(f) = G\,\eta\frac{e}{h\upsilon}\Phi_R(f) \qquad (2.11.4)$$

where Φ_R is the Fourier transform of the modulated received power at the photosensor. The variables η , e , h , and υ are quantum efficiency, electronic charge, Planck's constant and frequency of light, respectively. Quantum efficiency is the ratio of the number of liberated electrons to the number of incident photons. Hence the maximum possible value of η is one.

Amplifier output voltage is given by (2.11.5) .

$$V_S = S_o\,GR_{APD}\,I \qquad (2.11.5)$$

where S_o is the amplifier transfer function, R_{APD} is the APD load resistor, and I is the APD current.

In summary, the three noise sources present are:

(a) $(I_{sh}^*) = (2eIG^2F)^{1/2}$ is the multiplied shot noise originating in the APD.

(b) $(I_{th}^*) = \left\{\frac{4K_B\,T^o\,B}{R_{APD}}\right\}^{1/2}$ is the thermal noise arising from the amplifier's resistive elements.

(c) $(I_A^*) =$ equivalent noise current source of the amplifier.

$(V_A^*) =$ equivalent noise voltage source of the amplifier.

The sum of the noise current sources becomes (2.11.6).

$$(I_T^*)^2 = (I_{sh}^*)^2 + (I_{th}^*)^2 + (I_A^*)^2 \qquad (2.11.6)$$

which can also be expressed as

$$(I_T^*)^2 = (2eIG^2F) + (4K_B T^\circ B/R) + (I_A^*)^2 \qquad (2.11.7)$$

Hence the equivalent circuit is shown in figure 7 (A) and the reduced equivalent is shown in figure 7 (B).

The output noise voltage is obtained by integrating the noise sources over the range of the receiver bandwidth Δf .

$$V_N^2 = \int_{\Delta f} |S(f)|^2 (V_A^*)^2 df + \int_{\Delta f} \frac{|S(f)|^2 R^2 (I_T^*)^2 df}{|1 + j2\pi f CR|^2} df \qquad (2.11.8)$$

Substituting $S_o(1+j2\pi f CR)$ for $S(f)$ so that the overall transfer function is frequency independent and therefore allievating the problem of high frequency band limiting

$$V_N^2 = S_o^2 \int_0^{\Delta f} [(1 + 4\pi^2 f^2 C^2 R^2)(V_A^*)^2 + R^2 (I_T^*)^2] df \qquad (2.11.9)$$

The terms V_A^* and I_T^* are now independent of Δf therefore integration yields (2.11.10) .

$$V_N = S_o \left[1 + \frac{4}{3}\pi^2 (\Delta f)^2 C^2 R^2 (V_A^*)^2 + R^2 (I_T^*)^2\right]^{1/2} (\Delta f)^{1/2} \qquad (2.11.10)$$

The rms signal signal to noise ratio K is (2.11.11).

$$K = \frac{V_S}{V_N} = \frac{GIR}{V_N} \qquad (2.11.11)$$

In more detail

$$K = \frac{1}{\left\{\frac{(V_A^*)^2}{G^2}\left[\frac{1}{R^2} + \frac{4\pi^2}{3}(\Delta f)^2 C^2\right] + 2eIF + \frac{4kT}{G^2 R} + \frac{(I_A^*)}{G^2}\right\}^{1/2} \Delta^{1/2}} \qquad (2.11.12)$$

2.12 Probability of Error for an OOK system

An optical signal at the photodiode surface generates carrier pairs in random independent events whose probability of occurence in an incremental interval is proportional to the duration of the interval. This is known as a Poisson process. Given an average optical energy ξ_R arriving in a given period it would be expected to produce N carrier pairs.

$$N = \eta \frac{\xi_R}{\xi_{ph}} = \eta \frac{\xi_R}{h\upsilon} \tag{2.12.1}$$

where ξ_{ph} = photon energy

Because of the statistical nature of the interaction the actual number of carrier pairs varies about a mean value. The probability that the number of carriers produced is k is given by the Poisson probability distribution where shot noise is dominant. The term k is a discrete random value.

$$p_P(k;N) = \frac{\exp(-N)\cdot N^k}{k!} \tag{2.12.2}$$

In the situation where shot noise is negligible and thermal noise is dominant the carriers take on a Gaussian distribution about a mean of N carriers. The filtered signal noise voltage V_S and rms noise voltage V_N are sent to the decision logic during a given bit period. The signal voltage corresponds to the number N of carriers generated by the optical signal during the bit period. The noise voltage corresponds to an effective fluctuation about N whose rms value is taken to be σ_N. For Gaussian noise the probability that the total output voltage in a bit period is $V_S + V_N$ and corresponds to k carrier pairs generated in the photodiode.

$$p_G(k;N,\sigma_N) = \frac{1}{\sqrt{2\pi}\sigma_N}\exp\left[-\frac{(N-k)^2}{2\sigma_N^2}\right] \tag{2.12.3}$$

for the case where N average carriers for "1" are sent and zero carriers for "0" are sent. Choosing the threshold voltage $V_S/2$ for $N/2$ carrier pairs. The signal to noise is given by

$$K = \frac{V_S}{V_N} = \frac{N}{\sigma_N} \tag{2.12.4}$$

The total expression for probability of error for an OOK (On Off Keying) system where due to receiver imperfections and background illumination thermal noise is dominant is given by

$$P_e = \frac{1}{2}\left\{P_G(0/1) + P_G(1/0)\right\} \tag{2.12.5}$$

where the probability of "0" or "1" being transmitted is equal and substituting the Gaussian distribution results in

$$P_e = \frac{1}{2}\frac{1}{\sqrt{2\pi}\sigma_N}\left[\int_0^{N/2}\exp\left[-\frac{(N-k)^2}{2\sigma_N^2}\right]dk + \int_{N/2}^{\infty}\exp\left[-\frac{k^2}{2\sigma_N^2}\right]dk\right] \tag{2.12.6}$$

Since the two integrals are equal, by symmetry

$$P_e = \frac{1}{\sqrt{2\pi}\sigma_N}\int_{N/2}^{\infty}\exp\left[-\frac{k^2}{2\sigma_N^2}\right]dk \tag{2.12.7}$$

In a more familiar form the probability of error becomes

$$P_e = \mathrm{Erfc}\left(N/2\sigma_N\right) \tag{2.12.8}$$

or the probability of error can be expressed as

$$P_e = \text{Erfc}\left(K/2\right) \tag{2.12.9}$$

If shot and thermal noise have the same order of magnitude, an expression for the input to the decision circuit must first be obtained, in order to obtain the probability density function. The signal value seen after T seconds of integration is given by Sorenson [9] as

$$v = \frac{ekR}{T} + n_{th} \tag{2.12.10}$$

where e = electronic charge, k = number of electrons through resistor R in time T, and n_{th} = integrated thermal noise.

An expression for probability density of the receiver output voltage v follows from (2.12.10) by first conditioning on the number of photodetected counts k, then averaging over the avalanche statistics. Since n_{th} is Gaussian, the conditioned variable v is also Gaussian with mean μ and variance σ^2. Thus the receiver thermal noise converts the discrete counting variable k into the continuous observation variable v . The probability density of the detected receiver voltage v is given by

$$p_T(v) = \sum_{k=0}^{\infty} p_P(k/N)p_G(v,\mu,\sigma^2) \tag{2.12.11}$$

where N = average electron count, $\mu = 2eRk/T$, and $\sigma^2 = 4BT^0R/T$. The terms R, B, and T^0 represent APD load resistor, Boltzmann's constant, and receiver temperature in degrees Kelvin, respectively.

This particular situation of the combined effect of Poisson and Gaussian noise components will be examined in further detail in the next chapter.

CHAPTER THREE

COMBINATIONAL PPAM AND POSSIBLE RECEIVERS

3.1 Introduction

In this chapter a new modulation scheme is introduced. The proposed scheme consists of three dimensions. First, each symbol bit has a reverse "L" shape. The first half of the pulse is referenced as α_i and the second half of the pulse is referenced as β_i. Secondly, this reverse "L" shaped pulse is multi-leveled (i.e. PAM). Lastly, the reverse "L" shaped pulse is multi-slotted (i.e. PPM). This modulation scheme shall be refered to as combinational PPAM, henceforth. The combinational PPAM pulse shape and frame structure is shown in figure 8. In the combinational PPAM scheme the virtues of conventional PAM and PPM modulation techniques are exploited. The ability of PAM to carry more information than OOK in the same bandwidth is the first desired characteristic utilitised. Secondly, the immunity of PPM to ISI is the next feature that is highly desired. Modern optical fiber systems experience very little ISI, but systems that use open air as the propagation medium experience serious ISI due to scattering caused by moisture and oxygen atoms. It is for this reason that the effects of ISI are not neglected. The combination of these two conventional modulation schemes is used to produce a hybrid modulation scheme that is supposedly superior than either one of the basic schemes alone.

The analysis begins by considering the possible receivers. Following the optical detector there are $M-1$ integrator banks. The first integrator bank integrates from 0 to T, the second bank from T to 2T, and, the last integrator from $M-2$ to $M-1$. The $(M-1)$ to M region is used as a guard band area, hence no integrator bank is used here. The combinational pulse can appear in any slot of the frame

with equal probability. The result of all the integrators will be dumped into corresponding banks of threshold comparators. Two types of receivers are possible at this point: the conventional receiver and the ratio receiver. The conventional receiver integrates both α_i and β_i as one non-composite pulse and renders one of L possible decisions on the total power present in the sum of α_i and β_i. The ratio receiver integrates the first half of the slot T and the second half of the slot T separately and presents them to a bank of L ratio comparators. After the ratio of power in β_i to power in α_i has been calculated, one of L possible decisions are rendered

In section 3.2 the sub-optimal case is examined where the components α_i and β_i are integrated together a decision is based on the total power present in both components. In section 3.3 the combinational PPAM scheme is examined when the ratio receiver is used. The decision is now based on the ratio of the power in β_i to the power in α_i. In section 3.4 the performance of conventional PAM and PPM is compared to combinational PPAM.

3.2 The conventional combinational PPAM detector

In this section the performance of the combinational PPAM scheme is observed in a sub-optimal situation. The entire pulse shape is simply integrated and dumped to the comparator bank. The sub-optimal situation is used as reference, when the performance of the combinational scheme is observed with the ratio receiver which takes into account the reverse "L" shape of the pulse, in the next chapter. The sub-optimal receiver is shown in figure 9.

At the transmitter end of the fiber optic system the message source generates data in the following form

$$X(t) = \sum_{n=-\infty}^{+\infty} a_n \delta(t - nT) \tag{3.2.1}$$

where a_n is the multi-level data source where $a_n \epsilon (0,1,2, \cdots L)$. The term a_n assumes a non-zero value for 1 out of M slots and a zero value for the remaining $M-1$ out of M slots. There M slots per combinational PPAM frame, each T seconds in width.

This message source in turn modulates the transmitter optical source, which in this case is a laser. The laser current is then given by

$$X_C(t) = \sum_{n=-\infty}^{+\infty} r_n \tag{3.2.2}$$

where r_n is specified by

$$r_n = \begin{cases} \alpha_n & 0 \leq t \leq T_n/2 \\ \beta_n & T_n/2 \leq t \leq T_n \\ 0 & \textit{elsewhere} \end{cases} \tag{3.2.3}$$

where T_n is the slot period contained within the M by T frame.

After the electro-photo conversion the optical output of the laser is given by

$$X_L(t) = \sum_{n=-\infty}^{+\infty} r_n \, h_L(t - nT) \tag{3.2.4}$$

where $h_L(t)$ is the laser impulse response. Then the optical pulse after passing through the optical medium (i.e. in the optical fiber) the pulse is given by

$$p(t) = \sum_{n=-\infty}^{+\infty} r_n \, h_p(t - nT) \tag{3.2.5}$$

where $h_p(t) = h_l(t) * h_f(t)$ and where $h_f(t)$ is the impulse response of the optical fiber.

The photo-detector (i.e. the APD) converts the optical signal into its electrical replica. The output current of the detector can be described as a filtered randomly multiplied Poisson process. This output current is given by Hauk [5] as

$$X_S(t) = \sum_{n=1}^{k(t)} g_n \, e r_n \, h_s(t - nT - t_n) \tag{3.2.6}$$

where e is electonic charge.

Random processes have now been introduced into the received signal by the APD photodetector. An optical pulse $p(t)$ arrives every nT seconds and after time t_n, k(t) number of primary electrons are generated for this pulse. These primary electrons are then multiplied by a random gain (i.e. APD gain) g_n with an expected value of $<G>$. The terms $k(t), g_n$, and t_n are statistically independent random variables. The term h_s represents the impulse response of all the system elements between and including the laser and the photo-detector. Furthermore, the following shall hold true

$$\int_{-\infty}^{+\infty} h_s(t)dt = 1 \tag{3.2.7}$$

The probability that $k(t)$ electrons are emitted is given by the Poisson process given by Hauk [5] below

$$P[\, k(t) = N/\lambda(\tau),\ 0 \leq \tau \leq t\ ] = \frac{1}{N!}\left[\int_0^t \lambda(\tau)d\tau\right]^N \exp\left[-\int_0^t \lambda(\tau)d\tau\right] \tag{3.2.8}$$

The mean instantaneous rate of primary electrons produced by the received optical power $p(t)$ and thermal effects is

$$\lambda(t) = \frac{\eta}{h\upsilon} p(t) + \lambda_o \tag{3.2.9}$$

or

$$\lambda(t) = \frac{\eta}{h\upsilon} \sum_n r_n\, h_p(t - nT) + \lambda_o \tag{3.2.10}$$

where $\lambda \geq 0$ and η , $h\upsilon$ are quantum efficiency, and photon energy, respectively. The term λ_o corresponds the dark current and background illumination. Dark current is a residual current present even in the absence of optical signal input to the APD and is due to thermally generated carriers in the semiconductor material.

The input to the decision circuit is given by the following expression

$$Y(t) = [X_S(t) + X_{th}(t)] * h_R(t) \tag{3.2.11}$$

An ideal "brickwall" low pass filter $h_R(f)$ follows the APD photodetector. The filter is given by the following, in the frequency domain.

$$h_R(f) = \begin{cases} 1 & f_o > f \\ 0 & f_o < f \end{cases} \tag{3.2.12}$$

where f_o is the 3 dB corner frequency given by Nyquist as $\frac{1}{2T}$.

The inverse Fourier transform of (3.2.12) results in the following filter characteristic in the time domain

$$h_R(t) = 2f_o\, Sa\left(2\pi f_o\, t\right) \tag{3.2.13}$$

The input to the decision circuit is the sum of an inseparable component consisting of the received signal and shot noise $Y_S(t)$ and thermal noise $Y_{th}(t)$ after filtering.

$$Y(t) = Y_S(t) + Y_{th}(t) \tag{3.2.14}$$

where periodic sampling occurs at $t = nT$.

The expected signal m_S of the output of the photo-detector can be expressed by using Campbell's theorem, from Papoulis [6], by obtaining the first moment of a Poisson process as follows

$$m_S = E[Y_S(t)] = E[g_n] \int_{-\infty}^{+\infty} \lambda(\tau) e h(t-\tau) d\tau \tag{3.2.15}$$

where $h(t)$ is the impulse response of the entire fiber optic system, i.e. between the input to the transmitter and the input to the decision circuit.

The term $m_S(i)$ is the expected value of the pulse shape composed of α_i and β_i

$$m_S(i) = \frac{\eta}{h\upsilon}(eRA) < G > \int_{nT}^{(n+1)T} p(\tau) h(t-\tau) d\tau \tag{3.2.16}$$

where $< G > = E[g_n]$ is the expected APD gain and where $i \epsilon (1,2,3,\ldots,L)$

$$m_S(i) = \frac{\eta}{h\upsilon}(eRA)<G>\frac{(\alpha_i^2 T + \beta_i^2 T)}{2} \tag{3.2.17}$$

The variance of $Y_S(t)$ is found using Campbell's Theorem to obtain the second moment of a Poisson process

$$\sigma_S^2 = <G^2> \int_{-\infty}^{+\infty} \lambda(\tau) e h^2(t-\tau) d\tau \tag{3.2.18}$$

From Davidson [7] the second moment $<G^2>$ is obtained by taking the product of the excessive noise factor F_e in equation (2.10.19) and the square of the first moment (i.e. $<G^2> = F_e <G>^2$)

$$<G^2> = -(1-k)<G> + 2(1-k)<G>^2 + k<G>^3 \tag{3.2.19}$$

The variance $\sigma_S(i)$ for the transmitted pulse composed of α_i and β_i is given by

$$\sigma_S^2(i) = \frac{\eta}{h\upsilon}(eRA)^2<G^2> \int_{nT}^{(n+1)T} p(\tau) h^2(t-\tau) d\tau \tag{3.2.20}$$

where $i \in (1,2,3,\ldots,L)$

$$\sigma_S^2(i) = \frac{\eta}{h\upsilon}(eRA)^2<G^2>\frac{(\alpha_i^2 T + \beta_i^2 T)}{2} \tag{3.2.21}$$

The mean of the AWGN (Additive White Gaussian Noise) present at comparator i is quite simply

$$m_{th}(i) = E[Y_{th}] = 0 \tag{3.2.22}$$

The variance of the thermal noise is a function of the receiver filter characteristic. To obtain the variance of the thermal noise the following expression is used

$$\sigma_{th}^2 = E[Y_{th}^2(t)] = \frac{N_o}{2} \int_{-\infty}^{+\infty} \left| h_R(f) \right|^2 df \tag{3.2.23}$$

The variance of the AWGN present at comparator i is given by

$$\sigma_{th}^2(i) = \frac{N_o}{2T} \tag{3.2.24}$$

Two types of density functions are currently present: Poisson for the inseparable component consisting of the signal and the shot noise and Gaussian for the thermal noise component. Normally attempting to derive an equation for the probability of error that includes these two different density functions would be quite a laborious task indeed. Integration of the product of these two different probability density functions would require a great deal of computer time. Several options exists to minimize the intregration presented in equation (2.12.10).

One technique by Hubbard [8] approximates the Poisson distribution by a Gaussian distribution. The resulting Gaussian distribution can be easily evaluated using readily available Erf(x) tables and so the calculation of probability of error is greatly simplified. The Gaussian approximation for the Poisson density function of signal n and mean m is given by

$$p_P(n,m) = \left(\frac{1}{\sqrt{2\pi m}}\right)^{\frac{1}{1+a}} \exp\left(-\frac{2bm + (n-m)^2}{2m(1+a)}\right) \tag{3.2.25}$$

where $a = [0.0800u^2 - 0.230u + 1.26]^{-2}$, $b = [0.0667u^2 - 0.3933u + 0.810]^{-1}$ and $u = \ln(m)$.

The density function of the receiver, taking shot noise, and thermal noise, and assuming independence among the distributions becomes

$$p_R(x, m_{tot}, \sigma_{tot}) = \text{Erfc}\left(\frac{x - m_{tot}}{\sigma_{tot}}\right) \tag{3.2.26}$$

where $m_{tot} = m_S + m_{th}$, $\sigma_{tot} = \sqrt{\sigma_S^2 + \sigma_{th}^2}$. Through the use of Hubbard's approximation two probability functions have been reduced into one. The means and variances are simply added and plugged into the well known Erfc(x) function.

Since calculating the required values for the Erfc(x) is also a time consuming process on the computer, an approximation for the Erfc(x) by Hasting is used. This expression is shown below.

$$\text{Erfc(x)} = \phi(C_1 t + C_2 t^2 + C_3 t^3 + C_4 t^4 + C_5 t^5) \qquad (3.2.27)$$

where $t = \frac{1}{1 + Px}$ and $\phi = \frac{1}{\sqrt{2\pi}} \exp\left(-\frac{x^2}{2}\right)$

The constant terms are given by P=0.2316419, C_1=0.31938153, C_2=–0.356563782, C_3=1.78147937, C_4=–1.821255978, and C_5=1.330274429.

An even simpler method is available with a minimal affect on accuracy. According to Midwinter [4] when Gaussian noise is dominant the Poisson component can be approximated by a Gaussian distribution without resorting to Hubbard's technique. This is possible because when the m term is sufficiently large the Poisson distribution approaches the Gaussian distribution. This approximation turns out to be excellent for most modern fiber optics systems. Hence, the Poisson and Gaussian means and variances can be summed and placed directly into one Gaussian distribution. Only in the rare case where thermal variance σ_{th} is small would it be necessary to evaluate the error rate using the more comprehensive method previously described.

It is desired to choose an optimal value for the avalanche gain such that the error rate will be minimal. Hence the optimal value is determined by taking the partial derivative of the sum of the noise variances with respect to the avalanche

gain and equating to zero in equation (3.2.28).

$$\frac{\delta(\sigma_{th}^2 + \sigma_{sh}^2)}{\delta G} = 0 \tag{3.2.28}$$

In figure 11 the probability of error was plotted against the APD gain G for a typical OOK APD based receiver. It should noted that the optimal gain is not fixed but rather changes with optical input power as is illustrated by the family of curves shown in figure 11. For an APD gain less than 20 to 30 thermal noise dominates and for an APD gain greater than 20 to 30 shot noise dominates. Large values of APD gain degrades receiver performance because signal current is multiplied by G, while shot noise is multiplied $GF^{1/2}$ as was shown in the previous chapter. Recall noise factor F is always greater than unity and is an increasing function of G.

A practical fiber optic receiver is designed such that the avalanche diode is biased close to the value of the smallest signal level expected .

Where shot and thermal noise have the same order of magnitude the criterion for minimizing the probability of error is to maximize the S/N ratio shown below. The S/N is the ratio of the desired signal over the sum of shot and thermal noise as given by Midwinter [4].

$$S/N = \frac{P_S}{P_{sh} + P_{th}} = \frac{\left[\frac{\eta e < G > P_{op}}{hf}\right]^2 R}{\frac{2\eta e R B < G^2 > P_{op}}{hf} + 4K_B T^o B} \tag{3.2.29}$$

where P_{op} is the optical power incident to the APD and B is the receiver bandwidth.

The receiver structure for the PPAM detector consists of $M-1$ comparator

banks, one for each of the PPM slots and slot M has no comparator bank since it is used as a guard band. The front end of the receiver is simillar to that of other fiber optic systems. Each bank is sampled at a different instants nT corresponding to each of PPM slots. Then at each bank there are L comparators to detect the L possible levels of the PAM component of the received signal. The output of the each of the window comparators registers a true or "1" when the applied input has an amplitude between A_i and A_{i+1}. Then a parallel-to-serial converter forms a decision on all of the comparator outputs and renders a decision. This integrate-and-dump receiver structure is shown in figure 9.

Several scenerios are possible for the comparator banks. The first situation is where one of L transmitted symbol is arrives in a given slot. At this bank the transmitted signal S_i plus shot noise and thermal noise are all present. The probability of correct decision, given that pulse shape S_i was sent and received at this slot is given by $\Omega_S(i)$.

$$\Omega_S(i) = \int_{A_i}^{A_{i+1}} \sum_{n=0}^{+\infty} p_P(k/N)\, p_G(v, m_{th}, \sigma_{th}^2)\, dv \qquad (3.2.30)$$

where $A_i <$ total energy of S sub 1 $< A_{i+1}$. The thresholds A_i and A_{i+1} are specified by $A_i = m_{S_1}(i-1/2)$ and $A_{i+1} = m_{S_1}(i+1/2)$. The terms k, N, v, m, and, σ are defined in section 2.12. This expression can be simplified by using techniques previously described by Midwinter as follows.

$$\Omega_S(i) = \mathrm{Erfc}\left[\frac{m_S(i) - A_i}{\sqrt{\sigma_{th}^2(i) + \sigma_S^2(i)}}\right] - \left[\mathrm{Erfc}\frac{A_{i+1} - m_S(i)}{\sqrt{\sigma_{th}^2(i) + \sigma_S^2(i)}}\right] \qquad (3.2.31)$$

Up to this point only shot noise and thermal noise have been considered. A third source of error is also present. Power from neighbouring symbols also has a

detrimental on the desired signal. Although ISI is not a significant problem in fiber optic systems, it is included in the analysis for the case where another medium (i.e. open atmosphere) is used. The desired symbol can easily be corrupted by its nearest and even second and third nearest neighbours if the power levels of the neighbouring are comparable or greater than that of the desired signal. This ISI (Inter-Symbol Interference) component contains both a randomly varying element (a signal dependent on noise associated with the photon statistics) and a non-random component relating to the appropriate neighbouring symbol. In this analysis is assumed that ISI is significant only in the slot following that of the intended slot.

When the effect of ISI is considered on its closest neighbour, the respective mean becomes

$$m_I = E[Y_{ISI}(t)] = E[g_n] \int_{-\infty}^{+\infty} \lambda_I(\tau) eh(t-\tau) d\tau \qquad (3.2.32)$$

where $\lambda_I(\tau)$ is the mean instaneous rate of primary electrons produced by the ISI component.

Convolution of the receiver filter characteristic $h_R(f)$ and the exponentially decaying ISI component $\beta e^{-\gamma t}$ can be approximated by $1 - \exp(-\gamma T)$. Therefore

$$m_I(i) = <G> \frac{\eta}{h\upsilon}(eRA)\left(\frac{\beta_i}{\gamma}\right)[1 - \exp(-\gamma T)] \qquad (3.2.33)$$

And the corresponding variance is given by

$$\sigma_I^2 = <G^2> \int_{-\infty}^{+\infty} \lambda_I(\tau) eh^2(t-\tau) d\tau \qquad (3.2.34)$$

This yields

$$\sigma_I^2(i) = \langle G^2 \rangle \frac{\eta}{h\upsilon}(eRA)^2 \left[\frac{\beta_i}{\gamma} \right] [1 - \exp(-\gamma T)] \qquad (3.2.35)$$

Where the term γ is the decay factor of the interfering signal is dependent on the intensity of the ISI.

The second possible sceneraio possible occurs at the receiver bank directly following the slot where the transmitted symbol is present. In this case ISI plus shot and thermal noise are present at this slot. $\Omega_I(i)$ is probability that the ISI from pulse S_i in the previous slot, is falsely detected as the desired signal in this slot. $\Omega_I(i)$ consists of a Poisson component for the ISI and Gaussian component for the thermal noise.

$$\Omega_I(i) = \int_{A_i}^{A_{i+1}} \sum_{n=0}^{+\infty} p_P(n, m) p_G(v, \mu_{th}, \sigma_{th}) dv \qquad (3.2.36)$$

Using Midwinter's approximation the previous expression becomes

$$\Omega_I(i) = \text{Erfc}\left[\frac{m_I(i) - A_i}{\sqrt{\sigma_I^2(i) + \sigma_{th}^2(i)}} \right] - \left[\text{Erfc} \frac{A_{i+1} - m_I(i)}{\sqrt{\sigma_I^2(i) + \sigma_{th}^2(i)}} \right] \qquad (3.2.37)$$

The last possible scenerio is the case in which only thermal noise is present. This occurs in a slot that is not occupied by the received pulse or the ISI component. The corresponding expression for $\Omega_{th}(i)m$ is the probability the thermal noise is falsely detected as the desired pulse. This situation can occur in any slot preceding the slot that contains the transmitted signal or this situation can occur in any slot after the slot that contains the ISI component.

$$\Omega_{th}(i) = \int_{A_i}^{A_{i+1}} p_G(v, \mu_{th}, \sigma_{th}) dv \qquad (3.2.38)$$

Equation (3.2.38) can be simplified by using readily available Error Function

$$\Omega_{th}(i) = \mathrm{Erfc}\left(\frac{-A_i}{\sigma_{th}(i)}\right) - \left(\mathrm{Erfc}\frac{A_{i+1}}{\sigma_{th}(i)}\right) \qquad (3.2.39)$$

For an M slot L level combinational PPAM signal the probability of correct decision is given by a "true" decision for the pulse in its intended slot, a "false" decision for the ISI component of the signal in the following slot, and "false" decision for the thermal noise component in all other remaining slots. The overall expression for a combinational PPAM receiver's probability of error for an M slot and L level system is given by subtracting the probability of correct decision from unity.

$$P_e = \frac{1}{L}\sum_{i=1}^{L}\left[1 - \Omega_S(i)(1 - \Omega_I(i))(1 - \Omega_{th}(i))^{M-2}\right] \qquad (3.2.40)$$

To clarify the significance of equations (3.2.31), (3.2.38), and (3.2.39) a typical case will be examined to illustrate all the possible scenerios. For the case where $M=5$ and $L=4$ the slot that occupies $(n+4/5)T$ to $(n+1)T$ will be used as a guard band and hence no sampling takes place at $t=(n+1)T$. There exists four unique symbols S_1, S_2, S_3, and, S_4 which can occupy any of the first four slots. Each symbol S_i is a composite pulse formed from unique values of α_i and β_i. The component α_i is always smaller than β_i for reasons of minimizing ISI.

Bank 1 will receive a signal from the front end of receiver at sampling instant $t=(n+1/5)T$. Bank 2 will operate at sampling instant $t=(n+2/5)T$, bank 3 at sampling instant $t=(n+3/5)T$ and bank 4 at sampling instant $t=(n+4/5)T$. Each bank has four comparators to detect any one of the four possible symbols. Five possible outcomes are possible from the integrator bank. Symbol S_1, S_2, S_3, or S_4 has been detected. The other possible decision is that none of the four symbols has been detected. The outputs of all the integrator bank's comparators are fed into a parallel-to- serial converter and one of sixteen

possible outcomes is sent out. Hence, combinational PPAM can carry $M-1 \; x \; L$ bits of information. When two or more banks have detected a symbol means an error has occured and hence the system will disregard this data or attempt to correct it.

If a symbol has been transmitted in slot 1, at bank 1 one of possible four symbols plus shot and thermal noise will be present. At bank 2, ISI due to the symbol in slot 1 plus shot and thermal noise will be present. At banks 3, 4, and 5 only dark current and thermal noise is present. It is assumed that the ISI component is only significant in the slot immediately following the slot of transmitted signal.

When a symbol has been sent in slot 2, the output of banks 1, 4, and 5 consists of dark current and thermal noise. At bank 2 one of four possible symbols plus shot and thermal noise is present. Whereas in bank 3 ISI due to the symbol in slot 2 plus shot and thermal noise is present.

The third scenerio is when one of four possible symbols has been sent in slot 3. At banks 1, 2, and 5 only dark current and thermal noise is present. At bank 3 the symbol plus shot and thermal noise is present. At bank 4 ISI due to the symbol in the previous bank plus shot and thermal noise is present.

The last possible scenerio is when one of four possible symbols has been sent in slot 4. At banks 1,2 and 3 dark current and thermal noise is present. At bank 4 the symbol plus shot and thermal noise is present. The ISI of this symbol plus shot and thermal noise component is absorbed into the guard band of the frame (i.e. slot 5).

The effect of ISI from other frames is neglected in this thesis. When ISI leaks within its own frame, error can be easily spotted by virtue of PPM detection. A PPM detector expects a true or "1" decision from only one threshold

bank while expecting a false from all the remaining banks. Two or more true decisions means an error has occured and measures such as disregarding the data frame or error control correction can be employed. Therefore the guard band serves the purpose of minimizing inter-frame ISI and improving the overall error performance of the system.

3.3. The Ratio Detector as a PPAM detector

The structure of the ratio detector is essentially the same as that of the conventional receiver up until the decision threshold. At this point the decision is based on the ratio of β_i to that of α_i instead of just integrating and dumping, the entire pulse shape as one component, as was done previously. A new probability density function must be derived at this point because the receiver decision is based on a new random variable z. The random variable is the ratio of two random variables β and α (i.e. $z=\beta/\alpha$). Such a receiver is shown in figure 11. In this analysis the means and variances are derived separately for each component of the signal, as opposed to the combinational pulse as whole as was done previously. Then these components are plugged into the ratio PDF and probability of error can be found.

As in the previous section Campbell's theorem was used to evaluate the first and second moments of the shot noise dependant components. Hence the means for the individual α and β components become

$$m_{\alpha_s} = E[Y_{\alpha_s}(t)] = <G> \int_{-\infty}^{+\infty} \lambda(\tau) h(t-\tau) d\tau \qquad (3.3.1)$$

$$m_{\alpha_s}(i) = <G>(eRA)\frac{\eta}{h\upsilon}\frac{\alpha_i^2 T}{2} \qquad (3.3.2)$$

$$m_{\beta_S} = E[Y_{\beta_S}(t)] = <G> \int_{-\infty}^{+\infty} \lambda(\tau) h(t-\tau) d\tau \tag{3.3.3}$$

$$m_{\beta_S}(i) = <G>(eRA)\frac{\eta}{h\upsilon}\frac{\beta_i^2 T}{2} \tag{3.3.4}$$

Similarly the variances are found to be

$$\sigma_{\alpha_S}^2 = \; = <G^2> \int_{-\infty}^{+\infty} \lambda(\tau) h^2(t-\tau) d\tau \tag{3.3.5}$$

$$\sigma_{\alpha_S}^2(i) = <G^2>(eRA)^2\frac{\eta}{h\upsilon}\frac{\alpha_i^2 T}{2} \tag{3.3.6}$$

$$\sigma_{\beta_S}^2 = \; = <G^2> \int_{-\infty}^{+\infty} \lambda(\tau) h^2(t-\tau) d\tau \tag{3.3.7}$$

$$\sigma_{\beta_S}^2(i) = <G^2>(eRA)^2\frac{\eta}{h\upsilon}\frac{\beta_i^2 T}{2} \tag{3.3.8}$$

The means of the thermal noise components is simply

$$m_{\alpha_{th}}(i) = 0 \tag{3.3.9}$$

$$m_{\beta_{th}}(i) = 0 \tag{3.3.10}$$

The thermal variances are given by

$$\sigma_{\alpha_{th}}^2(i) = \frac{N_o}{4T} \tag{3.3.11}$$

$$\sigma_{\beta_{th}}^2(i) = \frac{N_o}{4T} \tag{3.3.12}$$

The mean of the ISI components are found in a similar fashion as before thus the convolution of the filter $h_R(t)$ and the ISI component $\beta_i e^{-\gamma t}$ yields

$$m_{\alpha_i}(i) = <G>(eRA)\frac{\eta}{h\upsilon}\frac{\beta_i}{\gamma}[1 - \exp(\gamma T/2)] \tag{3.3.13}$$

$$m_{\beta_i}(i) = <G>(eRA)\frac{\eta}{h\upsilon}\frac{\beta_i}{\gamma}[\exp(\gamma T/2) - \exp(\gamma T)] \tag{3.3.14}$$

The variances of ISI components are found as per section (3.2)

$$\sigma^2_{\alpha_i}(i) = <G^2>(eRA)^2\frac{\eta}{h\upsilon}\frac{\beta_i}{\gamma}[1 - \exp(\gamma T/2)] \tag{3.3.15}$$

$$\sigma^2_{\beta_i}(i) = <G^2>(eRA)^2\frac{\eta}{h\upsilon}\frac{\beta_i}{\gamma}[\exp(\gamma T/2) - \exp(\gamma T)] \tag{3.3.16}$$

The probability density function used for the conventional receiver is no longer valid. A new PDF is derived in APPENDIX A for the ratio receiver. The general form of the function for the ratio z of two random variables x and y is given below. The values β_i and α_i are substituted for x and y, after the derivation.

$$p_R(z) = \frac{1}{2\pi\sigma_x\sigma_y}\exp\left[-\frac{\sigma_x^2 m_y^2+\sigma_x^2 m_x^2}{2\sigma_x^2\sigma_y^2}\right] \tag{3.3.17}$$

$$*\left\{\frac{2\sigma_x^2\sigma_y^2}{\sigma_x^2+\sigma_y^2 z^2} - \frac{\sigma_x^2 m_y+\sigma_y^2 m_x z}{\sigma_x^2+\sigma_y^2 z^2}\exp\left[\frac{(\sigma_x^2 m_y+\sigma_y^2 m_x z)^2}{(2\sigma_x^2\sigma_y^2)(\sigma_x^2+\sigma_y^2 z^2)}\right]\right.$$

$$\left.*\frac{\sqrt{2\pi}\sigma_x\sigma_y}{\sqrt{\sigma_x^2+\sigma_y^2 z^2}}\left[1 - 2\mathrm{Erf}\left[\frac{\sigma_x^2 m_y+\sigma_y^2 m_x z}{\sigma_x\sigma_y\sqrt{\sigma_x^2+\sigma_y^2 z^2}}\right]\right]\right.$$

The probability of correct decision, the transmitted symbol S_i was detected in its intended slot, is given by

$$\Omega_S(i) = \int_{A_i}^{A_{i+1}} p_R(z, m_x, m_y, \sigma_x, \sigma_y)dz \tag{3.3.18}$$

where are given by $A_i = m_{\beta_i}/m_{\alpha_i}(i-1/2)$ and $A_{i+1} = m_{\beta_i}/m_{\alpha_i}(i+1/2)$

and where $m_x = m_{\alpha_S}(i) + m_{\alpha_{th}}(i)$, $m_y = m_{\beta_S}(i) + m_{\beta_{th}}(i)$,

$\sigma_x = \sqrt{\sigma^2_{\alpha_S}(i) + \sigma^2_{\alpha_{th}}(i)}$,and $\sigma_y = \sqrt{\sigma^2_{\beta_S}(i) + \sigma^2_{\beta_{th}}(i)}$.

The probability that the ISI of symbol S_i will cause an error in the slot following symbol S_i is given by

$$\Omega_I(i) = \int_{A_i}^{A_{i+1}} p_R(z, m_x, m_y, \sigma_x, \sigma_y)dz \tag{3.3.19}$$

where $m_x = m_{\alpha_I}(i) + m_{\alpha_{th}}(i)$, $m_y = m_{\beta_I}(i) + m_{\beta^{th}}(i)$,

$\sigma_x = \sqrt{\sigma^2_{\alpha_I}(i) + \sigma^2_{\alpha_{th}}(i)}$, and $\sigma_y = \sqrt{\sigma^2_{\beta_I} + \sigma^2_{\beta_{th}}(i)}$

The probability of error caused by thermal noise in a slot not occupied by a symbol S_i or its corresponding ISI is given by

$$\Omega_{th}(i) = \int_{A_i}^{A_{i+1}} p_R(z, m_{\alpha_{th}}(i), m_{\beta_{th}}(i), \sigma^2_{\alpha_{th}}(i), \sigma^2_{\beta_{th}}(i))dz \tag{3.3.20}$$

The probability of error for the entire system can be calculated from this point onwards as was done in section (3.2.36). Hence, probability of correct decision for the combinational PPAM symbol requires that the one of L unique pulse shapes is correctly detected as "true" in its intended slot. And the ISI component in the slot immediately following the pulse shape is not detected as "true" and the remaining slots containing only thermal noise are not detected as "true".

$$P_e = \frac{1}{L}\sum_{i=1}^{L}\left[1 - \Omega_S(i)(1 - \Omega_I(i))(1 - \Omega_{th}(i))^{M-2}\right] \tag{3.3.21}$$

3.4 Comparison of PPAM with conventional PAM and PPM systems

The probability of symbol error of an L-level PAM optic fiber system is given by Sorensen [9] by the following expression

$$P_{PAM} = 1 - \sum_{i=1}^{L} \left[\frac{1}{L} \int_{A_i}^{A_{i+1}} P_T(x, \mu_i, \sigma_i) dv \right] \tag{3.4.1}$$

where P_T is defined in equation (2.7.10). The above expression simply states that the probability of error for an L-level PAM system is simply unity minus the averaged sum of probabilities for correct decision for each of the L symbols. In figure 12 the probability of error versus average optical power per bit have been plotted for $L = 2,4,8,16,32,64,128$, and 256 levels using Gray coding. A receiver with a data rate of 100 mb/s temperature of $300K^{o}$, an APD load resistor of 50 ohms, a bandwidth of 175 mhz, a detector efficiency of 0.85 , a detector avalanche ionization coefficient of $k = 0.028$, and an optimal avalanche gain of 25 were assumed.

The expression for probability of error for an M slot PPM system, when symmetry is assumed is given by

$$P_{PPM} = 1 - q \sum_{i=0}^{M-1} \frac{\binom{M-1}{i}}{i+1} p^{i} (1-p)^{M-i-1} \tag{3.4.2}$$

where q is the probability that the level of the threshold logic is exceeded where the signal is present and p is the probability that the level of the threshold logic is exceeded where the signal is not present.

Expression (3.4.2) can simplified into the following expression by converting it into the form of the binominal distribution function and assuming $p \ll 1$

$$P_{PPM} = 1 - \frac{q}{pM}(1 - (1 - p)^M) \tag{3.4.3}$$

It evident from the expansion of (3.4.2) that the dominant term is the product Mp . If it assumed $Mp << 1$ then (3.4.2) is greatly simplified as follows

$$P_{PPM} = 1 - q(1 - p)^{M-1} \tag{3.4.4}$$

A simillar expression for the probability of symbol error for an M-position PPM optic fiber system is given by Sorensen as

$$P_{PPM} = 1 - \int_{-\infty}^{+\infty} P_T(x, \mu_1, \sigma_1) \left[\int_{-\infty}^{A_t} P_T(x, \mu_0, \sigma_0) dV' \right]^{M-1} dV \tag{3.4.5}$$

In figure 13 the probability of error versus average optical power per bit count has been plotted for $M = 2,4,8,16,32,64,128$ and 256 positions using Gray coding for a PPM system. The same receiver parameters as the PAM case have been used.

In figure 14 the probability of error versus average optical power per bit for the PPAM case using the conventional detector derived in equation 3.2.36. The same receiver parameters used in the PAM and PPM case have been used.

In figure 15 the probability of error versus average optical power per bit for the PPAM case using the ratio detector derived in equation 3.3.21. The same receiver parameters used in the PAM, PPM, and the conventional PPAM case have been used.

It was found the PPM system had the best performance in terms of bit error rate, however a price is paid in terms of a complicated receiver with stringent timing requirements. While the PAM system had the worsest performance in terms of bit error rate. The PPAM combinational system had a performance in

between that of conventional PAM and PPM systems. The conventional PPAM receiver had better performance than the PPAM ratio receiver in low to medium SNR scenerios, while the ratio receiver had better performance in high SNR scenerios. Overall all systems required more power per bit as the alphabet size was increased.

CHAPTER FOUR

PWM OPTICAL RECEIVER AND EQUALIZER

4.1 The PWM receiver and probability of error

In this chapter the performance of PWM (Pulse Width Modulation) is analysized and the corresponding equalizer is derived. In wide-band fiber optic systems PWM offers many advantages. The same bit error rate as PAM can be achie ed using less power with PWM. However, PWM suffers under conditions of ISI, hence an equalizer derived in the next section is expected to ameliorate the ISI problem.

The PWM signal source generates a PWM optical signal in the fc lowing form

$$X_L(t) = \sum_{i=-\infty}^{+\infty} r_j(t - iT) \tag{4.1.1}$$

where $j \epsilon(1,2,3,...,M-1)$ for an M slotted PWM symbol. Note that a pulse with a minimum width of one slot T/M to the maximum of $M-1$ slots of width T/M present in the PWM frame. The unused slot in position M is used as a guard band. After passing optic fiber with impulse response of $h_f(t)$ the received signal $p(t)$ assumes the following form

$$p(t) = h_{f(t)} X_L(t) \tag{4.1.2}$$

At the front end of the fiber optic PWM receiver an optical signal $p(t)$ arrives at the APD and is converted to a corresponding PAM voltage V_{out} via integration. Then a threshold decision is made on the level of this PAM signal.

$$V_{out} = <G> \left(\frac{\eta}{h\upsilon} \right) (eRA) \int_{nT}^{(n+1)T} p(\tau) h(t-\tau) d\tau \qquad (4.1.3)$$

The PWM receiver consists of an APD diode, amplifier with a gain of A and a filter with an impulse response $h(t)$. The bandwidth of the filter is B and can be given in terms of the pulse risetime as

$$B = \frac{0.7}{t_r} \qquad (4.1.4)$$

According to Xianda [10] it is desired to minimize the effect of the noise voltage n_t on the timing error $\Delta\tau$ so that the probability of error is minimized.

So therefore the threshold level A_{th} is chosen at the point of maximum slope as shown in figure 16.

$$\left| \frac{dV_{out}(t)}{dt} \right|_{\max} = \frac{n_t}{\Delta\tau} = \frac{V_{\max}}{t_r} \qquad (4.1.5)$$

At the sampling instant T the normalized random voltage is given by

$$X = \frac{n_t}{\sigma_T} \qquad (4.1.6)$$

The variance σ_T is a function of both thermal and shot noise, hence

$$\sigma_T = \sqrt{\sigma_{th}^2 + \sigma_{sh}^2} \qquad (4.1.7)$$

The variance of the signal and shot noise component is given by

$$\sigma_{sh}^2 = <G^2> \left(\frac{\eta}{h\upsilon} \right) (eRA)^2 \int_{nT}^{(n+1)T} p(\tau) h^2(t_m + nT - \tau) d\tau \qquad (4.1.8)$$

where $<G^2>$ was previously defined in equation (3.2.16). The term t_m corresponds to the mean pulse width of pulse m.

Using Midwinter's simplification only a Gaussian PDF (probability density function) is required to encompass both thermal and shot noises. It is assumed that the thermal noise is dominant and avalanche gain is much greater than unity. The simplification therefore sacrifices very little of the accuracy of the BER (bit error rate). Hence, the familiar Gaussian probability density function is used in the calculation of probability of error

$$P(X) = \frac{1}{\sqrt{2\pi}} \exp\left[\frac{-X^2}{2}\right] \tag{4.1.9}$$

The individual PDFs are specified by Xianda as

$$P_j(\tau) = \frac{J}{\sqrt{2\pi}} \exp\left[\frac{-(K(\tau - t_j))^2}{2}\right] \tag{4.1.10}$$

where t_j for $j = 1,2,3, \cdots, M$ correspond to the mean pulsewidths and τ_n for $n = 1,2,3, \cdots, M-1$ correspond to the optimal thresholds. The term J is given by

$$J = \frac{V_{max}}{\sigma_T t_r} \tag{4.1.11}$$

Hence the total probability of error P_e for an M-level PWM system is quite similar to that of the M-level PAM system described in section 3.4. The probability of error for the PWM case is given by Bayes law as follows

$$\begin{aligned} P_e = {} & p_1 P(2/1) + p_2 P(1/2) + p_2 P(3/2) + p_3 P(2/3) \\ & + p_3 P(4/3) + p_4 P(3/4) + p_4 P(5/4) + p_4 P(4/5) \\ & + \cdots + p_{M-1} P(M/M-1) + p_M P(M-1/M) \end{aligned} \tag{4.1.12}$$

where p_i is the probability that symbol r_i being sent and where $P(a/b)$ is the probability of error given that symbol r_b was sent by the transmitter and that

r_a was detected at the receiver.

The contributions of secondary terms such as $P(3/1)$, $P(4/1)$, and $P(4/2)$ are assumed negligible and hence not included in equation (4.1.10). If all pulses have been sufficiently randomized then

$$p_i = \frac{1}{M} \tag{4.1.13}$$

where $i = 1,2,3, \cdots, M$ for all i .

Figure 17 shows the probability of error versus SNR for the family of curves $M = 2, 4, 8, 16, 32,$ and 256 . The same system parameters as section 3.4 are used. Note, the PWM curves are similiar to those of the PAM case. The similiarity is due to the fact the incoming PWM is integrated and sampled. This results in a PAM signal present at the comparator banks and hence the similiar performance to a PAM receiver.

4.2 The PWM receiver equalizer

An ideal communication channel is modeled by constant gain and constant delay for all frequency components contained in the transmitted signal. However in a practical channel used in an optical fiber system many there exist factors exist that can corrupt the received signal. Gaussian noise, shot noise and dark current are inherently present in every receiver. Furthermore ISI is introduced due to the band-limited nature of the channel. It is possible to compensate for the non-ideal frequency response characteristic of the channel through the use of an equalizing filter at the receiver.

The transmitter sends discrete symbols at a rate of $1/T$ symbols per second and the corresponding receiver samples the symbols every $T + \tau_d$ seconds, where τ_d is the propagation delay introduced by the channel. Hence it is logical that a discrete time filter be used to compensate for channel discrepancies. Such a filter is better known as a transversal filter and assumes the form shown in figure 18.

The transversal filter consists of $(2K + 1)$ discrete time delay units z^{-1}. Each unit delays the signal by T seconds. The output of each delay unit is fed into an individual multiplier unit (also known as a tap weight coefficient) which multiplies the delayed signal by a preset value of C_n. Then all the output of tap weight coefficient are fed into a summer where the outputs of the summer $Z(t)$ is the equalized version of the input to the equalizer $Y(t)$. The preset coefficients are selected such that the signal $Z(t)$ resembles the data input to the transmitter $X(t)$ as close as possible.

In section 3 ISI was not examined for PPM and PAM since work has already been done in this area by Gagliardi and Messerchmitt, respectively. Hence, the focus here will be on the PWM system. In section 4.1 ISI was not considered in the PWM receiver, now in this chapter an equalizer for the optical PWM receiver

under conditions of ISI will be derived. Several different types of configurations exist for the transversal filter. The least complex is the LE (linear equalizer) which is examined in section 4.4 . Other more complicated forms include the DFE (decision feedback equalizer) . The PWM frame is of length $T = M\tau$ and each sub-slot is of length τ. The PWM receiver consists of $2k + 1$ equalizer banks, one for each unique PWM symbol. Each equalizer bank consists of M tap weight coefficients. The PWM receiver with equalizer is shown in figure 19.

At the front end of the PWM receiver the output of the optical detector assumes a current waveform $r(t)$

$$r(t)=\sum_{n}\delta(t-t_n)+n(t) \tag{4.2.1}$$

A PWM symbol is present at the output of the optical detector and is converted (usually via integrate and dump) into a PAM signal $x(t)$. The signal intensity obeys the following time varying Poisson statistics

$$\lambda(t) = \lambda_o + \sum_{k=-\infty}^{+\infty} V_k\, p(t-k\tau) \tag{4.2.2}$$

The term t_n is Poisson arrival times, $n(t)$ is a wide sense stationary process with autocorrelation R_n and noise power N_o . The derivation of the optimal equalizer begins at the output of the receiver filter which is given by

$$x(t) = \alpha\sum_{n}h(t-t_n) + \int n(u)h(t-u)du \tag{4.2.3}$$

where α is the constant term which replaces $\frac{\eta}{h\upsilon}$ and where $h(t)$ is the post detection filter.

The first step in finding an equalizer for the PWM receiver is to derive the the mean square error between the data symbol V_k and the sampled signal. This

has been done in APPENDIX B and is given by

$$\overline{e^2} = \alpha^2\lambda_o \int h^2(-u)du + \alpha^2 m_V \sum_m \int p(u - m\tau)h^2(-u)du \qquad (4.2.4)$$

$$+ \int\int R_n(u-s)h(-u)h(-s)duds + \alpha^2 \sum_n \sum_m r_{k-m}\, r_{k-n}(\Theta_{mn} - m_V^2)$$

$$- 2\alpha \sum_m \sum_n \Theta_{mn}\, r_{k-n} + (\Theta_{mn} - m_V^2) + 2\alpha m_V^2 \sum_m r_m$$

Recall, Θ_{mn} is the second moment of V_k, r_n is the convolution of $p(u + m\tau)$ and $h(u)$, and R_n is the autocorrelation of the thermal noise term. By differentiating with respect to h using variational calculus the optimal equalizer filter can be determined

$$2h(u)\left[\alpha^2\lambda_o + \alpha^2 m_V \sum_n p(t + (\overline{k-n})\tau)\right] + \int R_n(t-s)h(u)du \qquad (4.2.5)$$

$$+ \alpha^2 \sum_n \sum_m (\Theta_{mn} - m_V^2) r_{k-n}\, p(t + (\overline{k-n})\tau)$$

$$- 2\alpha \sum_n \sum_m \Theta_{mn}\, p(t + (\overline{k-n})\tau) + 2\alpha m_V^2 \sum_m p(t + (\overline{k-m})\tau) = 0$$

which becomes

$$\phi(u)h(-u) + \frac{1}{2}\int R_n(u-s)h(-s)ds \qquad (4.2.6)$$

$$+ \frac{1}{2}\alpha^2 \sum_n \sum_m (\Theta_{mn} - m_V^2) r_{k-m}\, p(t + (\overline{k-n})\tau)$$

$$- \alpha \sum_n \sum_m \Theta_{mn}\, p(t + (\overline{k-n})\tau) + \alpha m_V^2 \sum_m p(t + (\overline{k-m})\tau) = 0$$

where $\phi(t)$ represents the optical signal input to the equalizer filter $h(t)$ and so

$$\phi(t)h(-t) + \frac{1}{2}\int R_n(t-s)h(-s)ds = \qquad (4.2.7)$$

$$\left[\sum_m \sum_n [\alpha^2 \Theta_{mn} - \frac{1}{2}\alpha^2 r_{k-m}(\Theta_{mn} - m_V^2)] - \alpha^2 \sum_n m_V^2\right] p(t + (\overline{k-n})\tau)$$

Simplification yields

$$\phi(t)h(-t) + \frac{1}{2}\int R_n(t-s)h(-s)ds = \sum_m\sum_n(\Theta_{mn}\alpha^2(1 - \frac{1}{2}r_{k-m}) + \frac{1}{2}\alpha^2 m_V^2 r_{k-m}) - \alpha m_V^2 \quad (4.2.8)$$

where $h(-t)$ is given as follows

$$h(-t) = \sum_n C_n g(t + n\tau) \quad (4.2.9)$$

represents the optimal equalizing filter in terms of tap weight coefficients C_n and where $g(t)$ satifies the integral equation below

$$\phi(t)g(t) + \int_{-\infty}^{+\infty} R_n(t-s)g(s)ds = p(t) \quad (4.2.10)$$

Therefore an optimal filter for the PWM receiver would assume the coefficients

$$C_n = \sum_{m=-\infty}^{+\infty}\left[\Theta_{mn}(\alpha^2 - \frac{1}{2}\alpha^2 r_{k-m}) + \frac{1}{2}\alpha^2 m_V^2 r_{k-m}\right] - \alpha m_V^2 \quad (4.2.11)$$

$$C_n = \sum_{m=-\infty}^{+\infty}\Theta_{mn}\xi_{mn} + \sum_{m=-\infty}^{+\infty} r_{k-m}\gamma_{mn} + \alpha m_V^2 \quad (4.2.12)$$

where $\xi_{mn} = \alpha^2(1 - \frac{1}{2}r_{k-m})$ and $\gamma_{mn} = \frac{1}{2}\alpha^2 m_V^2$ for $-\varsigma \leq k \leq \varsigma$ and $-\varsigma \leq n \leq \varsigma$

where $\varsigma = \frac{(M-1)}{2}$

The equalizer tap coefficient for $n = 0$ is given by

$$C_0 = \sum_{m=-\infty}^{+\infty}\Theta_{m,0}\xi_{m,0} + \sum_{m=-\infty}^{+\infty} r_{k-m}\gamma_{m,0} - \alpha m_{V_2} \quad (4.2.13)$$

Expanding (4.2.13)

$$C_0 = \sum_{m=-\infty}^{-1} \Theta_{m,0}\xi_{m,0} + \alpha^2(1 - \frac{1}{2}r_{k-m})g + \sum_{m=1}^{+\infty} \Theta_{m,0}\xi_{m,0} \qquad (4.2.14)$$
$$\sum_{m=-\infty}^{-1} r_{k-m}\gamma_{m,0} + \frac{1}{2}\alpha^2 m_V^2 r_{k-m} + \frac{1}{2}\alpha^2 m_V^2 \sum_{m=1}^{\infty} r_{k-m} - \alpha m_V^2$$

Recall, from APPENDIX C that Θ_{mn} can assumeone of three values $y, g, or \Psi$ depending on the values of m and n. Hence, furthermore expansion yields

$$C_0 = \alpha^2 \sum_{m=-\infty}^{-\varsigma-1} \left[(1 - \frac{1}{2}r_{k-m})y + \frac{1}{2}m_V^2 r_{k-m} \right] \qquad (4.2.15)$$
$$+ \alpha^2 \sum_{m=-\varsigma}^{-1} \left[(1 - \frac{1}{2}r_{k-m})\Psi + \frac{1}{2}m_V^2 r_{k-m} \right] + \alpha^2(1 - \frac{1}{2}r_{k-m})g + m_V^2 r_{k-m} - \alpha m_V^2$$
$$+ \alpha^2 \sum_{m=1}^{\varsigma} \left[(1 - \frac{1}{2}r_{k-m})\Psi + \frac{1}{2}m_V^2 r_{k-m} \right] + \alpha^2 \sum_{m=\varsigma+1}^{+\infty} \left[(1 - \frac{1}{2}r_{k-m})y + \frac{1}{2}m_V^2 r_{k-m} \right]$$

Next the term C_1 is determined

$$C_1 = \sum_{m=-\infty}^{+\infty} \Theta_{m,1}\alpha\xi_{m,1} + \sum_{m=-\infty}^{+\infty} r_{k-m}\gamma_{m,1} - \alpha m_V^2 \qquad (4.2.16)$$

$$C_1 = \alpha^2 \sum_{m=-\infty}^{-\varsigma} \left[(1 - \frac{1}{2}r_{k-m})y + \frac{1}{2}m_V^2 r_{k-m} \right] \qquad (4.2.17)$$
$$+ \alpha^2 \sum_{m=-\varsigma+1}^{-1} \left[(1 - \frac{1}{2}r_{k-m})\Psi + \frac{1}{2}m_V^2 r_{k-m} \right] + \alpha^2(1 - \frac{1}{2}r_{k-m})g + \frac{1}{2}m_V^2 r_{k-m} - \alpha m_V^2$$
$$+ \alpha^2 \sum_{m=1}^{\varsigma+1} \left[(1 - \frac{1}{2}r_{k-m})\Psi + \frac{1}{2}m_V^2 r_{k-m} \right] + \alpha^2 \sum_{m=\varsigma+2}^{+\infty} \left[(1 - \frac{1}{2}r_{k-m})y + m_V^2 r_{k-m} \right]$$

For any i the general equation is

$$C_i = \alpha^2 \sum_{m=-\infty}^{-\varsigma-1+i} \left[(1 - \frac{1}{2}r_{k-m})y + \frac{1}{2}m_V^2 r_{k-m} \right] \qquad (4.2.18)$$
$$+ \alpha^2 \sum_{m=-\varsigma+i}^{-1} \left[(1 - \frac{1}{2}r_{k-m})\Psi + \frac{1}{2}m_V^2 r_{k-m} \right] + \alpha^2(1 - \frac{1}{2}r_{k-m})g + \frac{1}{2}m_V^2 r_{k-m} - \alpha m_V^2$$
$$+ \alpha^2 \sum_{m=1}^{\varsigma+i} \left[(1 - \frac{1}{2}r_{k-m})\Psi + \frac{1}{2}m_V^2 r_{k-m} \right] + \alpha^2 \sum_{m=\varsigma+1+i}^{+\infty} \left[(1 - \frac{1}{2}r_{k-m})y + m_V^2 r_{k-m} \right]$$

where $k - \frac{(M-1)}{2} \leq i \leq k + \frac{(M-1)}{2}$

Taking the z transform of C_i

$$
\begin{aligned}
C(z)^{(k)} = \alpha^2 \sum_{m=-\infty}^{-\varsigma-1+i} & \left[\frac{1}{2} z_k R\left(\frac{1}{z}\right)(m_V^2 - y) + y\right] z^{-m} \\
+ \alpha^2 \sum_{m=-\varsigma+i}^{-1} & \left[\frac{1}{2} z^k R\left(\frac{1}{z}\right)(m_V^2 - \Psi) + \Psi\right] z^{-m} \\
+ \alpha^2 \frac{1}{2} z^k & R\left(\frac{1}{z}\right)(m_V^2 - g) + \alpha^2 g - \alpha m_V^2 \\
+ \alpha^2 \sum_{m=1}^{\varsigma+i} & \left[\frac{1}{2} z^k R\left(\frac{1}{z}\right)(m_V^2 - \Psi) + \Psi\right] z^{-m} \\
+ \alpha^2 \sum_{m=\varsigma+1+i}^{+\infty} & \left[\frac{1}{2} z^k R\left(\frac{1}{z}\right)(m_V^2 - y) + y\right] z^{-m}
\end{aligned}
\tag{4.2.19}
$$

The solution for the tap weight coefficients will be found in the next chapter after finding $R\left(\frac{1}{z}\right)$.

4.3 Calculation of Receiver Pre-Equalizing Filter

In a typical fiber optic communication system the received individual pulse shape at time t is given by

$$p(t) = \begin{cases} an_e\, e^{-at} & \text{if } t>0 \\ 0 & \text{if } t<0 \end{cases} \tag{4.3.1}$$

The received optical power is Gaussian shaped where the term n_e represents the average number of electrons per pulse $p(t)$ and the term a is the pulse time constant in seconds. The function $\phi(t)$ in equation (4.3.2) was defined previously as the signal input at the equalizer. It is defined as the sum of the signal times the probability of a pulse in the slot and the signal times the probability of a pulse not in the slot. The probability of a pulse in the slot is given by m_V .

$$\phi(t) = (\lambda_o + \frac{am_V n_e\, e^{-at}}{(1-\beta)})m_V + (\lambda_o + am_V n_e\, e^{-at})(1-m_V) \tag{4.3.2}$$

where $\beta = e^{-a\tau}$

Simplification yields

$$\phi(t) = \lambda_o + an_e\, e^{-at}\left[1 + \frac{m_V \beta}{(1-\beta)}\right] \tag{4.3.3}$$

The equalizer assumes additive white Gaussian noise environment. Since a practical system is bandlimited, the thermal noise is also bandlimited. Therefore a noise whitening filter is required before the transversal equalizer. From Messerschmitt [1] the impulse response of the optimal filter preceding the transversal filter with tap coefficients C_i is given by

$$g(t) = \frac{p(t)}{\phi(t) + N_o} \tag{4.3.4}$$

Substituting (4.3.1) and (4.3.3) into (4.3.4)

$$g(t) = \frac{e^{-at}}{\frac{\lambda_o + N_o}{an_e} + m_V e^{-at}\left[1 + \frac{m_V \beta}{(1-\beta)}\right]} \tag{4.3.5}$$

To simplify (4.3.5) the following substitutions are made

$$\rho = \frac{\lambda_o + N_o}{an_e} \tag{4.3.6}$$

where ρ is the average number of noise electrons per time slot to signal electrons per transmitted symbol

$$\Delta = m_V \left[1 + \frac{m_V \beta}{(1-\beta)}\right] \tag{4.3.7}$$

Substituting (4.3.6) and (4.3.7) into (4.3.5) yields the following

$$g(t) = \frac{1}{e^{at}\rho + \Delta} \tag{4.3.8}$$

The convolution of pre-equalization filter and unequalization optical signal is calculated as follows

$$S_k = \sum_{m=l}^{+\infty} \int_{(m-1)\tau}^{m\tau} p(t+kT)g(t)dt \tag{4.3.9}$$

$$S_k = \sum_{m=l0}^{+\infty} \int^{\tau} \frac{an_e e^{-2au} e^{-2m\tau \cdot \tau}}{\rho + \Delta e^{-au}} \cdots du \tag{4.3.10}$$

where $l = 0$ for $k \geq 0$ and $l = -k$ for $k < 0$

To simplify the integration, partial fractions are used.

$$\frac{1}{e^{au}(\rho e^{au}+\Delta)} = \frac{A}{e^{au}} + \frac{B}{\rho e^{au}+\Delta} \tag{4.3.11}$$

Hence solving for (4.3.11) the A and B coefficients become $A = -\rho/\Delta$ and $B = 1/\Delta$

Therefore (4.3.10) now becomes

$$S_k = \int_0^{\tau} \frac{1}{\Delta e^{au}} du - \int_0^{\tau} \frac{\rho}{\rho\Delta e^{au} + \Delta^2} du \tag{4.3.12}$$

The integrations of equation (4.3.12) yields the following result

$$S_k = an_e \sum_{m=l}^{+\infty} \left[\frac{e^{au}}{\Delta} - \frac{\rho}{\Delta} \left(\frac{u}{\Delta} - \frac{1}{\Delta a} \ln(\Delta + \rho e^{au}) \right) \right] \tag{4.3.13}$$

$$S_k = an_e \sum_{m=l}^{+\infty} e^{-2m\tau - k\tau} \left[\frac{1}{\Delta} e^{-a\tau} - \frac{\rho\tau}{\Delta^2} + \left[\frac{\rho}{\Delta^2 a} \ln(\Delta + \rho e^{a\tau}) - \frac{1}{\Delta} - \frac{\rho}{\Delta^2 a} \ln(\Delta + \rho) \right] \right] \tag{4.3.14}$$

The constant terms in the square brackets shall be denoted by the term D.

$$D = \frac{1}{\Delta} \left(e^{-a\tau} - 1 \right) - \frac{\rho\tau}{\Delta^2} + \frac{\rho}{\Delta^2 a} \left[\ln(\Delta + \rho e^{a\tau}) - \ln(\Delta + \rho) \right] \tag{4.3.15}$$

Hence

$$S_k = an_e \sum_{m=l}^{+\infty} De^{-2m\tau - k\tau} \tag{4.3.16}$$

The cases for different K will considered

If $k > 0$ then $m = 0$

$$S_{k+} = De^{-k\tau} \sum_{m=0}^{+\infty} e^{-m\tau} = D^{k\tau a} \frac{1}{1 - \beta^2} \tag{4.3.17}$$

If $k < 0$ then $m = -k = |k|$

$$S_{k-} = De^{-k\tau} \sum_{m=|k|+1}^{+\infty} e^{-m\tau} \tag{4.3.18}$$

Using the following property

$$\sum_{i=0}^{n} x^i = \frac{(1-x^{n+1})}{(1-x)} \tag{4.3.19}$$

for $1 > x$

Hence (4.3.18) becomes

$$S_{k-} = De^{-k\tau a} \left[\frac{\beta^{2|k|}}{1-\beta^{+2}} \right] \tag{4.3.20}$$

Hence for all K the general expression is

$$S_k = \frac{S_{k+}}{2} \left(\frac{k}{|k|} + 1 \right) - \frac{S_{k-}}{2} \left(\frac{k}{|k|} - 1 \right) \tag{4.3.21}$$

Therefore

$$S_k = D \frac{\beta^{+|k|}}{(1-\beta^{+2})} \tag{4.3.22}$$

From Peled [11] the z-transform will be evaluated. When S_k where $k < 0$ is given by

$$S_{k-} = \frac{D}{1-\beta^2} \sum_{k=-\infty}^{-1} \beta^{|k|} z^{-k} = \frac{D}{1-\beta^2} \sum_{k=1}^{+\infty} \beta^k z^k \tag{4.3.23}$$

and S_k when $k > 0$ is given by

$$S_{k+} = \frac{D}{1-\beta^{+2}} \sum_{k=0}^{+\infty} \beta^{|k|} z^{-k} = \frac{D}{1-\beta^2} \sum_{k=0}^{+\infty} \beta^k z^{-k} \qquad (4.3.24)$$

Hence the z-transform becomes

$$S(z) = \frac{D}{1-\beta^2} \left[\frac{\beta z}{1-\beta z} + \frac{1}{1-\beta z^{-1}} \right] \qquad (4.3.25)$$

After simplification $S(z)$ becomes

$$S(z) = \frac{D}{(1-\beta z)(1-\beta/z)} \qquad (4.3.26)$$

where $S(z)$ is valid for the region of $|\beta| < |z| < 1/|\beta|$.

4.4 Calculation of LE-ZF equalizer coefficients and MSE

The simplest from of equalizer is the LE-ZF (Linear Equalizer Zero Forcing). The estimate of symbol X_k using the linear equalizer is given by

$$Z_k = \sum_{i=-k}^{k} C_i Y_{k-i} \tag{4.4.1}$$

where C_i are tap weight coefficients of the filter and Y_k is the equalizer input.

Ideally k approaches infinity, however in a practical equalizer k is chosen at the point where the system performance is no longer improved as the value for k is increased. With the ZF algorithm it is assumed the worst case of ISI (i.e. peak distortion) is present at the equalizer. From Proakis [12] the discrete time filter can be described in terms of its impulse response

$$q_n = \sum_{i=-\infty}^{+\infty} C_i s_{n-i} \tag{4.4.2}$$

where s_n is the impulse response of the channel and C_n is the impulse response of the equalizer. The output of the filter can be expressed as

$$Z_k = q_0 Y_k + \sum_{n \neq k} Y_n q_{k-n} + \sum_{i=-\infty}^{+\infty} C_i \eta_{k-i} \tag{4.4.3}$$

The first term represents the desired symbol, the second term is the ISI, and the third term is the noise term. The peak value of the ISI term (i.e. peak distortion) is given by W where W is a function of the tap weight coefficients.

$$W = \sum_{n=-\infty}^{+\infty} \left| \sum_{i=-\infty}^{+\infty} C_i s_{n-i} \right| - \left| \sum_{i=-\infty}^{+\infty} C_i s_{-i} \right| \tag{4.4.4}$$

It is possible for a filter having an infinite number of taps to completely eliminate

ISI. According to Proakis [12] ISI is eliminated (i.e. $W=0$) when the following conditions are met.

$$q_n = \sum_{i=-\infty}^{+\infty} C_i s_{n-i} = \begin{cases} 1 & n=0 \\ 0 & n \neq 0 \end{cases} \tag{4.4.5}$$

The z-transform yields a filter with the transfer function of

$$C(z) = \frac{1}{S(z)} \tag{4.4.6}$$

where $S(z)$ is the channel transfer function. In other words the transfer function is simply the inverse of the channel's tranfer function.

If a ZF equalizer of finite taps $2K+1$ is desired, the peak distortion is given by

$$W = \sum_{n=-K}^{K} \left| \sum_i C_i s_{n-i} \right| - \left| \sum_i C_i s_{-i} \right| \tag{4.4.7}$$

The minimum peak distortion is given by

$$W_0 = \frac{1}{|s_0|} \sum_{n=1}^{L} |s_n| \tag{4.4.8}$$

The coefficients are optimal when the sequence is orthogonal to the equalizer input sequence. Limitations exist with the ZF algorithm. The ZF solution is optimal only when $W_0<1$ otherwise when $W_0>1$ the solution is not optimal. Furthermore the ZF equalizer neglects the effect of additive white noise . With the MSE algorithm discussed in section 4.5 these limitations do not exist.

The equalizer coefficients for the PWM system using LE-ZF case will be calculated. The coefficients can be expressed as a function of S(z).

$$C(z) = \frac{1}{S(z)} = \frac{(1-\beta z)(1-\beta/z)}{D} \tag{4.4.9}$$

$$C(z) = \frac{(\beta^2+1)}{D} - \frac{\beta z}{D} - \frac{\beta/z}{D} \tag{4.4.10}$$

Hence the coefficients become simply

$$C_0 = \frac{(1+\beta^2)}{D} \tag{4.4.11.a}$$

$$C_{+1} = -\frac{\beta}{D} \tag{4.4.11.b}$$

$$C_{-1} = -\frac{\beta}{D} \tag{4.4.11.c}$$

To calculate the MSE (Mean Square Error)

$$\overline{e^2} = \alpha^2 \sum_n C_n^{(k)} r_n + \alpha^2 \sum_m \sum_n r_{k-m}\, r_{k-n}\, (\Theta_{mn} - m_V^2) \tag{4.4.12}$$

$$- 2\alpha \sum_m \sum_n \Theta_{mn}\, r_{k-n} + (\Theta_{mn} - m_V^2) + 2\alpha m_V^2 \sum_m r_m$$

where $\sum_n C_n\, r_n$ is given by

$$\sum_n C_n\, r_n = \phi(t)h(-t) + \int R_n(t-s)h(-t)dt \tag{4.4.13}$$

and where r_n is given by

$$r_n = \delta_n \tag{4.4.14}$$

For the ZF-LE all $C_n = C_n$ except $n=0$

The term r_{k-n} is given by

$$r_{k-n} = \begin{cases} 0 & \text{if } k \neq n \\ 1 & \text{if } k = n \end{cases} \tag{4.4.15}$$

After the appropriate substitutions are made the MSE for the ZF-LE is given by

$$\overline{e^2} = \frac{(1+\beta^2)}{D} + (\alpha^2+1)(g-m_V^2)-4\alpha(y+\Psi+\frac{g}{2})+2\alpha m_V^2 \qquad (4.4.17)$$

The curves for MSE versus rms pulse width for M=2,4,8,16,32,64,128, and 256 for ρ=1 and n_e = 1000 are plotted in figure 20.

4.5 Calculation of LE-MSE equalizer coefficients and MSE

With the MSE criterion the tap weights coefficients are adjusted to minimize the mean square value of the error.

$$\epsilon_k = X_k - Z_k \tag{4.5.1}$$

For complex-valued symbols, the MSE performance index J is given by

$$J = E \mid \epsilon_k \mid^2 = E \mid X_k - Z_k \mid^2 \tag{4.5.2}$$

The estimate Z_k is expressed as

$$Z_k = \sum_{i=-\infty}^{+\infty} C_i Y_{k-i} \tag{4.5.3}$$

In terms of the coefficients C_i and the input sequence Y_{k-i}

To minimize the error ϵ_k , ϵ_k is made othogonal to the input sequence Y_{k-i}

$$E(\epsilon_k Y^*_{k-l}) = 0 \tag{4.5.4}$$

or

$$\sum_{i=-\infty}^{+\infty} C_i E(Y_{k-i} Y^*_{k-i}) = E(Y_k Y_{k-l}) \tag{4.5.5}$$

where $\infty < l < +\infty$

From Proakis [12]

$$Y_k = \sum_{n=0}^{L} s_n X_{k-n} + \eta_k \tag{4.5.6}$$

Using equation (4.5.6) in equation (4.5.7)

$$E(Y_{k-i}\, Y^{*}_{k-l}) = \sum_{n=0}^{L} s_n^{*} s_{n+l-i} + N_o\, \delta_{ij} \tag{4.5.7}$$

$$E(Y_k\, Y^{*}_{k-l}) = \begin{cases} s^{*}_{-l} & -L \le l \le 0 \\ 0 & \text{otherwise} \end{cases} \tag{4.5.8}$$

Putting equation (4.5.7) and (4.5.8) into equation (4.5.6) and then taking the z-transform of both sides results in the following

$$C(z)[S(z)S^{*}(z^{-1}) + N_o] = S^{*}(z^{-1}) \tag{4.5.9}$$

Hence the transfer function for MSE criterion is

$$C(z) = \frac{S^{*}(z^{-1})}{S(z)S^{*}(z^{-1}) + N_o} = \frac{1}{S(z)S^{*}(z^{-1}) + N_o} \tag{4.5.10}$$

The equalizer coefficients for the LE-MSE case will be calculated.

From equations (4.2.22) and (4.2.40) the term r_j is specified as

$$r_j = \sum_m C_n^{(k)} S_{j-n} \tag{4.5.11}$$

where S_j is defined by equation (4.3.9).

The z-tranform of $r_j^{(k)}$ is given by

$$R^k(z) = S(z)C^k(z) \tag{4.5.12}$$

Using this fact in conjunction with equation (4.2.50) a general equation, the equalizer coefficients are obtained without knowing or needing $R(z)$

$$C^k(z) = \frac{D\,\alpha^2}{(1-\beta z)(1-\beta/z)} \sum_{m=-\infty}^{-\varsigma-1+i} \left[\frac{1}{2} z^k\, C\left(\frac{1}{z}\right)(m_V^2 - y)\right] z^{-m} \tag{4.5.13}$$

$$+ \alpha^2 y \sum_{m=-\infty}^{-\varsigma-1+i} z^{-m} + \frac{D\,\alpha^2}{(1-\beta z)(1-\beta/z)} \sum_{m=-\varsigma+i}^{-1} \left[\frac{1}{2} z^k\, C\left(\frac{1}{z}\right)(m_V^2 - \Psi)\right] z^{-m}$$

$$+\alpha^2\Psi\sum_{m=-\varsigma+i}^{-1}z^{-m}+\frac{D\alpha^2}{(1-\beta z)(1-\beta/z)}\left[\frac{1}{2}z^k C\left(\frac{1}{z}\right)(m_V^2-g)\right]+\alpha^2 g-\alpha m_V^2$$
$$+\frac{D\alpha^2}{(1-\beta z)(1-\beta/z)}\sum_{m=1}^{\varsigma+i}\left[\frac{1}{2}z^k C\left(\frac{1}{z}\right)(m_V^2-\Psi)\right]z^{-m}+\alpha^2\Psi\sum_{m=1}^{\varsigma+i}z^{-m}$$
$$+\frac{D\alpha^2}{(1-\beta z)(1-\beta/z)}\sum_{m=\varsigma+1+i}^{+\infty}\left[\frac{1}{2}z^k C\left(\frac{1}{z}\right)(m_V^2 C-y)\right]z^{-m}+\alpha^2 y\sum_{\varsigma+1+i}^{+\infty}z^{-m}$$

Completing the z-transform the solution is expressed as follows

$$C(z)=\frac{\alpha^2}{2}z^k S(z)E(z)C\left(\frac{1}{z}\right)+\alpha^2 F(z) \tag{4.5.14}$$

where the transforms S(z), F(z), and E(z) are defined below

$$S(z)=\begin{cases}\dfrac{D}{(1-\beta z)(1-\beta/z)} & |\beta|<|z|<|1/\beta|\\ 0 & \text{elsewhere}\end{cases} \tag{4.5.15}$$

$$F(z)=\begin{cases}\dfrac{y}{1-z}+\displaystyle\sum_{m=0}^{\varsigma-i}(\Psi-y)z^m-\Psi & z<1\\ g & z=0\\ \dfrac{y}{1-z^{-1}}+\displaystyle\sum_{m=0}^{\varsigma+i}(\Psi-y)z^{-m}-\Psi & z>1\end{cases} \tag{4.5.16}$$

$$E(z)=\begin{cases}\dfrac{m_V^2-y}{1-z}+\displaystyle\sum_{m=0}^{\varsigma-i}(y-\Psi)z^m-(m_V^2-\Psi) & z<1\\ m_V^2-g & z=0\\ \dfrac{m_V^2-y}{1-z^{-1}}+\displaystyle\sum_{m=0}^{\varsigma+i}(y-\Psi)z^{-m}-(m_V^2-\Psi) & z>1\end{cases} \tag{4.5.17}$$

After expansion of all z-transforms and grouping of like terms the following row

generating equations for the augemented matrix are obtained.

$$C_i^k = \frac{\alpha^2 D}{2}(m_V^2-\Theta)\sum_{n=0}^{c_--i}\left[\sum_{j=0}^{c_--i-n} C_{L_2-j}\,\beta^{|2L_1+n|}\right] \tag{4.5.18}$$

for $L_1 < i \leq 0$ and where $c_- = L_2-4L_1+k$

and

$$C_i^k = \frac{\alpha^2 D}{2}(m_V^2-\Theta)\sum_{n=0}^{c_+-i}\left[\sum_{j=0}^{c_+-i-n} C_{L_1-j}\,\beta^{|2L_2+n|}\right] \tag{4.5.19}$$

for $0 \leq i < L_2$ and where $c_+ = L_1-4L_2+k$

By substituting all the values between $-\varsigma$ and $+\varsigma$ a set of M simultaneous equations is obtained. Using a numerical method such as the Gauss-Jordan algorithm these equalizer coefficients can be solved. In figure 21 the MSE versus rms pulse width has been plotted for 2,4,8,16,32,64,128, and 256 for $\rho = 1$ and $n_e = 1000$.

CHAPTER FIVE

CONCLUSION

In the second chapter it was seen that in fiber optic communication systems there exist many factors that can corrupt the transmitted data en route to the user. Several sources of noises exist. These include APD shot noise, thermal resistor noise, and amplifier noise. Furthermore, in the second chapter it was seen that a residual dark current is present in the APD. And finally ISI from neighbouring symbols also seriously corrupts the received signal. It was found the optimal performance of a fiber optic system is highly dependant on the value of APD gain $<G>$. This value for $<G>$ is dependant on thermal noise, shot noise, and received optical power.

In chapter three the behaviour of the combinational PPAM scheme was compared with that of conventional PAM and PPM schemes on fair basis using equivalent power budgets and data rates. It was found that PPAM scheme had better performance than the PAM scheme, but the conventional PPM scheme performed better than the PPAM scheme. The PPAM scheme has high immunity to ISI due its PPM nature and the spectral efficiency of PAM due to its multilevel composite construction.

The performance of the conventional receiver and that of the ratio receiver were compared in the case of the PPAM signal. The ratio receiver had superior performance in environments with moderate to high S/N levels and inferior performance in environments with low S/N levels for ratio receiver as compared to the conventional integrate-and-dump receiver.

In chapter four the performance of a PWM system was evaluated. Using techniques similar to that of Messerschmitt [1] and Gagliardi [2] an equalizer for

the PWM receiver in the presence of ISI was developed. Optimal Equalizers using the LE-ZF and LE-MSE criterion were calculated and analyzed. It was found that the LE-MSE criterion had better performance than the LE-ZF criterion for larger values of M. However, for smaller values of M , namely $M = 2$, 4,and 8, the performance of the equalizer was not significantly improved by resorting to the ZF-MSE scheme.

Further work could be done in the area of equalization of PWM over a fiber optic channel. The cases of the DF-ZF and DF-MSE are unexplored. It is expected that the performance of this class of decision feedback equalizers would be superior to that of the linear equalizers examined in chapter 4. Using chapter 4 as a basis and incorporating coefficients of the feedback filter into the equation of the mean square error, the DF-ZF and DF-MSE for PWM signals could be found in a similiar fashion to Messerschmitt [1].

REFERENCES

[1] Messerschmitt, David G., "Minimum MSE Equalization of Digital Fiber Optic Systems ", IEEE Transactions on Communications, Vol COM-26, No.7, July, 1978

[2] Gagliardi, R.M., " MSE Linear Equalization for the optical PPM channel", National Telecommunications Conference 1980 , Houston, Texas, December, 1980

[3] Gowar, John, Optical Communications Systems , Prentice-Hall, London, 1984

[4] Midwinter, John, E., Optical Fiber for Transmission , John Wiley & Sons, New York, 1979

[5] Hauk, Waldemar, et al., "The Calculation of Error Rates for Optical Fiber Systems", IEEE Transactions on Communications, Vol. COM-26, No.7, July 1978

[6] Papoulis, A., Probability, Random Variables, and Stochastic Processes Mc Graw-Hill, 1965

[7] Davidson, F.M. et al., "Gaussian Approximation versus Nearly Exact Performance Analysis of Optical Communication Systems with PPM Signaling and APD Receivers", IEEE Transactions on Communications, Vol. COM-36, No.11, November, 1988

[8] Hubbard, W.M., " Approximation of a Poisson Distribution by a Gaussian Distribution ", Proceedings of the IEEE, September, 1970

[9] Sorensen, N., and R. Gagliardi, "Performance of Optical Receivers with Avalanche Photodetection", IEEE Transactions on Communications, Vol COM-27, No.9, September, 1979

[10] Nanda, D., et al., " Four Level Pulse Width Modulation for Fiber Optic Communications ", IEEE Transcactions on Communications, Vol COM-30, No. 8, August, 1982

[11] Peled, Abraham, and Bede Liu Digital Signal Processing John Wiley & Sons, New York, 1976

[12] Proakis, John G., Digital Communications , Mc Graw-Hill, New York, 1983

APPENDIX A

DERIVATION OF THE PDF OF THE RATIO RECEIVER

The probability density function for the ratio receiver is the ratio of two independent one-dimensional normal density functions. The individual functions are given by

$$f_x(x) = \frac{1}{\sqrt{2\pi}\sigma_x}\exp\left[-\frac{(x - m_x)^2}{2\sigma_x^2}\right] \tag{A.1}$$

and

$$f_y(y) = \frac{1}{\sqrt{2\pi}\sigma_y}\exp\left[-\frac{(y - m_y)^2}{2\sigma_y^2}\right] \tag{A.2}$$

From Papoulis [6] the resulting two-dimensional joint probability distribution function is given by

$$f_z(z) = \int_{-\infty}^{+\infty} |\, y \,| f_{xy}(zy, y)\, dy \tag{A.3}$$

where the random variable $z = x/y$

By substituting (A.1) and (A.2) into (A.3) the result becomes

$$f_z(z) = \int_{-\infty}^{+\infty} \frac{|\, y \,|}{2\pi\sigma_x\sigma_y}\exp\left[-\frac{(y - m_y)^2}{2\sigma_y^2} - \frac{(zy - m_x)^2}{2\sigma_x^2}\right] dy \tag{A.4}$$

To simplify the integration the following substitution is made

$$u = y^2\left[\frac{\sigma_x^2 + \sigma_y^2 z^2}{2\sigma_x^2\sigma_y^2}\right] - 2y\left[\frac{\sigma_x^2 m_y + \sigma_y^2 m_x z}{2\sigma_x^2\sigma_y^2}\right] + \left[\frac{\sigma_x^2 m_y^2 + \sigma_y^2 m_x^2}{2\sigma_x^2\sigma_y^2}\right] \tag{A.5}$$

This reduces equation (A.4) to

$$f_z(z) = \int_{-\infty}^{0} \frac{-y}{2\pi\sigma_x\sigma_y}\exp(-u)dy + \int_{0}^{+\infty} \frac{y}{2\pi\sigma_x\sigma_y}\exp(-u)dy \qquad \text{(A.6)}$$

Equation (A.6) will now be put in a form which will allow for the completion of the square by replacing all constants terms with a, b, c, and, d

$$a = \frac{\sigma_x^2 + \sigma_y^2 z^2}{2\sigma_x^2\sigma_y^2} \qquad \text{(A.7)}$$

$$b = \frac{\sigma_x^2 m_y + \sigma_y^2 m_x z}{\sigma_x^2 + \sigma_y^2 z^2} \qquad \text{(A.8)}$$

$$c = \frac{\sigma_x^2 m_y^2 + \sigma_y^2 m_x^2}{\sigma_x^2 + \sigma_y^2 z^2} \qquad \text{(A.9)}$$

$$d = \frac{1}{2\pi\sigma_x\sigma_y} \qquad \text{(A.10)}$$

Hence equation (A.5) becomes

$$u = a(y^2 - 2yb + c) \qquad \text{(A.11)}$$

Completing the square for (A.11)

$$u = a(y - b)^2 + a(c - b^2) \qquad \text{(A 12)}$$

Using the result of (A.12) equation into (A.6) becomes

$$f_z(z) = d\int_{-\infty}^{0} -y\exp(-a(y-b)^2 - a(c-b^2))dy \qquad \text{(A.13)}$$
$$+d\int_{0}^{+\infty} y\exp(-a(y-b)^2 - a(c-b^2))dy$$

Let $z = y - b$ and $dz = dy$ and equation (A.13) becomes

$$f_z(z) = -d\int_{-\infty}^{-b}(z+b)\exp(-az^2)\exp(-a(c-b^2)dz + d\int_{-b}^{+\infty}(z+b)\exp(-az^2)\exp(-a(c-b^2)dz \tag{A.14}$$

Separating (A.14) into four integrals

$$\begin{aligned} f_z(z) = {} & -d\exp(-a(c-b^2))\int_{-\infty}^{-b} z\exp(-az^2)dz \\ & +d\exp(-a(c-b^2))\int_{-b}^{+\infty} z\exp(-az^2)dz \\ & -db\exp(-a(c-b^2))\int_{-\infty}^{-b}\exp(-az^2)dz \\ & +db\exp(-a(c-b^2))\int_{-b}^{+\infty}\exp(-az^2)dz \end{aligned} \tag{A.15}$$

The first integral can be integrated by letting $u = z^2$ and $du = 2zdz$

$$I_1 = \frac{d\exp(-ac)}{2a} \tag{A.16}$$

Similarly the second integral also becomes

$$I_2 = \frac{d\exp(-ac)}{2a} \tag{A.17}$$

The third integral assumes the form of the Erf function and the fourth integral assumes the form of the Erfc function after some manipulation. The third integral is given by

$$I_3 = -db\exp(-a(c-b^2))\sqrt{\frac{\pi}{a}}\mathrm{Erf}(-b\sqrt{2a}) \tag{A.18}$$

and the fourth integral becomes

$$I_4 = db \exp(-a\,(c - b^2))\sqrt{\frac{\pi}{a}}\mathrm{Erfc}(-b\sqrt{2a}) \qquad \text{(A.19)}$$

The final solution is simply the sum of these four integrals

$$f(z) = d\exp(-ac)\left[\frac{1}{a} - b\exp(ab^2)\sqrt{\frac{\pi}{a}}(1 - 2\mathrm{Erf}(-b\sqrt{2a}))\right] \qquad \text{(A.20)}$$

The final solution for the ratio detector probability density function becomes

$$f(z) = \frac{1}{2\pi\sigma_x\sigma_y}\exp\left[-\frac{\sigma_x^2 m_y^2+\sigma_x^2 m_x^2}{2\sigma_x^2\sigma_y^2}\right] \qquad \text{(A.21)}$$

$$*\left\{\frac{2\sigma_x^2\sigma_y^2}{\sigma_x^2+\sigma_y^2 z^2} - \frac{\sigma_x^2 m_y+\sigma_y^2 m_x z}{\sigma_x^2+\sigma_y^2 z^2}\exp\left[\frac{(\sigma_x^2 m_y+\sigma_y^2 m_x z)^2}{(2\sigma_x^2\sigma_y^2)(\sigma_x^2+\sigma_y^2 z^2)}\right]\right.$$

$$\left.*\frac{\sqrt{2\pi}\sigma_x\sigma_y}{\sqrt{\sigma_x^2+\sigma_y^2 z^2}}\left[1 - 2\mathrm{Erf}\left[\frac{\sigma_x^2 m_y+\sigma_y^2 m_x z}{\sigma_x\sigma_y\sqrt{\sigma_x^2+\sigma_y^2 z^2}}\right]\right]\right.$$

The constants of the pdf are verified when the pdf is integrated from $-\infty$ to $+\infty$ and results in unity. The ratio receiver pdf is plotted with the conventional gaussian pdf in figure 22. All means are set to zero and all variances are set to unity.

APPENDIX B

DERIVATION OF MEAN SQUARE ERROR OF V_k

From Messerschmitt [1] the mean square error between the data symbol V_k and the sampled signal $x(k\tau)$ is given by

$$\overline{e^2} = E(A-C)^2 = E(A^2) - 2E(AC) + E(C^2) \tag{B.1}$$

where $A = x(k\tau) - V_k$. The term A is the difference between the each sample and the current data digit. The minimum of the previous equation is found by differentiation. The term C is selected for minimal mean square error which occurs when

$$\frac{dA}{dC} = -2E(A) + 2E(C) = 0 \tag{B.2}$$

Therefore the minimum value of $\overline{e^2}$ occurs when

$$C = E(A) \tag{B.3}$$

Therefore the optimized mean square error becomes

$$\overline{e^2} = E(A^2) - E^2(A) \tag{B.4}$$

The first component of (B.4) is found to be

$$E(A^2) = E(x^2(k\tau)) - 2E(V_k\, x(k\tau)) + E(V_k^2) \tag{B.5}$$

The second component of (B.4) is found to be

$$E^2(A) = E^2(x(k\tau)) + E^2(V_k) - 2E(V_k)E(x(k\tau)) \tag{B.6}$$

Hence (B.5) and (B.6) yield

$$\overline{e^2} = \sigma_V^2 + \sigma_{x(k\tau)}^2 - 2E(V_k\, x(k\tau)) + 2E(V_k)E(x(k\tau)) \tag{B.7}$$

There are four components in (B.7) to be evaluated. The σ_V^2 term will be evaluated first.

$$E(V_k) = m_V = \frac{1}{2} \tag{B.8}$$

The derivation of m_V is given in APPENDIX C.

$$E(V_k^2) = E(V_{k-n}\, V_{k-m})_{m=n} = \Theta_{mn} \tag{B.9}$$

The term Θ_{mn} is defined below and is calculated in APPENDIX D.

$$\Theta_{mn} = \begin{cases} g = \dfrac{1}{2} & m = n \\ \Psi = \dfrac{(M-2)}{3(M-1)} & m \neq n \text{ same frame} \\ y = \dfrac{1}{4} & m \neq n \text{ different frame} \end{cases} \tag{B.10}$$

$$\sigma_V^2 = E(V_k^2) - E^2(V_k) \tag{B.11}$$

Hence, the first component is given by

$$\sigma_V^2 = \Theta_{mn} - m_V^2 \tag{B.12}$$

Now the second component will be evualated

$$E(x(k\tau)) = E\left[\alpha \sum_n h(k\tau - t_n) + \int n(u)h(t-u)\,du\right] \tag{B.13}$$

From Papoulis [6] Campbell's theorem shall be introduced and used extensively in following derivations. For a filtered Poisson process $s(t) = \sum_n h(t-t_n)$ where t_n are random time points, the first and second moments are given by (B.14) and

(B.15) respectively

$$E[s(t)] = \lambda(\tau)\int h(t-\tau)d\tau \tag{B.14}$$

$$E[s^2(t)] = \lambda^2(\tau)\left[\int h(t-\tau)d\tau\right]^2 + \lambda(\tau)\int h^2(t-\tau)d\tau \tag{B.15}$$

and from Campbell's theorem this equation can be restated as

$$E(x(k\tau)) = \alpha\int\lambda(u)h(k\tau-u)du \tag{B.16}$$

$$E(x(k\tau)) = \alpha\lambda_o\int h(u)du + \alpha\sum_m V_m\int p(u+m\tau)h(-u)du \tag{B.17}$$

Averaging over data V_k

$$E(x(kT)) = \alpha\lambda_o\int h(u)du + \alpha m_V\sum_m r_m \tag{B.18}$$

where

$$r_m = \int p(u+m\tau)h(-u)du \tag{B.19}$$

Therefore

$$E^2(x(k\tau)) = \alpha^2\lambda_o^2\left(\int h(u)du\right)^2 + 2\alpha^2 m_V\lambda_o\sum_m r_m \int h(u)du \tag{B.20}$$

$$+ \alpha^2 m_V^2\sum_n\sum_m r_{k-n}\, r_{k-m}$$

Next the term $E(x^2(k\tau))$ will be evaluated

$$E(x^2(k\tau)) = E\left[\left\{\alpha\sum_n h(k\tau-t_n) + \int n(u)h(t-u)du\right\}\right. \tag{B.21}$$

$$\left.\left[\left\{\alpha\sum_m h(k\tau-t_m) + \int n(u)h(t-u)du\right\}\right]\right.$$

The product of the dissimilar terms is zero, therefore

$$E\left(x^2(k\tau)\right) = E\left[\alpha^2 \sum_n h(k\tau - t_n) \sum_m h(k\tau - t_m)\right] + E\left[\left(\int n(u) h(t-u)\right)^2\right] \tag{B.22}$$

Again from Campbell's theorem the result becomes

$$E\left(x^2(k\tau)\right) = \alpha^2 \lambda(u) \int h^2(k\tau - u)\,du + \alpha^2 \lambda(u)^2 \left(\int h(k\tau - u)\,du\right)^2 + \int\int R_n(u-s) h(-u) h(-s)\,du\,ds \tag{B.23}$$

Expanding equation (B.23)

$$E\left(x^2(k\tau)\right) = \alpha^2 \int \left[\lambda_o + \sum_m V_m\, p(u - m\tau)\right] h^2(k\tau - u)\,du + \alpha^2 \left[\int \left[\lambda_o + \sum_m V_m\, p(u - m\tau)\right] h(k\tau - u)\right]^2 + \int\int R_n(u-s) h(-u) h(-s)\,du\,ds \tag{B.24}$$

Further expansion yields

$$E\left(x^2(k\tau)\right) = \alpha^2 \lambda_o \int h^2(u)\,du + \alpha^2 m_V \sum_m \int p(u - m\tau) h^2(k\tau - u)\,du + \alpha^2 \lambda_o^2 \left(\int h(u)\,du\right)^2 + 2\alpha^2 m_V \lambda_o \sum_m r_m \int h(u)\,du + \int\int R_n(u-s) h(-u) h(-s)\,du\,ds + \alpha^2 \left[\sum_m V_m \int p(u - m\tau) h(-u)\,du\right]^2 \tag{B.25}$$

Hence

$$\sigma^2_{x(k\tau)} = \alpha^2 \lambda_o \int h^2(u)\,du + \alpha^2 m_V \sum_m r_m \int h(-u)\,du + \alpha^2 \left[\sum_m V_m \int p(u - m\tau) h(-u)\,du\right]^2 - \alpha^2 m_V^2 \sum_m \sum_n r_{k-m}\, r_{k-n} \tag{B.26}$$

$$+ \int\int R_n (u-s)h(-u)h(-s)\,du\,ds$$

or

$$\sigma^2_{x(k\tau)} = \alpha^2\lambda_o \int h^2(u)\,du + \alpha^2 m_V \sum_m \int p(u-m\tau)h^2(-u)\,du \tag{B.27}$$

$$+ \int\int R_n (u-s)h(-u)h(-s)\,du\,ds + \alpha^2 \sum_n \sum_m r_{k-m}\, r_{k-n} (\Theta_{mn} - m_V^2)$$

The third term $E(V_k\, x(k\tau))$ will now be evaluated

$$E(V_k\, x(k\tau)) = \alpha V_k \lambda_o \int h(u)\,du + V_k \sum_m V_m \int p(u-nT)h(-u)\,du \tag{B.28}$$

where $k > m$

after averaging over V_k equation (B.28) becomes

$$E(V_k\, x(k\tau)) = \alpha\lambda_o\, m_V \int h(u)\,du + \alpha \sum_n \sum_m V_m\, V_{k-n} \int p(u-m\tau)h(-u)\,du \tag{B.29}$$

$$E(V_k\, x(k\tau) = \alpha\lambda_o\, m_V \int h(u)\,du + \alpha \sum_m \sum_n E[V_m\, V_{k-n}]\, r_{k-m} \tag{B.30}$$

$$E(V_k\, x(k\tau) = \alpha\lambda_o\, m_V \int h(u)\,du + \alpha \sum_m \sum_n \Theta_{mn}\, r_{k-n} \tag{B.31}$$

The complete expression for mean square error becomes

$$\overline{e^2} = \alpha^2\lambda_o \int h^2(-u)\,du + \alpha^2 m_V \sum_m \int p(u-m\tau)h^2(-u)\,du \tag{B.31}$$

$$+ \int\int R_n (u-s)h(-u)h(-s)\,du\,ds + \alpha^2 \sum_n \sum_m r_{k-m}\, r_{k-n} (\Theta_{mn} - m_V^2)$$

$$- 2\alpha \sum_m \sum_n \Theta_{mn}\, r_{k-n} + (\Theta_{mn} - m_V^2) + 2\alpha m_V^2 \sum_m r_m$$

APPENDIX C

DERIVATION OF FIRST MOMENT OF V_k

The first moment of a random variable from Papoulis [6] is given by

$$E(x) = \sum_i p_i x_i \tag{C.1}$$

where random variable x takes on values x_i with probability p_i

The first momemnt of the PWM symbol V_k is

$$m_V = E(V_k) = \frac{1}{M-1} \sum_{i=1}^{M-1} \frac{i}{M} \tag{C.2}$$

The summation counts up $M-1$ instead M, since the M th slot is used a guard band. Therefore this slot is always empty. This helps allievates the ISI problem somewhat, in particular the situation where a wide PWM pulse precedes a thin PWM pulse.

Using the following formula from the CRC (Cleveland Rubber Company) mathematical handbook

$$\sum_{i=1}^{N} i = \frac{N(N+1)}{2} \tag{C.3}$$

the closed form of equation of equation (C.2) becomes

$$m_V = \frac{1}{2} \tag{C.4}$$

APPENDIX D

DERIVATION OF SECOND MOMENT OF V_k

The correlation of $V_n\ V_m$ is given by Papoulis [6] as the joint moment below

$$E(V_n\ V_m) = \sum_n \sum_m v_n\ v_m\ p_{nm} \tag{D.1}$$

where p_{nm} is the probability of that both values v_n and v_m occur simultaneously. The probability p_{nm} is equal $\frac{1}{M-1}$.

The theta function Θ_{mn} represents the the sequence $E(V_m\ V_n)$. It can take three different values depending on the loaction of n and m .

$$\Theta_{mn} = E[V_m\ V_n] = \begin{cases} g & m = n \\ \Psi & m \neq n \text{ same frame} \\ y & m \neq n \text{ different frames} \end{cases} \tag{D.2}$$

The first scenerio where $m = n$ is given by the variable g

$$g = E(V_n\ V_m) = \sum_{k=1}^{M-1} v_k\ p_k \tag{D.3}$$

where k is the event where $m = n$

Using the result of APPENDIX C the term g becomes

$$g = \frac{1}{2} \tag{D.4}$$

When $m \neq n$ and n and m are in the same frame the theta function is given by the term Ψ

$$\Psi = \frac{1}{(M-1)}\left[\frac{\binom{2}{2}}{\binom{M}{2}} + \frac{\binom{3}{2}}{\binom{M}{2}} + \frac{\binom{4}{2}}{\binom{M}{2}} + \cdots + \frac{\binom{(M-1)}{2}}{\binom{M}{2}}\right] \tag{D.5}$$

Equation (D.5) can be simplified into the following form

$$\Psi = \frac{(M-2)!}{(M-1)M!}\left[\frac{2!}{0!} + \frac{3!}{1!} + \frac{4!}{2!} + \frac{5!}{3!} + \cdots + \frac{(M-1)!}{(M-3)!}\right] \tag{D.6}$$

Equation (D.6) can be further simplified as

$$\Psi = \frac{(M-2)!}{(M-1)M!}\left[\sum_{k=1}^{M-1}(k^2 - k)\right] \tag{D.7}$$

Using equation (C.3) and the following formula from the CRC handbook

$$\sum_{i=1}^{N} i^2 = \frac{N(N+1)(2N+1)}{6} \tag{D.8}$$

the closed form of equation (D.7) is given by

$$\Psi = \frac{(M-2)!}{M!}\left[\frac{M(2M-1)}{6} - \frac{M}{2}\right] \tag{D.9}$$

Further simplification yields

$$\Psi = \frac{(M-2)}{(3M-3)} \tag{D.10}$$

For very large values of M the term Ψ approaches

$$\Psi = \lim_{M\to\infty} \frac{(M-2)}{3(M-1)} = \frac{1}{3} \tag{D.11}$$

It should be noted that Ψ is only valid when $M \geq 2$.

When $m \neq n$ and symbols m and n are in the different frames the Θ_{nm} function is represented by y

$$y = E(V_n)E(V_m) \tag{D.12}$$

using the result from (C.4) the solution is given by

$$y = m_V^2 = \frac{1}{4} \tag{D.13}$$

In summary it can be said the Θ_{mn} is defined as following

$$\Theta_{mn} = E[V_m V_n] = \begin{cases} g = \frac{1}{2} & m = n \\ \Psi = \frac{(M-2)}{3(M-1)} & m \neq n \text{ same frame} \\ y = \frac{1}{4} & m \neq n \text{ different frames} \end{cases} \tag{D.14}$$

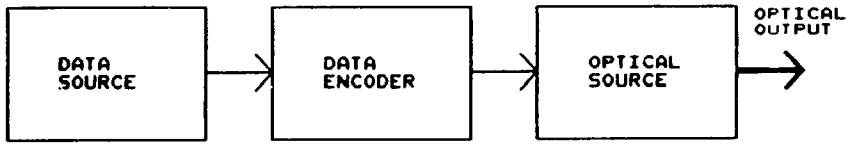

FIGURE 1(A) FIBER OPTIC TRANSMITTER

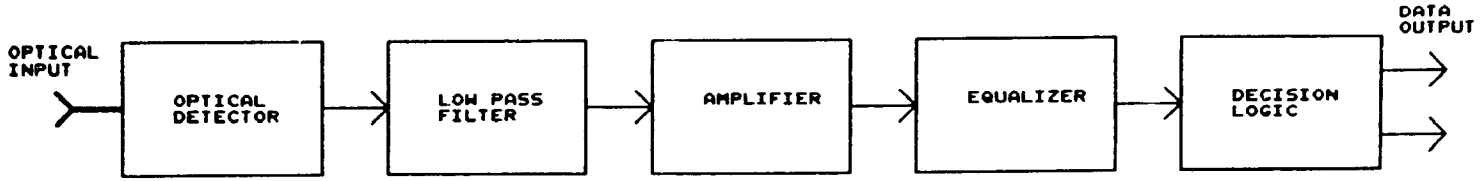

FIGURE 1(B) FIBER OPTIC RECEIVER

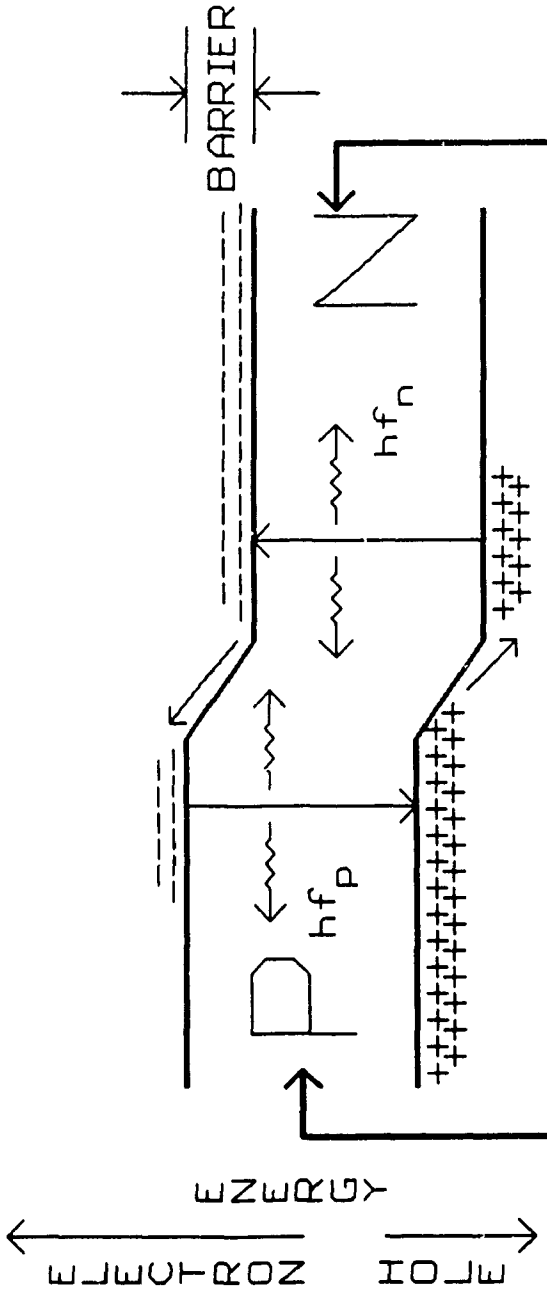

Figure 2 OPERATION OF THE PN JUNCTION LED

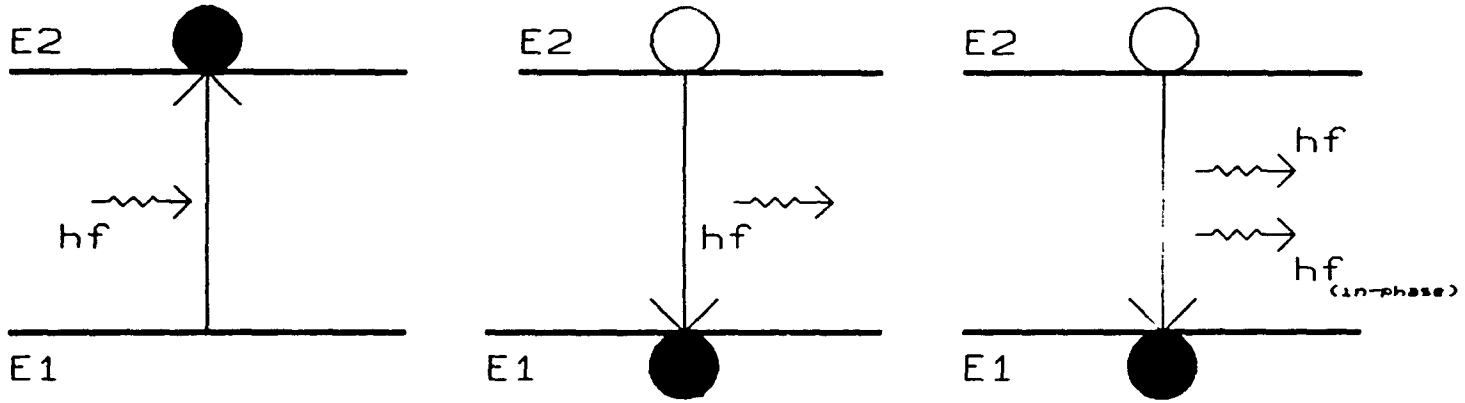

FIGURE 3 MECHANISMS OF LASER ACTION

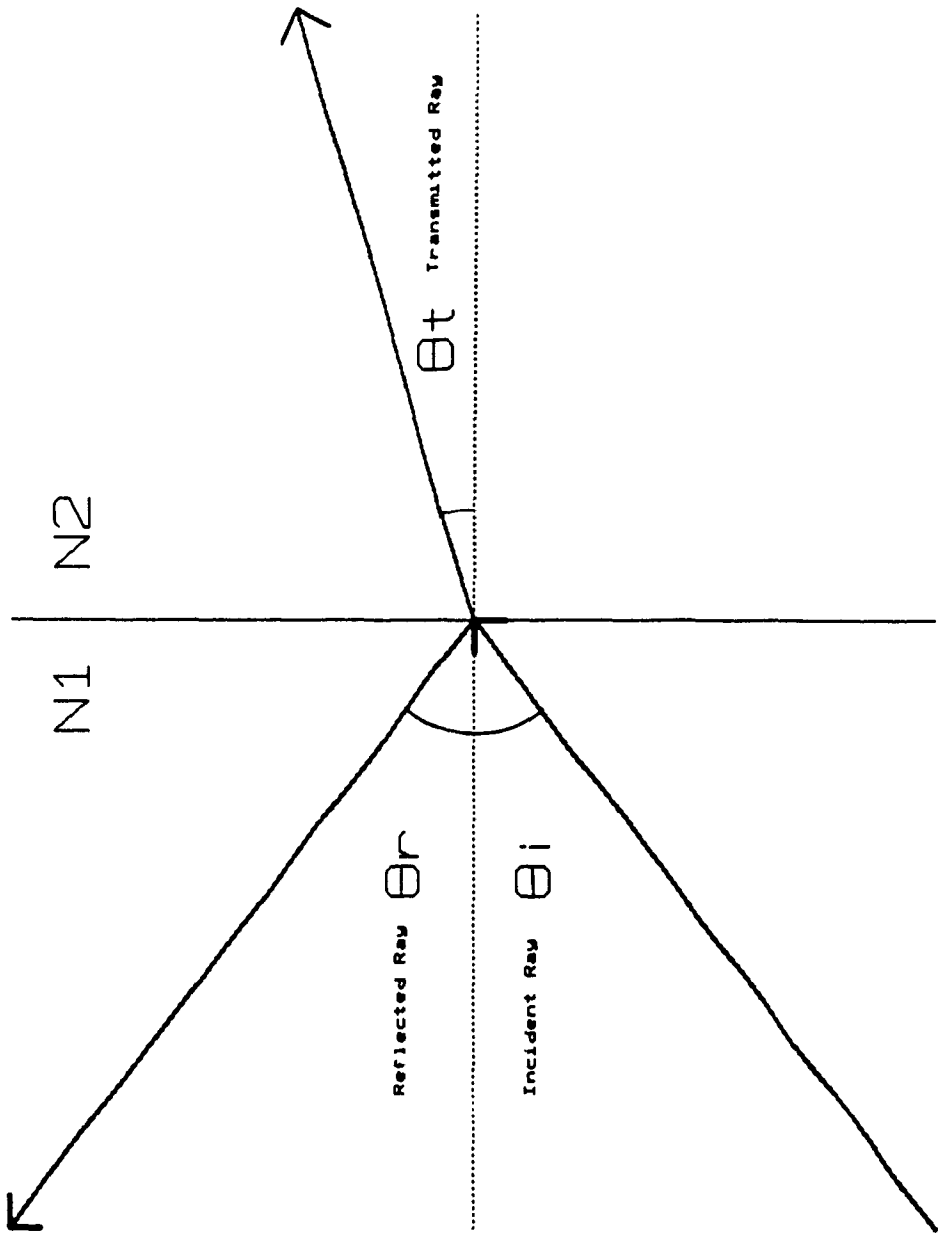

FIGURE 4 BEHAVIOUR OF LIGHT AT A BOUNDARY INTERFACE

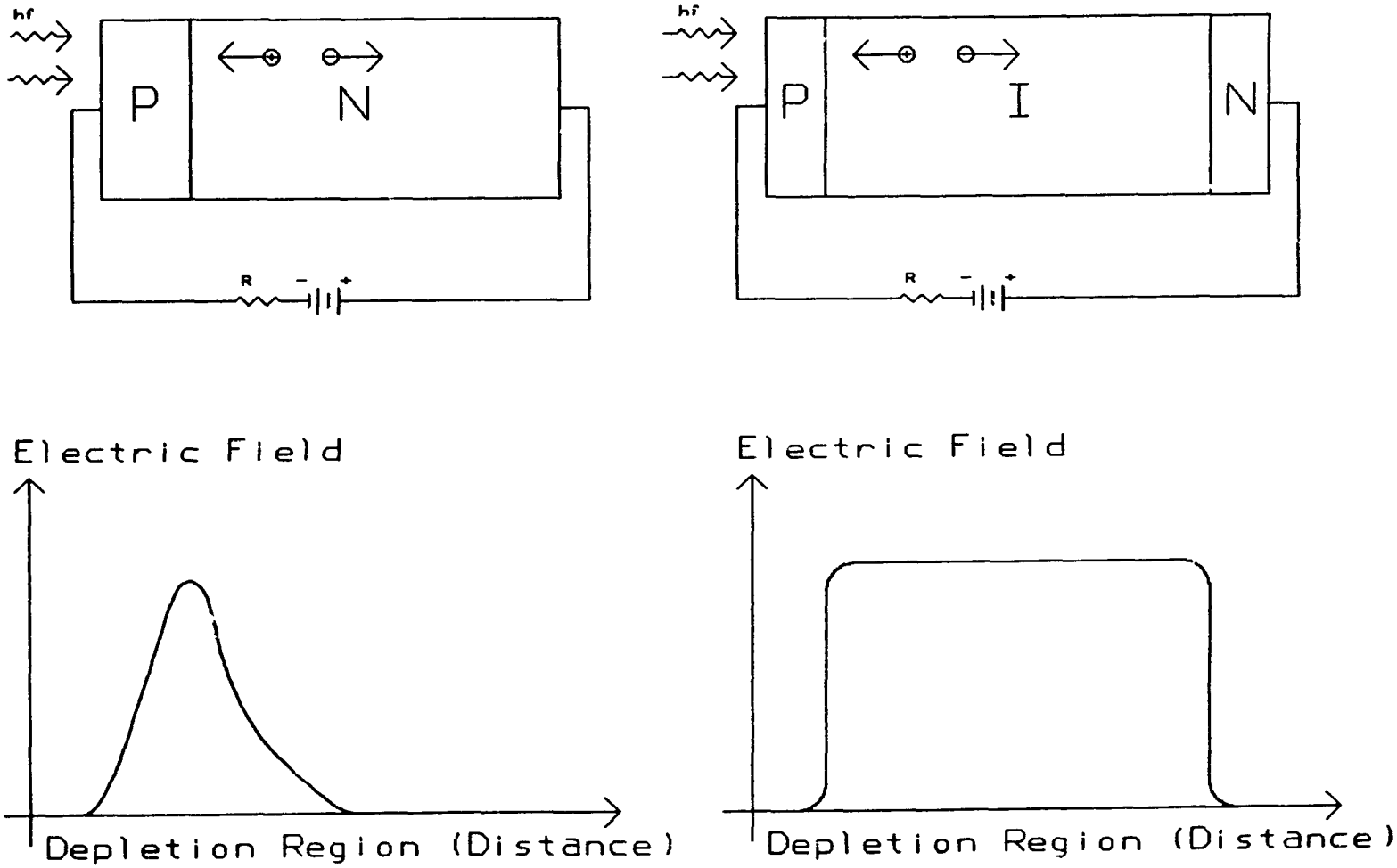

FIGURE 5 PN AND PIN DIODE CONSTRUCTION

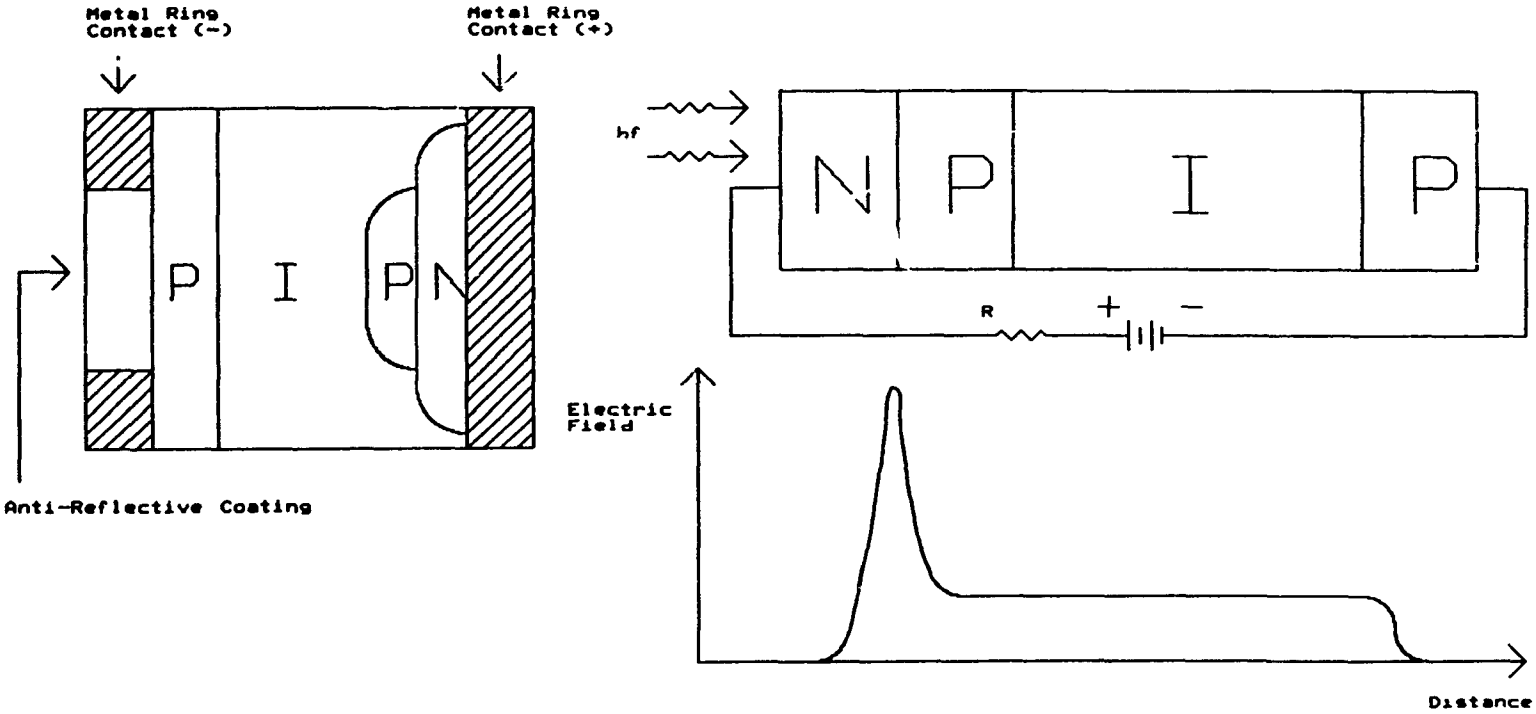

Figure 6(A) APD Construction (B) APD Electric Field Distribution

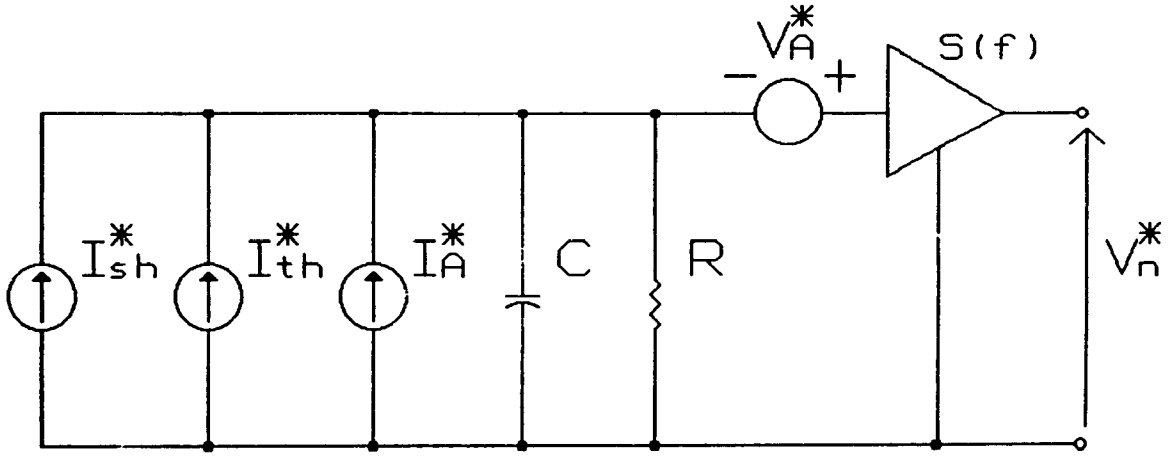

FIGURE 7(A) Noise Equivalent of an APD Amplifier

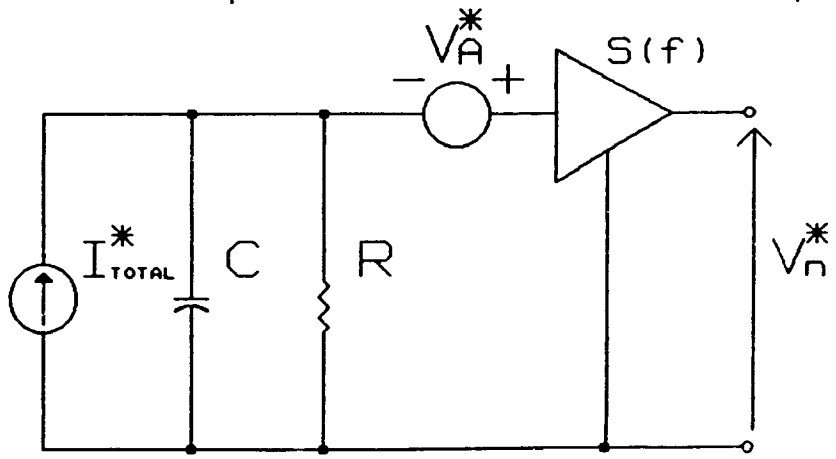

FIGURE 7(B) Reduced Noise Equivalent of an APD Amplifier

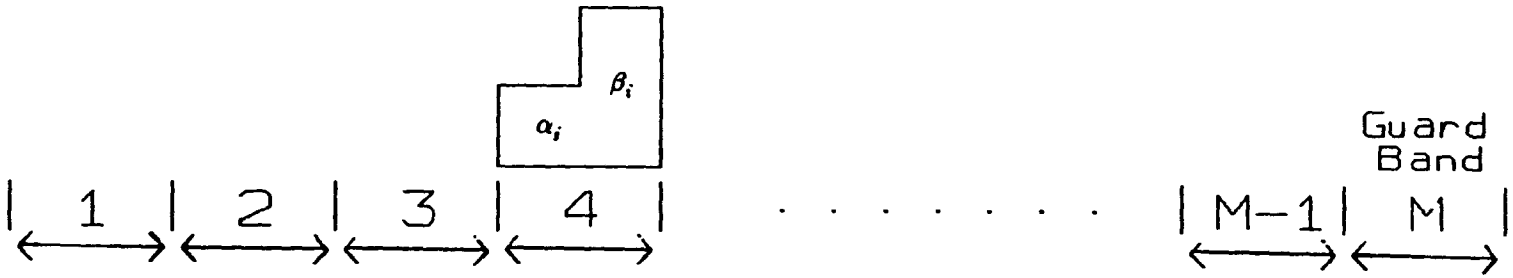

Figure 8 Combinational PPAM Pulse and Frame Structure

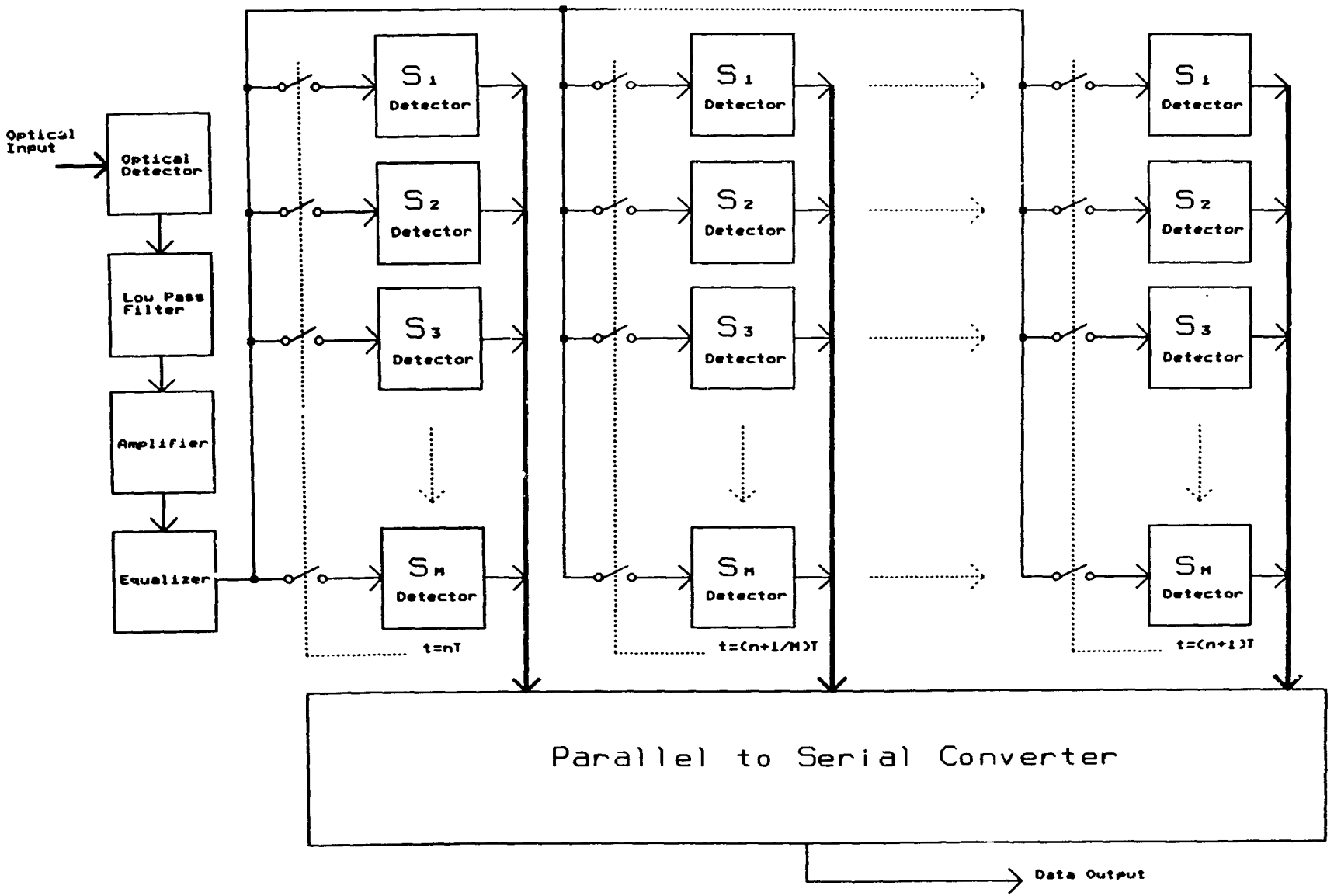

FIGURE 9 Conventional PPAM Reciever Structure

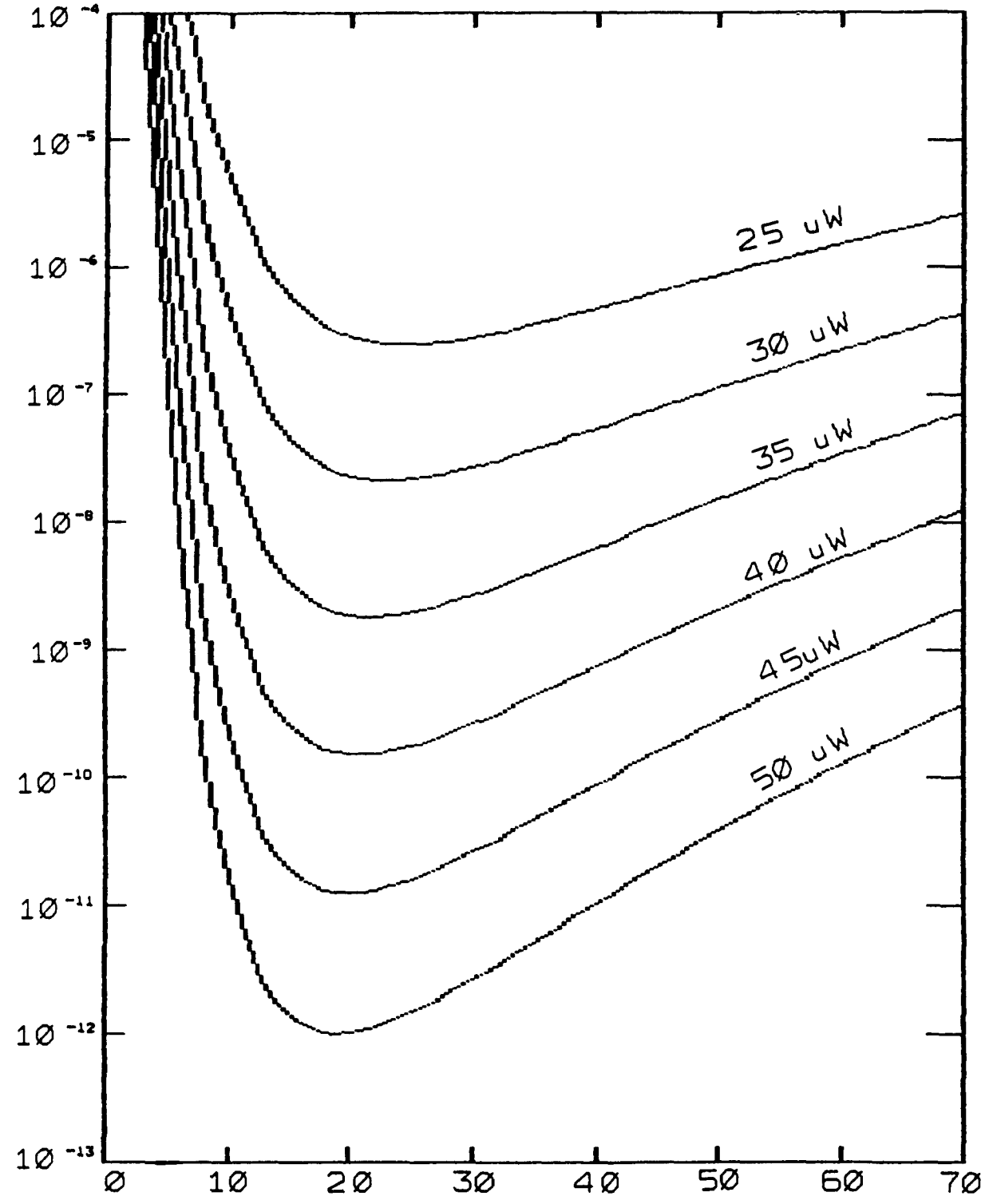

FIGURE 10 Probability of Error versus APD Gain <G>

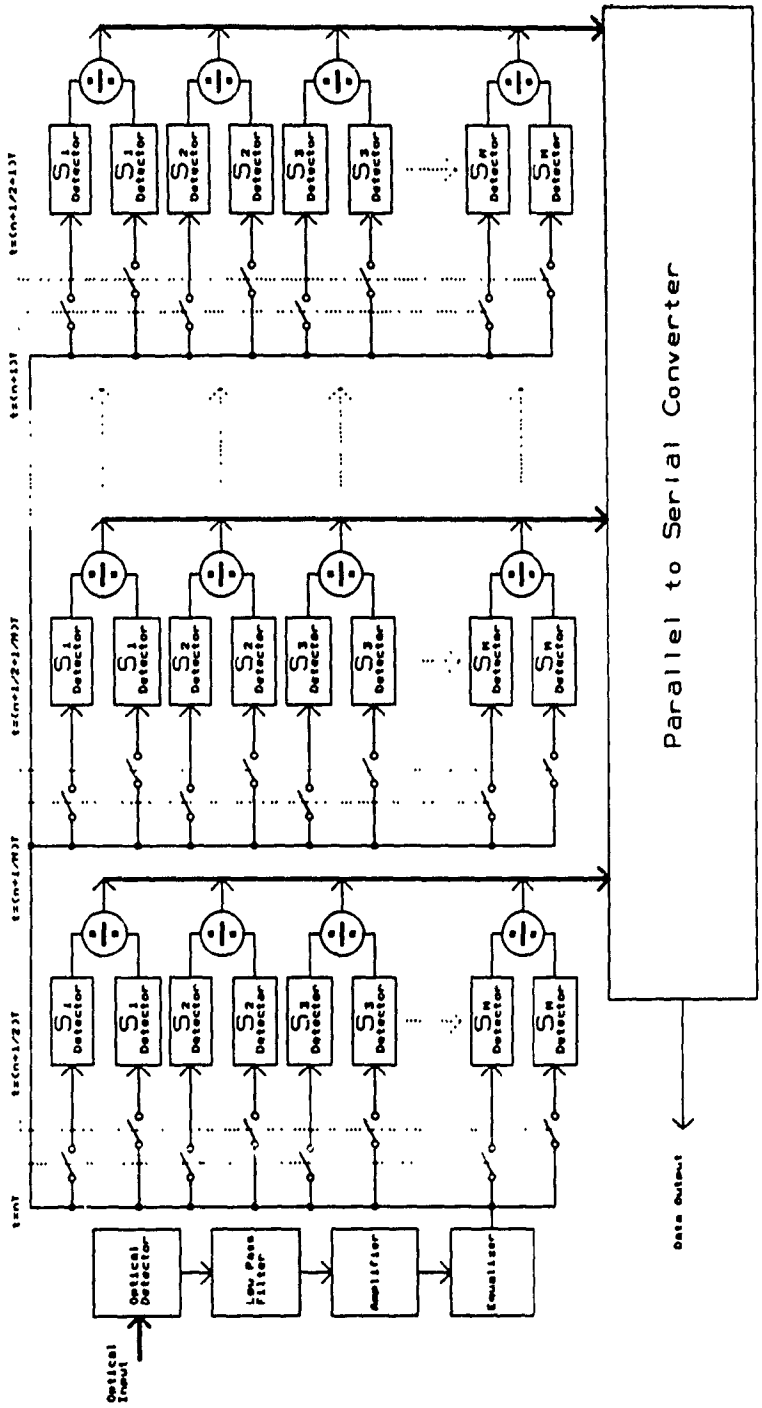

FIGURE 11 PPAM Ratio Receiver Structure

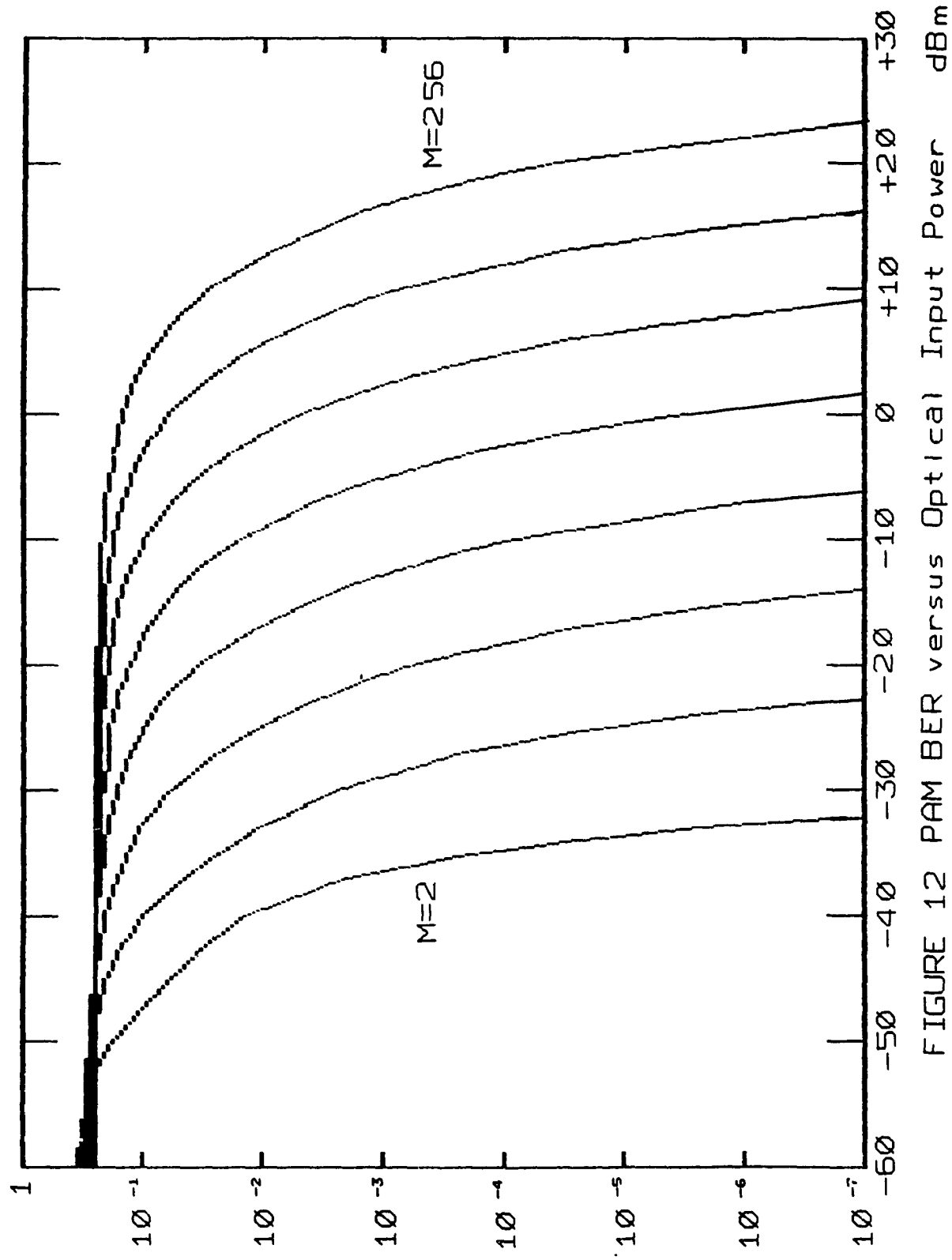

FIGURE 12 PAM BER versus Optical Input Power

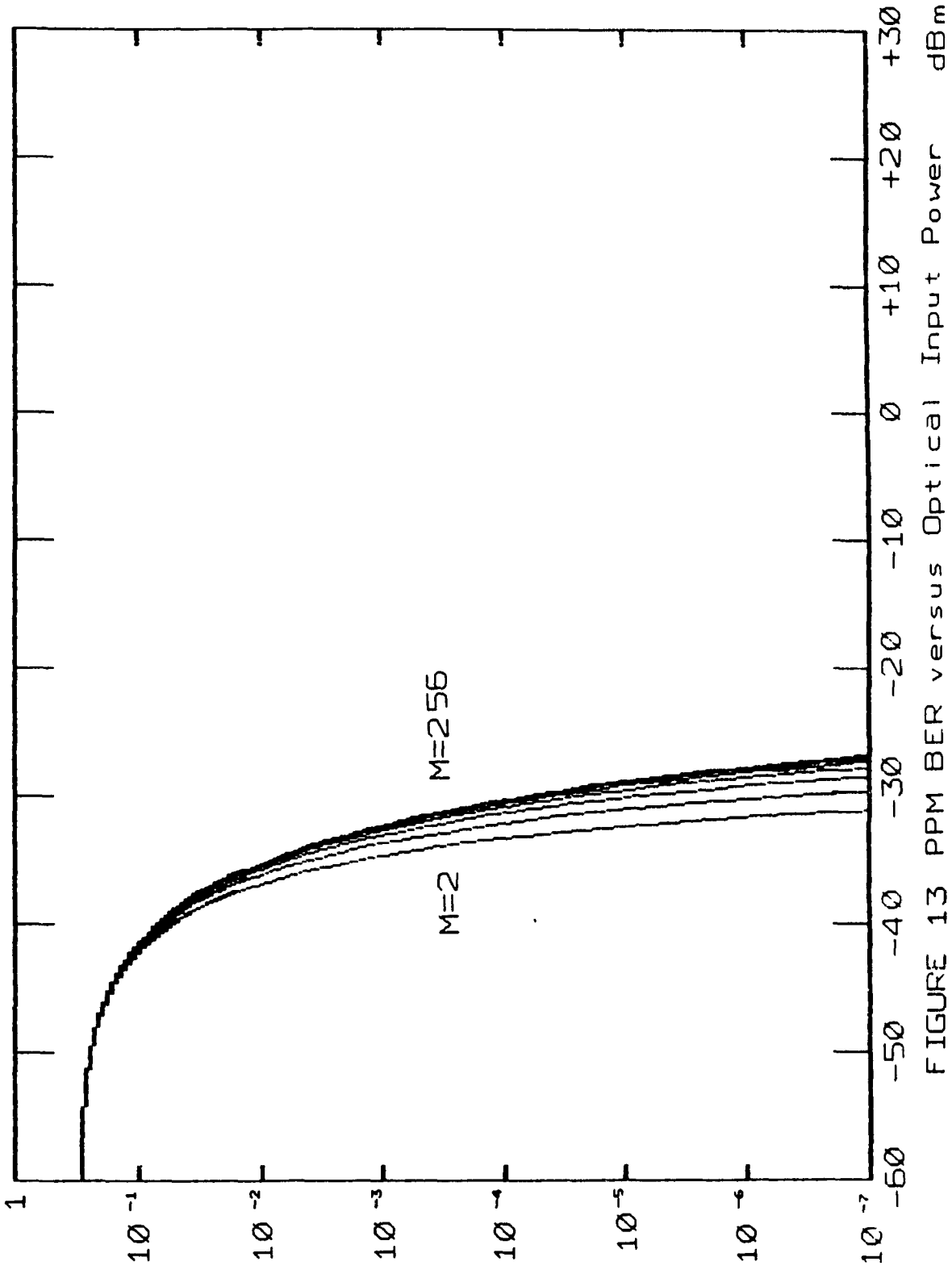

FIGURE 13 PPM BER versus Optical Input Power

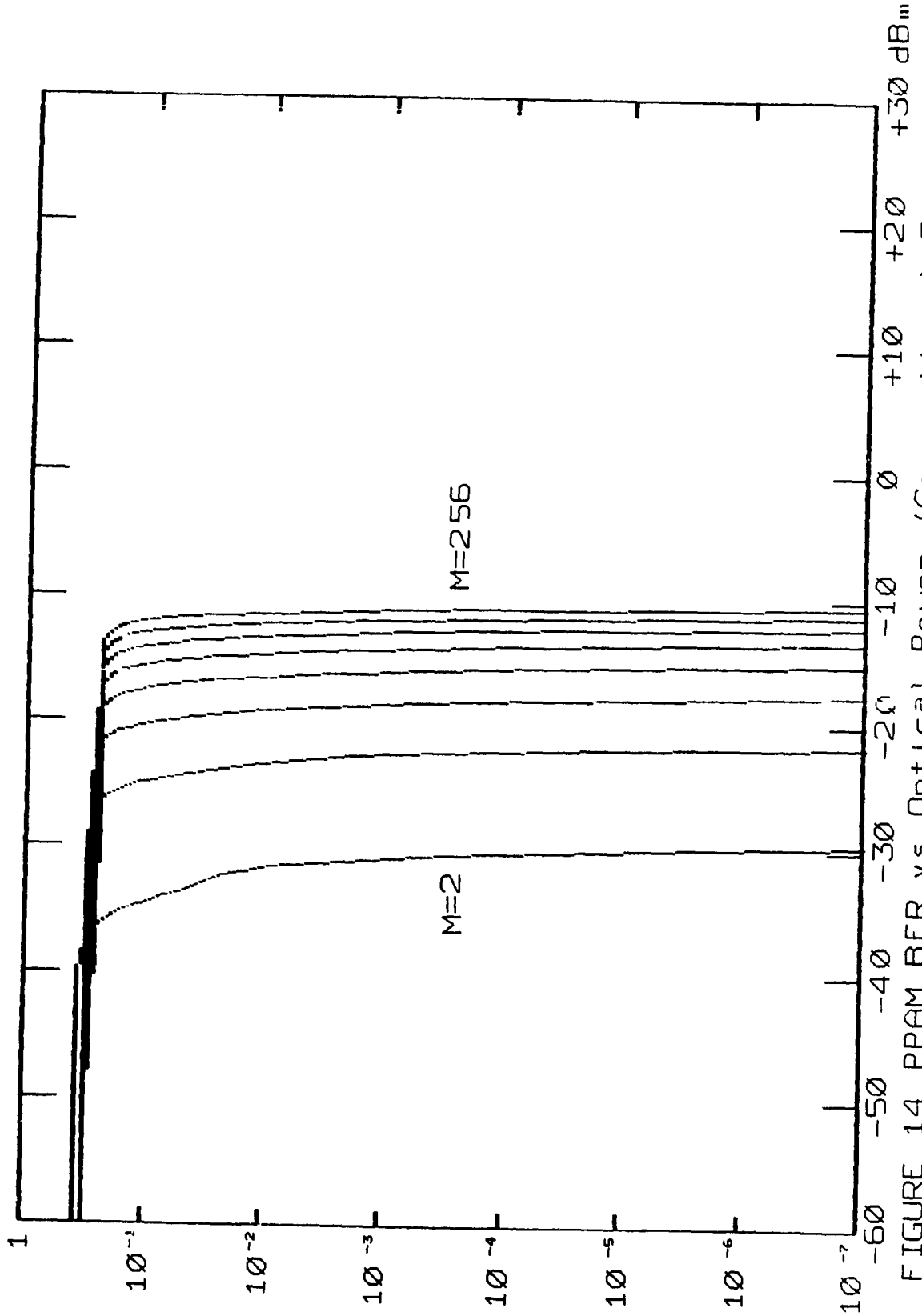

FIGURE 14 PPAM BER vs Optical Power (Conventional Receiver)

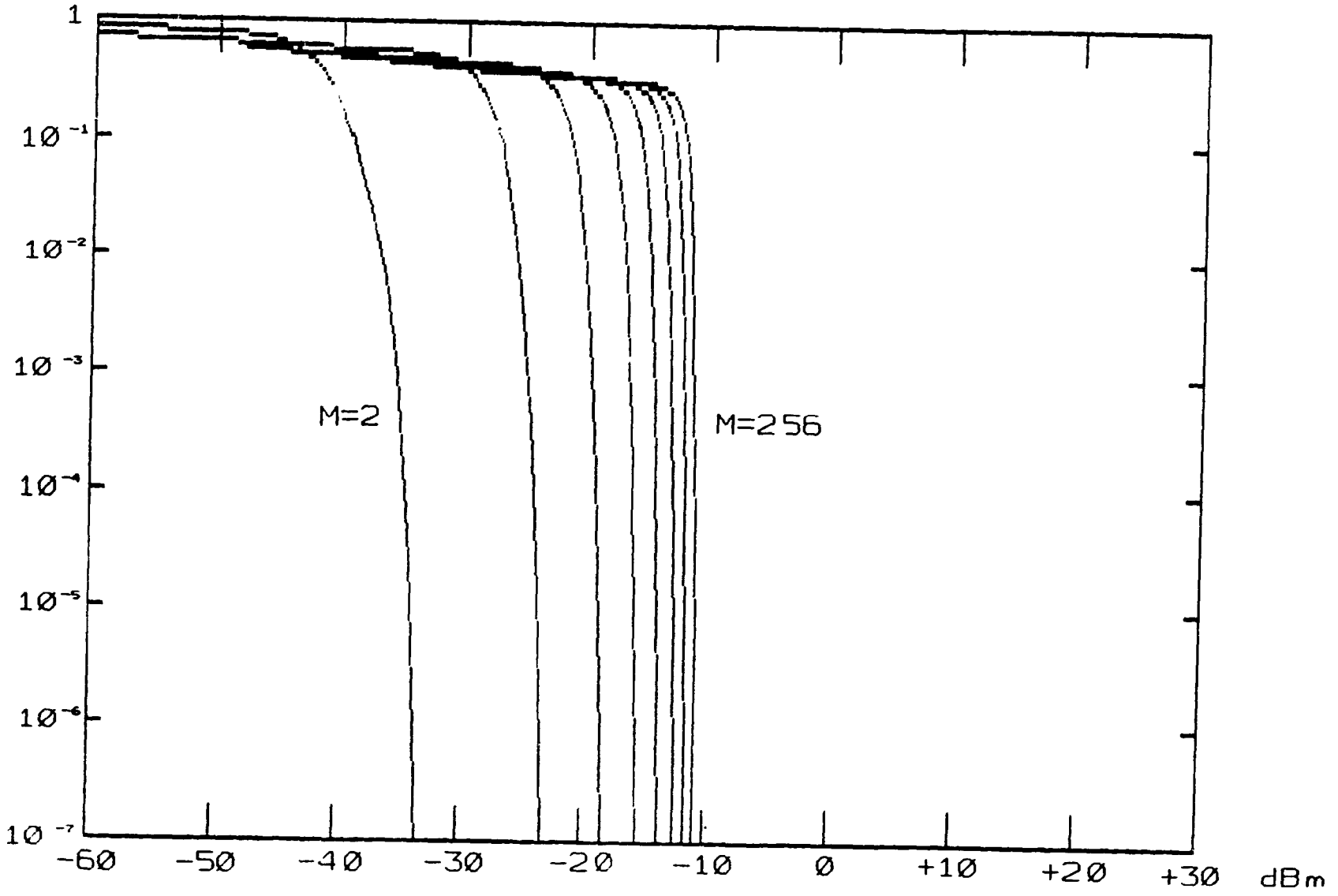

FIGURE 15 PPAM BER vs Optical Power (Ratio Receiver) I

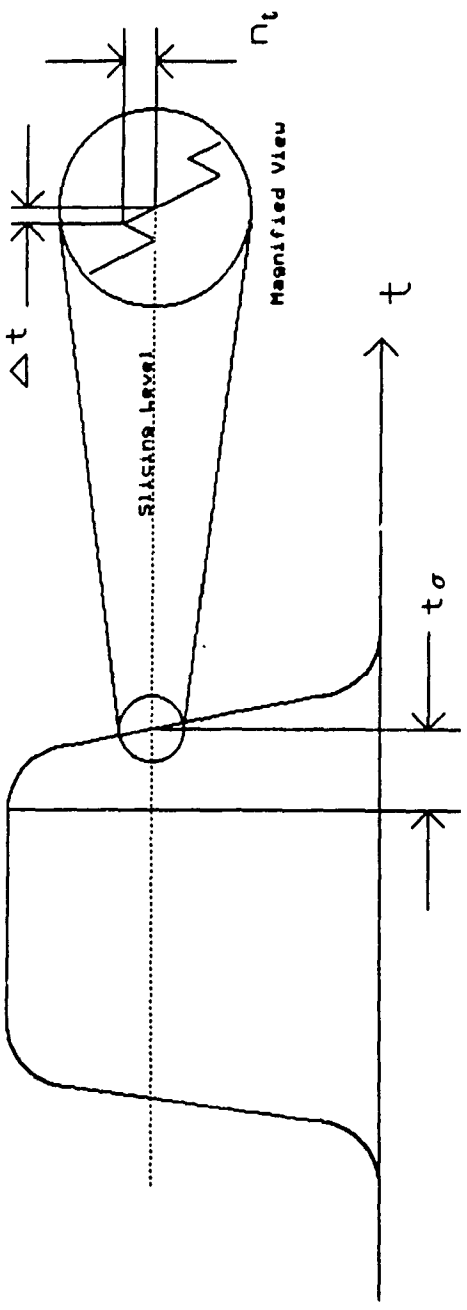

FIGURE 16 Noise Amplitude and Timing Error Relationship

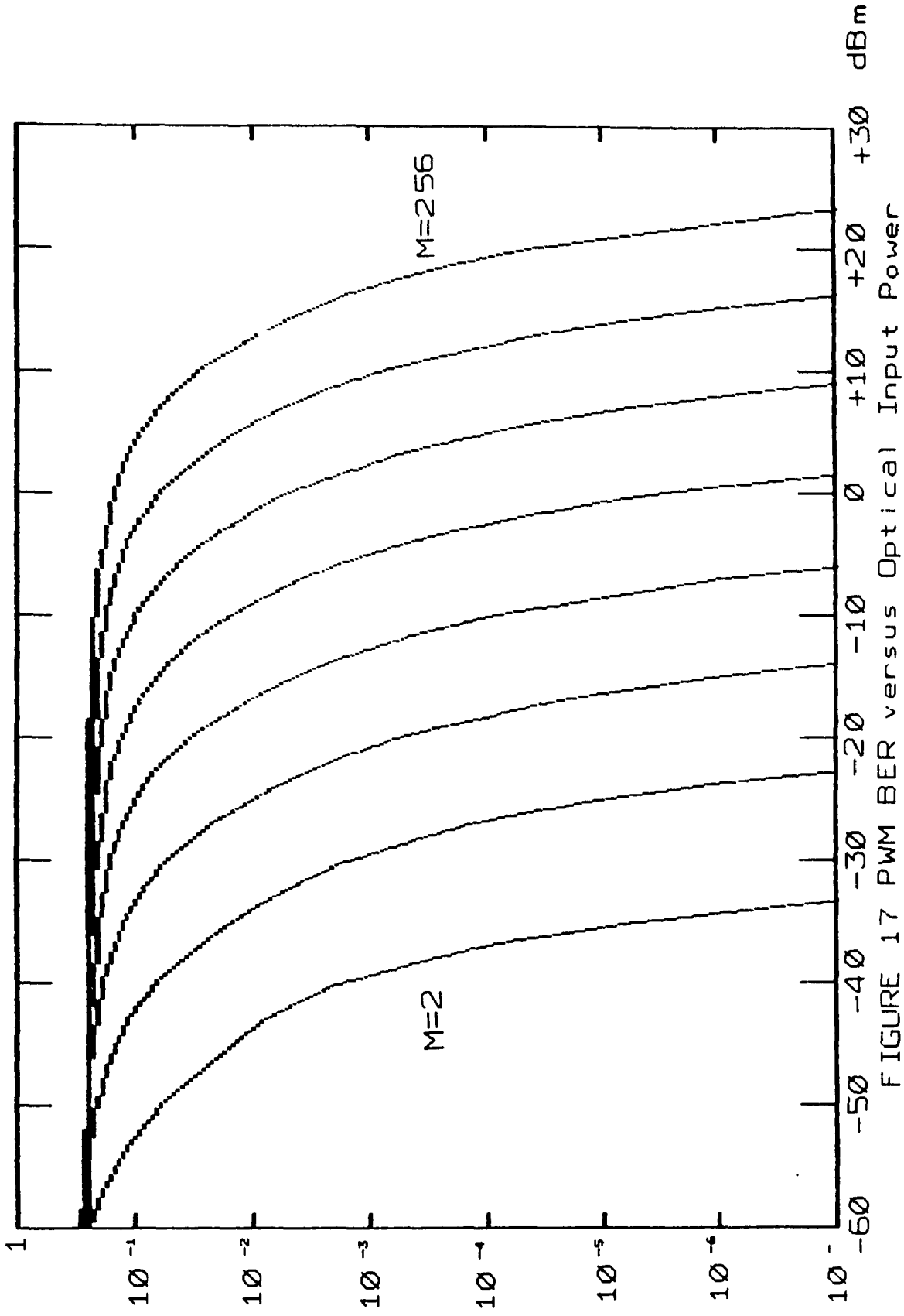

FIGURE 17 PWM BER versus Optical Input Power

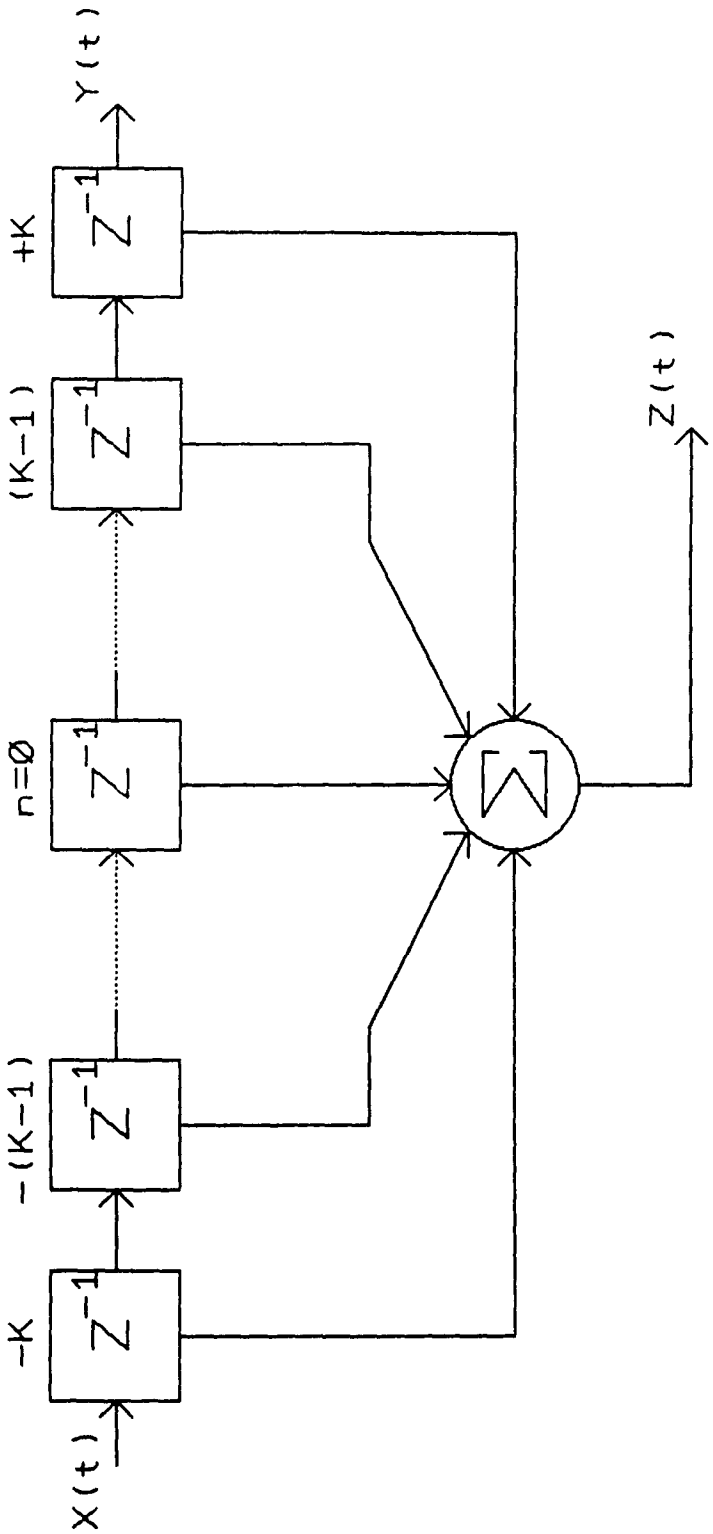

FIGURE 18 Transversal Filter

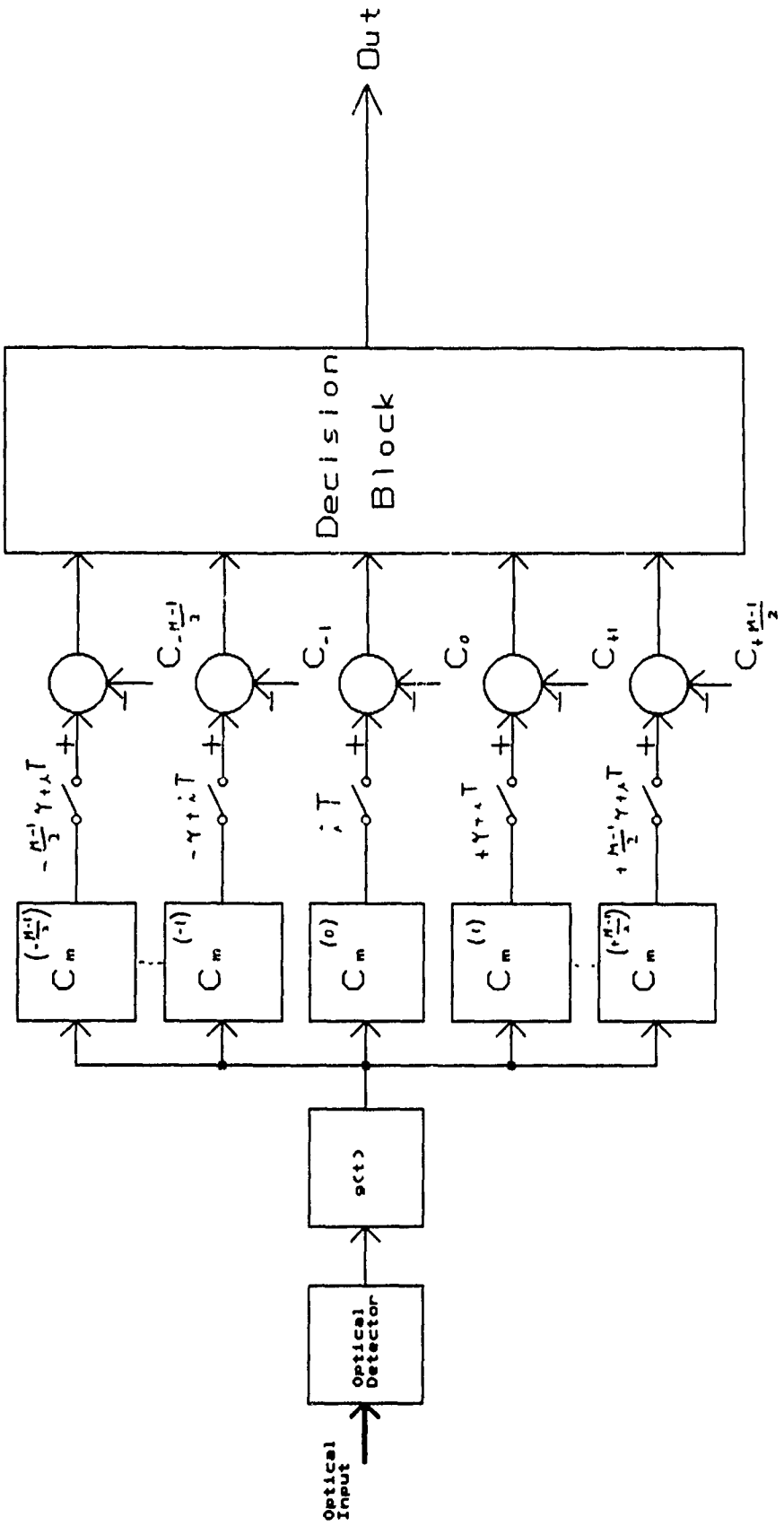

FIGURE 19 PWM Receiver with Equalizer

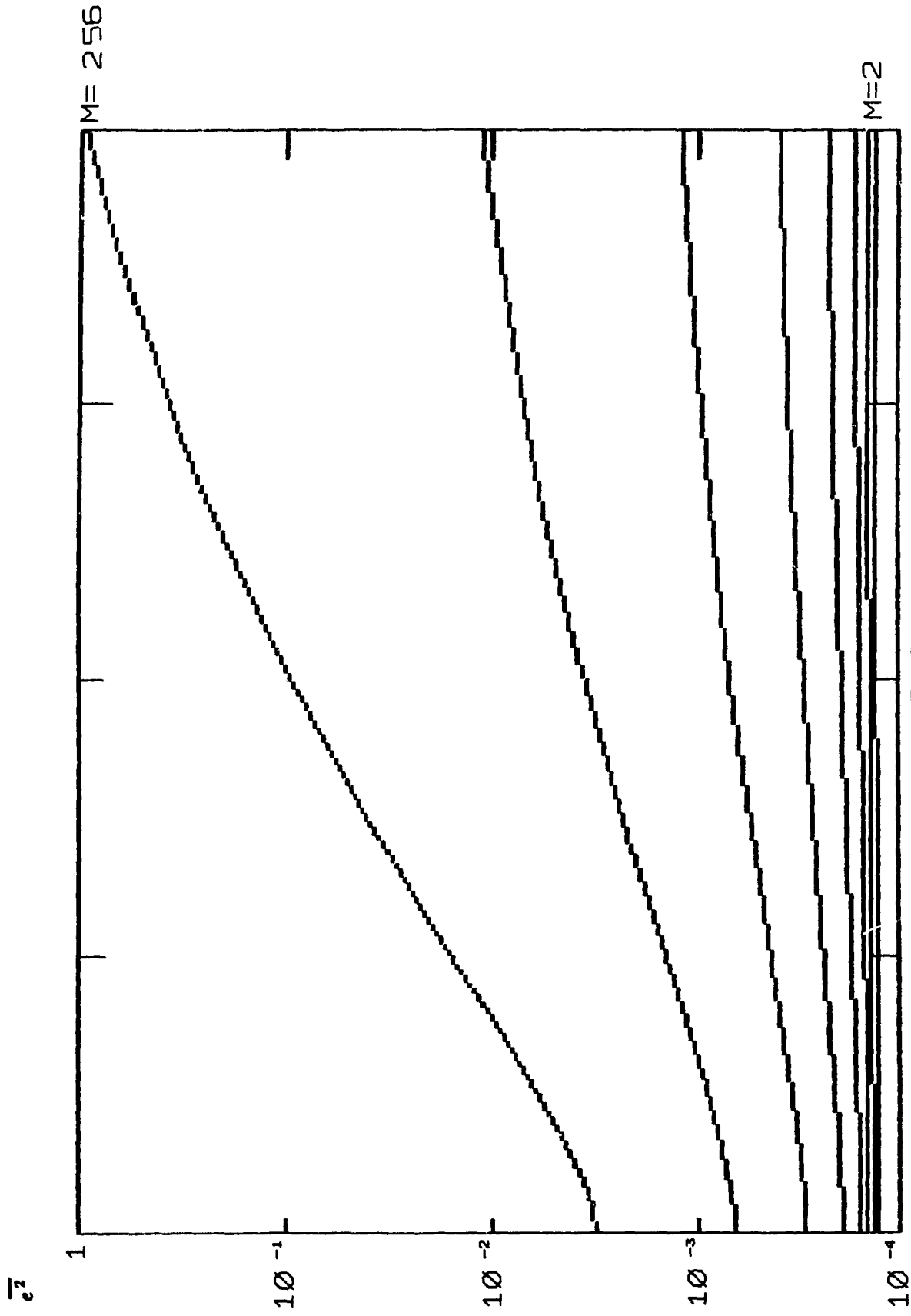

FIGURE 20 MSE versus RMS pulse width for ZF-LE

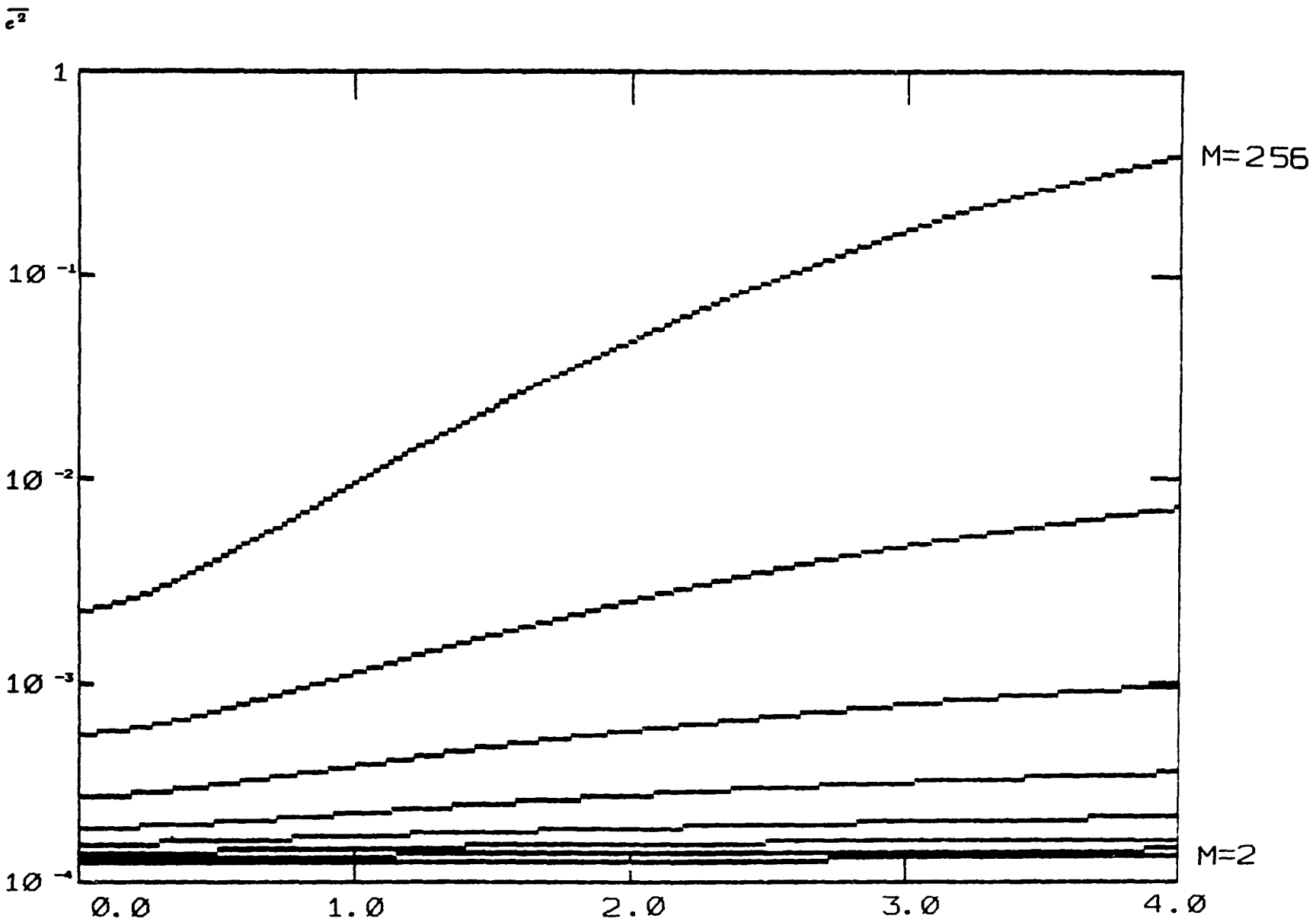

Figure 21 MSE versus RMS pulse width for MSE-LE

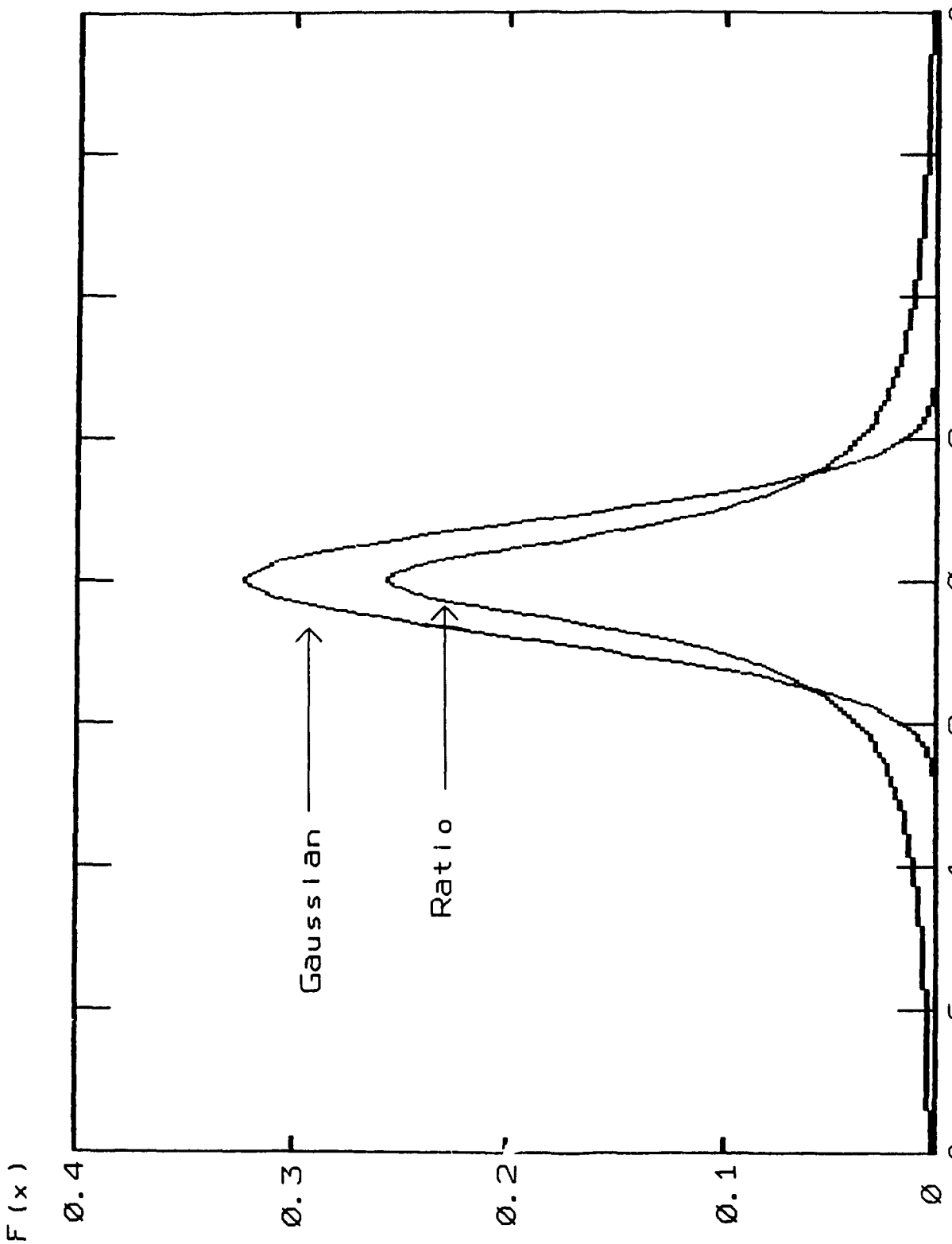

Figure 22 Comparison of Gaussian and Ratio PDF